Research on submerged inclined-plate breakwater for wave control

メタデータ	
	言語: eng
	出版者:
	公開日: 2018-04-09
	キーワード (Ja):
	キーワード (En):
	作成者: 王, 禹龍
	メールアドレス:
	所属:
URL	https://oacis.repo.nii.ac.jp/records/1526

Master's Thesis

RESEARCH ON SUBMERGED INCLINED-PLATE BREAKWATER FOR WAVE CONTROL

September 2017

Graduate School of Marine Science and Technology

Tokyo University of Marine Science and Technology

Master's Course of Marine System Engineering

YULONG WANG

Abstract

A structure designed and constructed for decreasing wave height is usually called breakwater in coastal engineering. Breakwaters are important structures to create appropriate environment for nearshore. Submerged plate structures, permeable structures usually supported by steal piles, are widely proposed as breakwater. Submerged horizontal-plate structures are believed to have some good features and performance in harsh natural conditions with harmony to surroundings, reasonable construction cost by fewer maintenances and shorter construction periods; practical experiences show that submerged horizontal-plates are quite effective in shoreline restoration. Meanwhile, submerged inclined-plate breakwaters structure inherit features from horizontal ones, and can be adopted in many fishing ports to meet the variation of tide. While compared to a conventional breakwater depending on the gravity as a solid structure, a submerged inclined-plate breakwater is limited to some extent on wave control performance to serve as a predominant prior option.

The motivation behind the present research was to enhance the performance of inclined-plate breakwater for wave control, and stages of work were carried out to accomplishment of the objective.

Specifically, wave deformation over the inclined-plate breakwater was evaluated based on velocity potential theory; wave deformation considering wave breaking over inclined-plate breakwater was investigated; an improvement scheme of inclined-plate breakwater for better wave control performance was purposed and tested. For the first stage of objective, a step-like

approximation method was developed to evaluate the reflection and transmission coefficients of a submerged inclined-plate breakwater; in the analytical model, the inclined-plate was assumed to comprise a series of small horizontal plates in different water depth, and each small horizontal plate region can be resolved by utilizing eigenfunction matching method (Ijima, T., et al., 1970) to analyze horizontal plate breakwater. Then a wave flume experiment with a physical model was conducted to investigate wave control performance with the consideration of wave breaking; wave energy dissipation coefficient in different breakwater configurations and wave conditions was evaluated. An improvement scheme for wave control with consideration of roughness and porosity was tested and its main influencing factors was studied.

A comparison between the analytical model results and former experimental results (Aoyama, T., et al., 1988) indicates that wave breaking at shallow submergence is a significant factor for water wave. It is the reason that the shallow submerged-plate plays a critical role on wave breaking. It is found from the experiment that wave steepness is another crucial factor for wave control. The comparison also shows the inclined-plate breakwater should be quite long (usually 0.25 times of wave length, which is 20~30 meters long) if this breakwater is as effective as the conventional breakwater. The consequent aim is to improve the performance of breakwater focusing on the plate roughness and the plate porosity by adding serrated blocks and making slot gaps on the plate. A wave flume experiment is conducted to measure wave height in different breakwater configuration and wave conditions, and then to calculate the reflection, transmission and wave energy dissipation coefficients.

Discussion starts with wave breaking analysis over the plate. Higher wave is easier to break over the plate; for the plate with roughness, wave breaking is earlier than that when plate is smooth. It is because the cubes on the plate disturb flow along plate direction which release more wave energy; for plate with slots, flow exchanges easier than solid plate both vertically and horizontally. On the contrary, wave breaks easily on solid plate due to continuous obstruction.

Acknowledgements

I would like to thank all the people who contributed in any ways to my work described in my thesis. First and foremost, I would like to thank my supervisor, Professor Akio Okayasu, for accepting me into his laboratory. During my first time to study abroad, he provided me extraordinary experience in Japanese by giving me abundant information focus on my interests before choosing research topic, supporting me various activities and conference, and demanding a high quality of work strictly.

Additionally, I would like to thank Professor Tsuyoshi Ikeya who had provided me extremely suggestions, who was the inspiration for developing idea of inclined plate model. Every time I went into the office of Professor Ikeya, I opened the door of the temple of knowledge, in his narrative, once printed on the pages of the theory become alive with full of anecdotes and stories which cannot read from books. Professor Ikeya is an inspiring priest more than a teaching preacher who engaging me in innovative ideas, my accomplishment would never have achieved without his enlightenment on numerical modelling and wave flume experiments during all my study. Acknowledgement also to Professor Kazuo Tani, and Associate Professor Daisuke Inazu for their advising in my work.

Every result described in my thesis was accomplished with the help and supports of fellow lab mates. I greatly benefited from Doctor Dejun Feng's sophisticated logic because he could always discover faults or in my story, his concentration on solving practical difficulties, his ability to explain a complex idea to an operable experimental design and his encouragement on my further

study in Japan.

Mr. Lianhui Wu was the first person who helped me on admitting before I came to Japan, deeply affected by his action style of clear propose, I gained a lot new views on thinking about and resolving problems. In addition, he was an extremely reliable source of Japanese knowledge, and I am grateful for his help during my life in campus.

Mr. Yoshiyuki Uno, who was researcher when I came in laboratory and became a doctor candidate years later, is a charming and cautious buddy in our laboratory, his enthusiasm warms me. Acknowledgement also greet to Mr. Yugeng Du, alumnus in Dalian and fortunately we became lab mates; Mr. Yuya Hanai, my tutor in lab and he is a sun shine boy who gave me a deep impression. In the same time, I am also grateful to Mr. Tianning Chen, Mr. Masahiro Sagehashi, Mr. Taihei Akatsuka, Ms. Nanami Noguchi, Ms. Narumi Konno, Mr. Akihiro Tomita, Mr. Shotaro Suzuki and Mr. Haijun Zhu.

I would like to thank the various instructors and members of the JCK program with whom we had memorable friendship in these two years, greetings also give to them who have not already mentioned: Miss. Jin, Miss. Kim, Miss. Qu and Miss. Shen, who gave me kind care in Japan. My program fellows, Mr. Yazhou Xie, Mr. Hao Cui, Ms. Yifei Wang, Mr. Hao Mei, Ms. Yiwen Hu, Mr. Yufei Liu, Mr. Jing'en Zhou, Mr. Jinxin Zhou and Ms. Xiaolin Ma, we spend time together in campus during workshops and courses. They provided a friendly and cooperative atmosphere when we are studying together, useful feedback and insightful comments to my work.

I also had the opportunity to know other friends during oceanic study, Mr. Xuanyu Liu, who tirelessly and with much enthusiasm over the discussion. Additionally, I also thank Ms. Yi Han for her gift from Antarctica and Australia.

I am grateful to Professor Zichang Shangguan of Dalian Ocean University and Japanese Government Scholarship that allowed me to pursue my graduate

Contents

List of Figures

xi

List of Tables

List of Symbols

$A_{j,n}$: n-th component unknown complex coefficient in inclined plate model

$\mathcal{A}_n$: n-th component unknown complex coefficient

A_1, A_2 :   Fourier constants

a_I :   amplitude of incident wave

a_R :   amplitude of reflected wave

B :   projection length of plate on x axis

$B_{j,n}$: n-th component unknown complex coefficient in inclined plate model

$\mathcal{B}_n$: n-th component unknown complex coefficient

B_1, B_2 :   Fourier constants

$C_{j,n}$: n-th component unknown complex coefficient in inclined plate model

$\mathcal{C}_n$: n-th component unknown complex coefficient

D :   middle point submergence of plate

$D_{j,n}$: n-th component unknown complex coefficient in inclined plate model

$\mathcal{D}_n$: n-th component unknown complex coefficient

d :   submerged depth of horizontal plate

d_j :   plate submergence in inclined plate model

$E_{j,n}$: n-th component unknown complex coefficient in inclined plate model

$\mathcal{E}_n$: n-th component unknown complex coefficient

$F_{j,n}$: n-th component unknown complex coefficient in inclined plate model

$\mathcal{F}_n$: n-th component unknown complex coefficient

$\mathcal{G}_n$: n-th component unknown complex coefficient

g :   acceleration of gravity

H :   wave height

$\bar{H}$	:	mean wave height
$H_{1/3}$	:	significant wave height
$\mathcal{H}_n$	:	n-th component unknown complex coefficient
h	:	water depth
j	:	plate element number in inclined plate model
$\mathcal{K}_R$	:	reflection coefficient
$\mathcal{K}_T$	:	transmission coefficient
k	:	wave number
k_n	:	roots of dispersion relation equation
	:	n-th component wave number of free surface wave region
	:	n-th mode evanescent wave number
$\hat{k}_n$	:	none dimensional value, $\hat{k}_n = k_n h$
k_n^d	:	n-th component eigenvalue of d water depth region
k_n^h	:	n-th component eigenvalue of h water depth region
$k_{0,n}$	:	n-th component wave number of none plate region in inclined plate model
$k_{j,n}$	:	n-th component wave number of above plate region in inclined plate model
L		wave length
l	:	half of the horizontal plate length
l_j	:	plate element length in inclined plate model
M_j	:	coefficient matrix of j element
$\mathcal{S}_n^{\mathcal{CE}}$	:	n-th component combination unknown complex coefficient
$\mathcal{T}_n^{\mathcal{DF}}$	:	n-th component combination unknown complex coefficient
T	:	wave period
$\bar{T}$	:	mean wave period
$T_{1/3}$	:	significant wave period
t	:	time
$\mathcal{X}_n$	:	orthogonal value of free surface wave region
x	:	horizontal coordinate
x_j	:	element middle point coordinate value in inclined plate model
$\mathcal{Y}_{nm}$	:	orthogonal value of region above and beneath plate
$\mathcal{Z}_n$	:	orthogonal value of region beneath plate

z	:	vertical coordinate
Δl	:	distance between the two wave gauges
$Z(kz)$	:	eigenfunction of none plate region
$E(\kappa z)$	:	combination eigenfunction of region above and beneath plate
$Z(\lambda z)$	:	eigenfunction of region beneath plate
$E(k_{0,n}z)$	:	eigenfunction of none plate region in inclined plate model
$Z(k_{j,n}z)$	:	eigenfunction of above plate region in inclined plate model
$\Lambda(\lambda_{j,n}z)$	:	eigenfunction of beneath plate region in inclined plate model
Ω	:	2-dimensional plain water region
α	:	$= \omega^2/g$
$\hat{\alpha}$	:	none dimensional value, $\hat{\alpha} = \alpha h$
δ_j	:	plate element thickness in inclined plate model
δ_{mn}	:	Kronecker delta
ε_I	:	phase
ε_R	:	phase
η	:	wave surface elevation
η_I	:	wave surface elevation due to incident wave
η_R	:	wave surface elevation due to reflected wave
θ	:	plate inclination
κ_n	:	n-th combination eigenvalue of region above and beneath plate
λ_n	:	n-th component eigenvalue of wave region beneath plate
$\lambda_{j,n}$	:	n-th component wave number of beneath plate region in inclined plate model
σ	:	angular frequency of wave in flume
φ	:	phase
ϕ	:	time independent part of velocity potential
ω	:	angular frequency

Chapter 1
Introduction

1.1 General Introduction to Breakwater

A structure designed and constructed for decreasing wave height are usually called breakwaters in coastal engineering. Breakwaters are important constructions to create appropriate environment for nearshore zones in harbors or to protect shorelines.

Due to the increasing demands from land to nearshore, offshore and ocean development during centuries, breakwater had constantly evolved fast at a single glance. It was believed that breakwater had a long history in human civilization, in the period of Wuyue, which was an independent coastal kingdom founded during the Five Dynasties and Ten Kingdoms (907–960) of Chinese history, overhaul the seawall and breakwater is one of its important national policies; from the gleaned information, the first breakwater ever constructed in the United State is the Delaware Breakwater near Cape Henlopen, Delaware, which was constructed from 1828 to 1869 by rubbles stacking randomly with 5276 foot long, 43.5 foot high from the sea bottom, 1 on 3 sea side slop and its cross section shows below in Figure 1-1 (Alonzo, 1971).

Concrete blocks met more favors than rock-mound due to harsh wave conditions. To improve the stability of rock mound breakwater, concrete blocks began to protect the surface of breakwater with a steeper slope, which was 1 on

2. A secondary armor of rocks was laid between breakwater core and concrete blocks, which is usually constructed in where natural rock is insufficient or wave height is large. An example of concrete block on rock mound breakwater is illustrated in Figure 1-2 (Alonzo, 1971) which shows the breakwater at Naval Air Station, Coco Solo in Panama Canal.
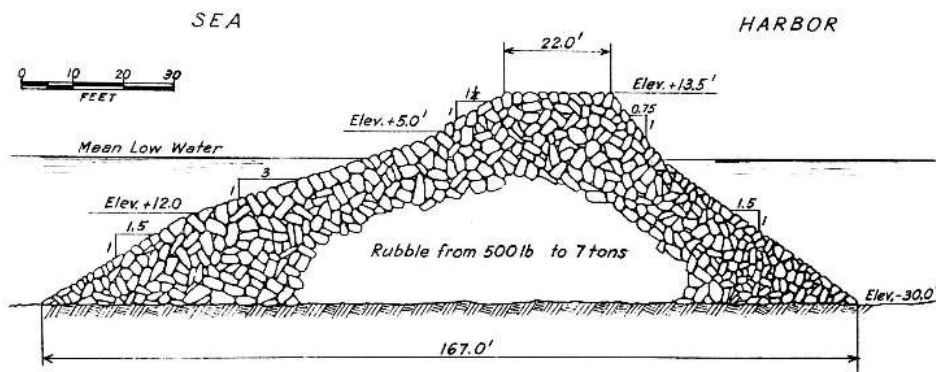
Figure 1-1   First rock-mound breakwater constructed in the U.S.
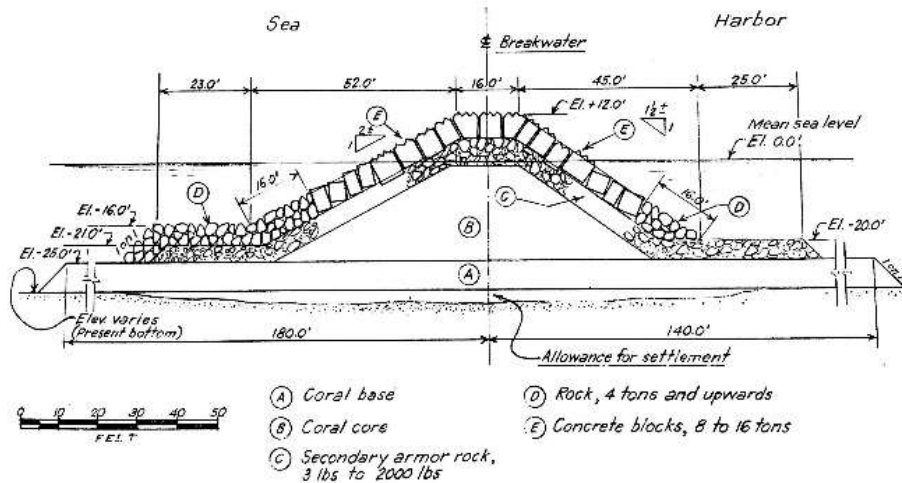
Figure 1-2   Cross section through concrete block armored breakwater.
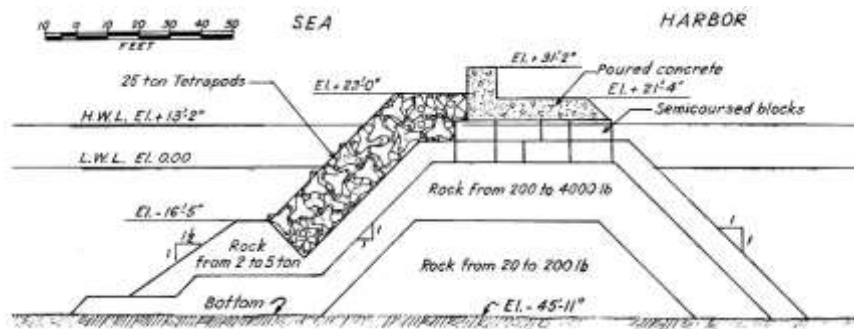
Figure 1-3　Cross section through tetrapod armored breakwater.

The irregular concrete unit armor has the advantage over standard shape concrete blocks in permitting steeper slopes and lighter weight, which improve the stability of concrete block armored breakwater, and varieties of irregular shaped concrete armor units were designed and implemented. In 1955, the main breakwater at Safi was extended with utilizing 25-ton tetrapods on 1 on 1 slope of rock mound breakwater on sea side as shown in Figure 1-3 (Alonzo, 1971).

Breakwater with steeper slope gradually extended dual functions for the sake of navigation and mooring to load and unload cargos. And then developed concrete caissons which reducing construction period with high structural stability and minimal maintenance cost.

The story for conventional breakwaters tells a rough route map of human exploration activities from terrestrial to deeper oceanic field and the evolution of the breakwaters. While with so many challenges facing in offshore which sea water in regions exchange slow, hard coastal structures change dynamical environmental boundary conditions and seascape is hard to accessible that a submerged plate breakwater gives an alternative solution. From this motivation, it was interesting to estimate some new alternative type breakwater concern on both engineering and environmental issues, which is done in the next sub-sections.

1.2 Submerged Inclined-plate Breakwater

Submerged plate structures, permeable structures from sea side to lee side direction which usually comprise of an impermeable plate supported by steal piles are widely proposed as a promising type of breakwaters in offshore zone.

Submerged horizontal-plate structures are believed to have some good features and performance in harsh natural conditions with harmony to surroundings, reasonable construction cost due to free maintenance and its short construction period; practical experiences show that submerged horizontal plates are quite effective in fishing banking and shoreline restoration. In 1990s Nippon Steel Corporation developed a type of breakwater, an H-shaped slit plate jacket type breakwater which was called CALMOS, with the Public Works Research Institute of the Ministry of Construction Company for Kanbara Beach under the jurisdiction of the Japan Ministry of Construction.
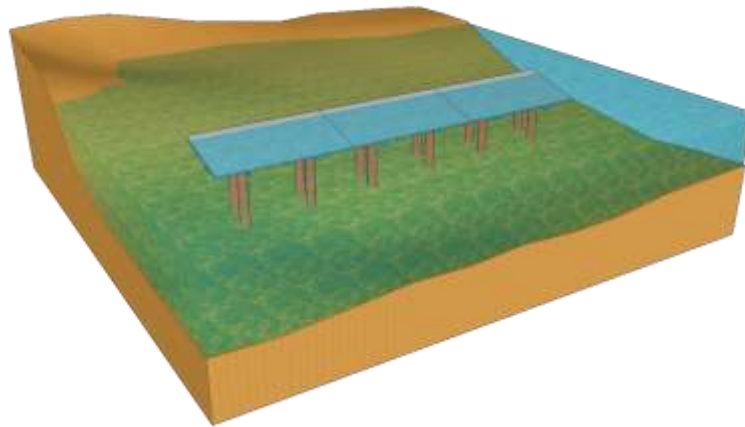
Figure 1-4   Sketch of submerged inclined-plate breakwater in offshore.

Submerged inclined-plate breakwater structure inherits features from horizontal breakwater, and be adopted in many sites to meet the fluctuation of tide variation. Due to the tidal change in realize situation, a fixed to bottom submerged inclined plate breakwater cannot ensure to work just beneath the water surface constantly. While some engineering examples which had completed or being constructed can give some perspective sights to discuss. As introduced before, Nippon Steel Corporation also developed a sloped-plate type breakwater, called the PSR which was built at the west wharf of Nippon Steel's Kimitsu Works. A breakwater constructed at Yobito Fishery Harbor in Hokkaido by using the PSR technique considered environmental condition of fishery habitat conservation, soft ground and tranquility of waterway. Researches (Kimura *et al.*, 1991; Okubo *et al.*, 1994; Aoyama *et al.*, 1997) showed submerged inclined plate breakwater worked with additional functions which are significant on coastal sand beach restoration, harbor and waterway protection and fishery resource recovery bank.

1.3 Literature Review

The first research (Ijima *et al.*, 1970) in Japan studied the transition and reflection coefficients of fixed surface plate and double horizontal plates with impermeable material between plates by integrate series of potential velocity equations on the plate boundaries. This research suggested that the longer plate obstruct or shorter wave fluctuate the more flux energy will dissipate in the model.

It is also worth mentioning one of the following study (Yu, 2002) did not appreciate plate inclination as it is not clear how validity range; the assumed reason is that the submerged ratio is fixed to 0.3, which is not effective for wave control when regard plate as breakwater. He reviewed historical developments of submerged horizontal plate for offshore wave control and proposed his understanding on mechanism which plate divides flow into free surface and pressure flow to different the phase velocity; Wave motion over submerged plate is equivalent to propagating over a bottom seated block.; analytical, numerical and semi-empirical methods had compared; known results of kinds numerical and experimental are summarized in detail; he also gave discussions on some prospective researches.

However, results of physical experiments (Rao *et al.*, 2009; Yagci *et al.*, 2014) reveals conclusions of wave transmission characteristics over a submerged plate breakwater. The plate oriented at an angle is more effective when the ratio of submergence is less; the transmission coefficient of submerged inclined plate varies significantly along the increasing of inclination; the energy dissipation performance of plate is increased with the inclination angle, since it is well known that wave reflection would certainly increase as the inclination angle increases over a certain value; inclined inclination reveals better performance on transmission than horizontal plate.

Kinds of methods are also researched in plate type wave generation. A numerical method was employed (Raichlen and Lee, 1978) for determining the characteristics of waves generated by a hinged inclined-plate wave generator operating in a constant depth channel. A semi-analytical method discussed (Wu, 1988) for the same purpose claims simpler, more flexible than that numerical method, and this method is in good agreement with laboratory data. Wave control, somehow, reverse to wave generation. Methods are also surveyed comprehensively for inclined-plate wave control. A hyper singular-integral equation formulation of the problem is obtained (Midya *et al.*, 2001) by an appropriate use of Green's Integral Theorem followed by utilization of boundary condition on the plate. Researches inherit this framework with similarity. A method of eigenfunction expansion used (Wang and Shen, 1999) and (Meylan and Peter, 2009) for horizontal plate or plate group in two-dimensional velocity potential in mathematical analysis will be introduced and utilized in inclined plate.

Practical engineering development approaches on submerged inclined plate breakwater for offshore wave control always come up the horizontal plate's, as shifting from the horizontal plate to the inclined plate is also regarded as a configuration improvement. To provide an insight into the study of wave control research of a submerged inclined plate, historical developments of both horizontal and inclined plate breakwater are presented in the following sections: horizontal plates and inclined plates respectively in which main configurations and experiments details are included. Literatures are reviewed representatively and listed in Table 1-1.

In previous experimental studies, a comparison (Aoyama *et al.*, 1988) between the 0-degree and 10-degree submerged plate breakwater was conducted and it is found that slope plate decreases the transmission of wave; an upward and downward plate comparison (Murakami *et al.*, 1995) found upward is effective in wave control; a study (Rao *et al.*, 2009) in a wider inclination range from 0-degree to 90-degree with a 15-degree interval found that only 60-degree

Table 1-1　　Representative Configurations of Former Experiments.

Sources	Sketch	Sources	Sketch
Yu, 2002		Yagci *et al.*, 2014	
Neelamani and Rajendran, 2002		Fujita *et al.*, 1992	
Neelamani and Rajendran, 2002		Cho and Kim, 2008	
Aoyama *et al.*, 1988		Shirlal, 2013	
Parsons and Martin, 1995		Sundar *et al.*, 2003	
Rao *et al.*, 2009		Teh and Ismail, 2013	
		Koraim, 2013	

is effective (coefficient of transmission less than 0.6) for entire range of wave when submergence is quite small enough; A recent study (Yagci *et al.*, 2014) shows the increase of inclination gain prominent wave energy dissipation, for instance, 15-degree. This discovery fits with Murakami's experimental figures when the inclination increasing from 0 degree to 10 degree derives higher rate. Base on the previous study, an inclination of 0-degree is necessary and a common discussed 15-degree is recommended to test and contrast the improvement of breakwater. Research on step-type-breakwater (Fujita *et al.*, 1992) in flume experiment revealed good engineering performance: the dissipation well as regular wave even for irregular waves. It can be ensured that transmittance and reflectance are less enough even tide change of 2 meter, comparing single horizontal plate, step-type-breakwater reduced wave force acting on plate.

1.4 Research Purpose

More and more submerged inclined plate breakwaters are loading into offshore to protect nature shoreline and artificial structure. While compared to conventional breakwater depend on its gravity by solid structure, submerged inclined plate breakwater is limited to some extend on wave control performance to serve as a predominant prior option. Therefore, it is necessary to do research which aims to evaluate the wave deformation over the inclined plate breakwater, to discover the dissipation mechanisms and to propose improvement based on inclined plate breakwater.

Methods had developed for revealing the interaction between wave and plate in a numerical way or semi analytical way. While the conventional numerical methods and techniques, such as the finite element method and boundary element method, cost much time and restoration on fluid region or structure discrete when calculating despite the accuracy. In this research, a step-like approximation method based on velocity potential theory was developed to estimate the refection and transmission coefficients which are effected by different submerged plate inclination and relative submergence mainly. A semi analytical solution is obtained by approximation rather than desecrating wave field or objects in water, which is faster than the method of finite element method and boundary element method.

By studying the basic mechanisms of submerged inclined plate breakwater, by using semi-analytical and experiments, additional type of inclined plate schemes is proposed to improve the performance of breakwater by adding serrated blocks and digging gaps with slots on the plate. A two-dimensional wave experiment is conducted to measure their wave height and then calculate the reflection, transmission and wave energy dissipation coefficient.

1.5 Review of Chapters

In this chapter, a general introduction to submerged inclined plate breakwater is made in the terms of breakwater historical evolution. Related researches on submerged horizontal and inclined plate breakwater are reviewed on both methodology and experiments. The initial motivation behind present research is to evaluate the wave deformation over a submerged inclined breakwater, to discover the dissipation mechanisms and to propose improvement based on the inclined plate breakwater.

In chapter 2, an approximation method is developed based on linear velocity potential theory. Before developing the method, the application of eigenfunction matching method to a single submerged horizontal plate is well introduced in detail to make it easier to understand the submerged inclined-plate model. In the application of model, two previews numerical results are compared with corresponding variables which show prefect agreement; in addition, former results from wave flume is also compared.

In chapter 3, several clues obtained from chapter 2 lead requirements to improve the submerged inclined breakwater with lower transmission coefficient and more wave breaking. Plate roughness and plate porosity are researched too with the consideration of inclination and incident wave characters, water depth to wave length ratio, wave steepness and wave height to submergence ratio are studied respectively and comprehensively.

In chapter 4, conclusions are drawn with an outline map, to give a brief story of this research.

The appendix part introduces several methods in numerical calculation with core coding presented.

Chapter 2

Analytical Study

In this chapter, a patching technique named eigenfunction matching method for the semi-analytical solution of wave deformation over the submerged inclined-plate will be employed during approximating the inclined-plate model; as the Galerkin method is assumed to be most effective on accuracy and speed (Yu, 1995), this method has been considered when dealing with the reflection, transmission and the fluid force acting on the plate comparing to the point collocation method or segment collocation method. For the need of minimizing the error along the patching boundaries based on linear potential wave theory, the weighted residual approximation was applied for the minimizing work: velocity potential and its normal derivative on each side of the inner boundaries should be continue; choose the eigenfunction terms in general solution of velocity potential in each fluid region as the weighing function because of their satisfaction to orthogonality condition. By properly choosing weighting function, a set of linear algebraic equation which contains unknown variables will be obtained and leads final solution of these unknown variables.

Before developing the analytical model, the two-dimensional wave and plate problem is defined by boundary value problem and solved based on velocity potential theory and the eigenfunction matching method. The verification of model application shows this model works well with satisfaction on accuracy when tested by experimental results conducted by former researchers.

2.1 Eigenfunction Matching Method

This part introduced the Eigenfunction Matching Method which is utilized to solving two-dimensional wave and signal horizontal-plate problem. The water consists of a region with a free surface from the left to right and a submerged plate through which no flow is possible. The solutions of problem, mainly discussed as reflection and transmission coefficients, were obtained based on the linear velocity potential theory.

2.1.1 Problem Description

At first, we simply it when the waves are normally incident, so that it is a truly two-dimensional case. The sketch and symbols definition of problem showed in Figure 2-1.
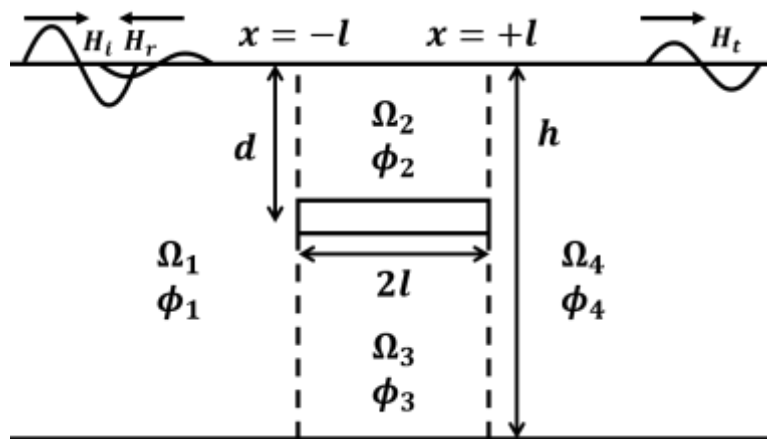
Figure 2-1   Symbol Definition for Horizontal Plate Element in Regions.

2.1.2　Governing Equation and Boundary Condition

A Cartesian coordinate system (x, y, z) is adopted with the z-axis directed vertically upwards and within the plane of undisturbed free surface. For purely two-dimensional wave motion problem, the dependence on y will be omitted at first and, throughout, time is denoted by t.

Conservation of mass requires ϕ satisfies Laplace's equation throughout the fluid,

$$\nabla^2 \phi = \frac{\partial^2 \phi}{\partial x^2} + \frac{\partial^2 \phi}{\partial z^2} = 0 \tag{2.1}$$

where ϕ is velocity potential.

The water depth is constant finite h and the z-direction points vertically upward with the water surface at $z = 0$ and the sea floor at $z = -h$.

$$\frac{\partial^2 \phi}{\partial t^2} + g \frac{\partial \phi}{\partial z} = 0, \qquad \text{on} \quad z = 0 \tag{2.2}$$

$$\frac{\partial \phi}{\partial z} = 0, \qquad \text{on} \quad z = -h \tag{2.3}$$

The fixed plate surface boundary satisfies

$$\frac{\partial \phi}{\partial z} = 0, \qquad \text{on} \quad z = -d \tag{2.4}$$

We must also apply the Somerfield radiation condition as $|x| \to \infty$, this implies the only wave at positive infinity is propagating away and the negative infinity there is a unit incident wave and a wave propagating away.

$$\lim_{|x| \to \infty} \sqrt{|x|} \left(\frac{\partial}{\partial x} - ik \right) \phi(x) = 0 \tag{2.5}$$

2.1.3 General Solution to Boundary Value Problem

Here introduces the conventional method for solving this Dinchlet boundary value problem called separation of variables.

In free surface region, named Ω_1, Ω_2, and Ω_4, the water and plate boundary gives a general solution for velocity potential and relation called linear dispersion relation.

$$\frac{\omega^2}{g} + k_n \tan k_n h = 0 \quad n = 0, 1, 2 \cdots \qquad (2.6)$$

$$\phi(x, z) = \sum_{n=0}^{\infty} (\mathcal{A}_n e^{k_n x} + \mathcal{B}_n e^{-k_n x}) \cos k_n(z + h) \qquad (2.7)$$

where the k_n is roots of dispersion relation equation, it is worth to note that the equation has an infinite sequence of positive real roots and negative roots which will be denoted as $\{\pm k_n; n = 1, 2, 3 \cdots\}$, for convenience we can consider only positive because both positive and negative root lead same general solution for velocity potential, details about calculations are introduced in appendix.

When ω^2/g and h equal to 1, the intersection of $f(k_n) = -\omega^2/g\, k_n$ and $f(k_n) = \tan k_n h$, it can be confirmed that $k_n h \in ((n - 1/2\,\pi), n\pi)$, details about calculations are introduced in appendix A.

In addition to the real roots, there is also a pair of imaginary roots which will similarly be denoted by $\{\pm k_0; k_0 = -ik\}$, where k is the positive root of another type dispersion relation equation.

$$\frac{\omega^2}{g} = k \tanh kh \qquad (2.8)$$

In the region beneath plate, named Ω_3, the water and plate boundary gives a general solution for velocity potential.

- 14 -

$$\phi(x,z) = \sum_{-}^{\infty} \left(\mathcal{G}_n e^{\lambda_n x} + \mathcal{H}_n e^{-\lambda_n x} \right) \cos \lambda_n (z+h) \qquad (2.9)$$

$$\lambda_n = \frac{n\pi}{h-d} \quad n = 0, 1, 2 \cdots \qquad (2.10)$$

To make solution meaningful, the outer region boundary should be defined. It is convenient that we choose $\mathcal{A}_n$, $\mathcal{C}_n$, $\mathcal{E}_n$, $\mathcal{G}_n$, which are complex coefficients corresponding the wave from negative to positive direction.

The Eq. (2.5) shows that in the left region only reflected wave, in the right region only transmitted wave propagate to outer region. Adding incident wave $\mathcal{A}_0 e^{-k_0^h(x+l)}$ form the left region, we obtain the general expressions of the celocity potential, reflected and transmitted coefficients can be calculated as $\mathcal{K}_R$ and $\mathcal{K}_T$.

$$\phi_1(x,z) = -\frac{ig}{\omega} \left[\mathcal{A}_0 e^{-k_0^h(x+l)} Z(k_0^h z) + \sum_{n=0}^{\infty} \mathcal{B}_n e^{k_n^h(x+l)} Z(k_n^h z) \right]$$

$$\phi_2(x,z) = -\frac{ig}{\omega} \left[\sum_{n=0}^{\infty} \left(\mathcal{C}_n e^{-k_n^d(x+l)} + \mathcal{D}_n e^{k_n^d(x-l)} \right) Z(k_n^d z) \right]$$

$$\qquad (2.11)$$

$$\phi_3(x,z) = -\frac{ig}{\omega} \left[\sum_{n=0}^{\infty} \left(\mathcal{E}_n e^{-\lambda_n(x+l)} + \mathcal{F}_n e^{\lambda_n(x-l)} \right) Z(\lambda_n z) \right]$$

$$\phi_4(x,z) = -\frac{ig}{\omega} \left[\sum_{n=0}^{\infty} \mathcal{G}_n e^{-k_n^h(x-l)} Z(k_n^h z) \right]$$

where $Z(kz)$ and $Z(\lambda z)$ are called eigenfunctions or vertical functions.

$$Z(k_n^h z) = \frac{\cos k_n^h(z+h)}{\cos k_n^h h}$$

$$Z(k_n^d z) = \frac{\cos k_n^d(z+d)}{\cos k_n^d h} \qquad (2.12)$$

$$Z(\lambda_n z) = \cos \lambda_n(z+h)$$

where

$$-\frac{\omega^2}{g} = k_n^h \tan k_n^h h = k_n^d \tan k_n^d d$$

$$\lambda_n = \frac{n\pi}{h-d} \qquad n = 0, 1, 2 \cdots$$

(2.13)

and then the coefficients are derived.

$$\mathcal{K}_R = \left|\frac{\mathcal{B}_0}{\mathcal{A}_0}\right|$$

$$\mathcal{K}_T = \left|\frac{\mathcal{G}_0}{\mathcal{A}_0}\right|$$

(2.14)

$$\mathcal{K}_R{}^2 + \mathcal{K}_T{}^2 = 1$$

2.1.4 Semi-analytical Solution to Horizontal Plate Problem

Besides the boundary condition, we should consider matching boundary conditions at each end of plate.

$$\phi_1 = \begin{cases} \phi_2, \\ \phi_3, \end{cases} \quad x = -l;$$

$$\phi_4 = \begin{cases} \phi_2, \\ \phi_3, \end{cases} \quad x = +l;$$

$$\frac{\partial \phi_1}{\partial x} = \begin{cases} \dfrac{\partial \phi_2}{\partial x} & -d < z < 0, \\ \dfrac{\partial \phi_3}{\partial x} & -h < z < -d, \end{cases} \quad x = -l; \qquad (2.15)$$

$$\frac{\partial \phi_4}{\partial x} = \begin{cases} \dfrac{\partial \phi_2}{\partial x} & -d < z < 0, \\ \dfrac{\partial \phi_3}{\partial x} & -h < z < -d, \end{cases} \quad x = +l.$$

By taking the advantage of orthogonality of eigenfunctions (details refer to appendix B), an equation set consisted by four linear equations can be short for below, more details are introduced in appendix. For $-h < z < 0$ and $m = 0, 1, 2, \cdots, N$.

$$-\sum_{n=0}^{N} \mathcal{B}_n \mathcal{X}_n + \sum_{n=0}^{N} \mathcal{S}_n^{\mathcal{CE}} \mathcal{Y}_{nm} + \sum_{n=0}^{N} \mathcal{T}_n^{\mathcal{DF}} e^{-2\kappa_n l} \mathcal{Y}_{nm} = \mathcal{A}_0 \mathcal{X}_0 \delta_{0m}$$

$$-\sum_{n=0}^{N} k_n^h \mathcal{B}_n \mathcal{X}_n - \sum_{n=0}^{N} \kappa_n \mathcal{S}_n^{\mathcal{CE}} \mathcal{Y}_{nm} + \sum_{n=0}^{N} \kappa_n \mathcal{T}_n^{\mathcal{DF}} e^{-2\kappa_n l} \mathcal{Y}_{nm} = -k_0^h \mathcal{A}_0 \mathcal{X}_0 \delta_{0m}$$

$$\sum_{n=0}^{N} \mathcal{S}_n^{\mathcal{CE}} e^{-2\kappa_n l} \mathcal{Y}_{nm} + \sum_{n=0}^{N} \mathcal{T}_n^{\mathcal{DF}} \mathcal{Y}_{nm} - \sum_{n=0}^{N} \mathcal{G}_n \mathcal{X}_n = 0$$

$$-\sum_{n=0}^{N} \kappa_n \mathcal{S}_n^{\mathcal{CE}} e^{-2\kappa_n l} \mathcal{Y}_{nm} + \sum_{n=0}^{N} \kappa_n \mathcal{T}_n^{\mathcal{DF}} \mathcal{Y}_{nm} + \sum_{n=0}^{N} k_n^h \mathcal{G}_n \mathcal{X}_n = 0$$

(2.16)

It is a linear system equation, we can rewrite it into matrix form.

$$\begin{bmatrix} -\mathcal{X}_n & \mathcal{Y}_{nm} & \mathcal{Y}_{nm}e^{-2\kappa_n l} & -\mathcal{X}_n \\ -\mathcal{X}_n k_n^h & -\mathcal{Y}_{nm}\kappa_n & \mathcal{Y}_{nm}\kappa_n e^{-2\kappa_n l} & \mathcal{X}_n k_n^h \\ \square & \mathcal{Y}_{nm}e^{-2\kappa_n l} & \mathcal{Y}_{nm} & \square \\ \square & -\mathcal{Y}_{nm}\kappa_n e^{-2\kappa_n l} & \mathcal{Y}_{nm}\kappa_n & \square \end{bmatrix}_{(4N+4)\times(4N+4)} \begin{bmatrix} \mathcal{B}_n \\ \mathcal{S}_n^{\mathcal{CE}} \\ \mathcal{T}_n^{\mathcal{DF}} \\ \mathcal{G}_n \end{bmatrix}_{(4N+4)\times 1} = \begin{bmatrix} \mathcal{A}_0\mathcal{X}_0\delta_{0m} \\ -k_0^h\mathcal{A}_0\delta_{0m} \\ \square \\ \square \end{bmatrix}_{(4N+4)\times 1} \qquad (2.17)$$

2.2 Model for Submerged Inclined Plate Breakwater

The Eigenfunction Matching Method has been utilized to solve two-dimensional wave and signal horizontal-plate problem. However, a limitation of this method is that the boundary of regions should be rectangular in both horizontal and vertical directions though it is more efficient on either memory cost or accuracy than the Boundary Elements Method and Finite Elements Method that are widely used for plate boundary value problem.

Based on the assumption that the horizontal step plates group is equivalent to an inclined plate which impediments wave and wave induced velocity along the plate length, the gap between method limitation and need mention above can be bridged. The total horizontal length of step equal to the projection of the inclined plate in horizontal axis; the total vertical height of step equal to the projection of the inclined plate in vertical axis. Another idea is also available that we disperse the inclined plate in Figure 2-2 to finite pieces of horizontal step plates as shown in Figure 2-3. The inference that the discrete approximates inclined plate after assumption seems rational when the discrete is fine enough. So, next we can formulate the problem in an analytical way.

2.2.1 Formulation for an Inclined Plate Model

Without loss of generality, a discrete model for inclined plate depicted below in Figure 2-3, which a similar was found in the research on step-type-breakwater by (Fujita *et al.*, 1992) in flume experiment: three horizontal plate elements are submerged in wave fluid with a uniform water depth corresponding to $z = -h$; each of plates are described by denotes separately, j represents the order of plate
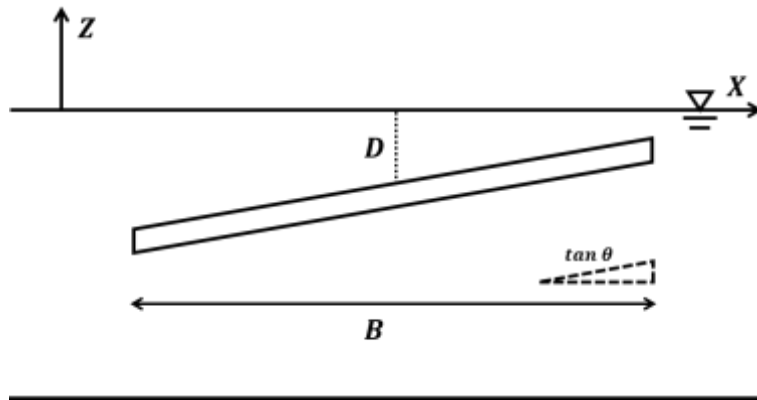
Figure 2-2   Conception Sketch of the Inclined plate.
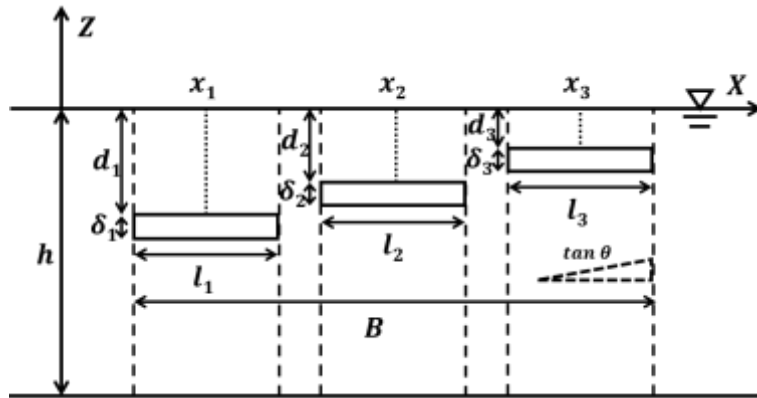
Figure 2-3   Symbol Definition for Dispersed Inclined Plate.
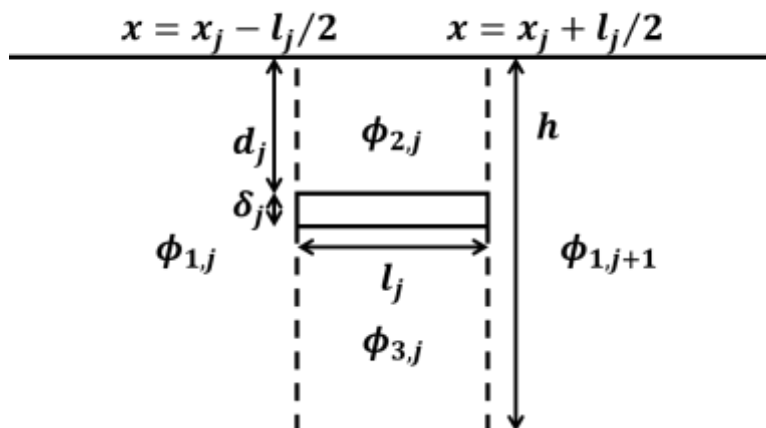
Figure 2-4   Symbol Definition for Horizontal Plate Element in Regions.

element, l_j represents the plate element length, δ_j represents the plate element thickness, d_j represents the plate submergence, x_j represents the middle point coordinate value on horizontal axis, free water surface elevation is at $z = -h$.

An arbitrary plate element which is denoted with j can be analyzed like an independent horizontal plate. The fluid regions around plate element j, $\phi_{1,j}$, $\phi_{2,j}$, $\phi_{3,j}$ and $\phi_{1,j+1}$, are defined in Figure 2-4; region beneath plate element is compressed fluid and the others are free surface water regions; the dash lines on $x_j \pm l_j/2$ are fancied boundaries clinging to both sides of vertical boundaries of plate element.

Discretization of inclined plate is described by Eq. (2.18) to Eq. (2.20),

$$B = \sum_{j=1}^{J} l_j \qquad (2.18)$$

$$D = \frac{1}{J}\sum_{j=1}^{J} d_j \qquad (2.19)$$

$$\tan\theta = \frac{(d_J - d_1)}{B} \qquad (2.20)$$

where, B is the projection length of plate on x axis; D is the middle point submergence of plate; θ is the plate inclination.

Upon assuming the fluid is inviscid and incompressible, the irrotational free surface flow on uniform water depth can be described by

$$\nabla^2\phi = \frac{\partial^2\phi_{i,j}}{\partial x^2} + \frac{\partial^2\phi_{i,j}}{\partial z^2} = 0, \qquad i = 1,2,3 \qquad (2.21)$$

$$\frac{\partial\phi_{i,j}}{\partial z} - \frac{\omega^2}{g}\phi_{i,j} = 0 \quad on \quad z = 0, \qquad i = 1,2 \qquad (2.22)$$

$$\frac{\partial\phi_{i,j}}{\partial z} = 0 \quad on \quad z = -h, \qquad i = 1,3 \qquad (2.23)$$

where, ϕ is the time independent part of the velocity potential corresponding to different fluid regions. Eq. (2.21) is the governing equation, and Eqs. (2.22) and (2.23) are the boundary conditions on free surface and bottom respectively.

The velocity potential will be derived by separation of variable to get the general expression as Eqs. (2.24)

$$\phi_{1,j}(x,z) = -\frac{ig}{\omega}\left[\sum_{n=0}^{\infty}\left(A_{j,n}e^{-k_{0,n}x} + B_{j,n}e^{k_{0,n}x}\right)\mathrm{E}_n\left(k_{0,n}z\right)\right]$$

$$\phi_{2,j}(x,z) = -\frac{ig}{\omega}\left[\sum_{n=0}^{\infty}\left(C_{j,n}e^{-k_{j,n}x} + D_{j,n}e^{k_{j,n}x}\right)\mathrm{Z}_n\left(k_{j,n}z\right)\right]$$

(2.24)

in which, $k_{0,n}$ and $k_{j,n}$ are complex root of dispersion relation in Eqs (2.25)

$$\frac{\omega^2}{g} + k_{0,n}\tan k_{0,n}h = 0 \quad n = 0,1,2\cdots$$

$$\frac{\omega^2}{g} + k_{j,n}\tan k_{j,n}d_j = 0 \quad n = 0,1,2\cdots$$

(2.25)

the complex equations are more efficient to be solved by using a numerical method such as the Newton-Raphson method which is detailed introduced (Linton and McIver, 2001) and appendix which briefly introduced the method of solving the linear dispersion relationship.

While the additional boundaries of region beneath plate element are described in Eqs. (2.26)

$$\frac{\partial\phi_{2,j}}{\partial z} = 0 \quad on \quad z = -d_j, \qquad x_j - l_j/2 < x < x_j + l_j/2$$

$$\frac{\partial\phi_{3,j}}{\partial z} = 0 \quad on \quad z = -d_j + \delta_j, \qquad x_j - l_j/2 < x < x_j + l_j/2$$

$$\frac{\partial\phi_{1,j}}{\partial x} = 0 \quad on \quad x = x_j - l_j/2, \qquad -d_j - \delta_j < z < -d_j$$

$$\frac{\partial\phi_{1,j+1}}{\partial x} = 0 \quad on \quad x = x_j + l_j/2, \qquad -d_j - \delta_j < z < -d_j$$

(2.26)

and the general form of solution of velocity potential is represented below in Eq. (2.27), it is also a form of flow between plate and bottom.

$$\phi_{3,j}(x,z) = -\frac{ig}{\omega}\left[E_{j,0} + F_{j,0}x + \sum_{n=1}^{\infty}\left(E_{j,n}e^{-\lambda_{j,n}x} + F_{j,n}e^{\lambda_{j,n}x}\right)\Lambda_n(\lambda_{j,n}z)\right] \quad (\,2.27\,)$$

in which $\lambda_{j,n}$ is describe in Eq. (2.28).

$$\lambda_{j,n} = -\frac{n\pi}{h - d_j - \delta_j} \quad n = 0, 1, 2 \cdots \quad (\,2.28\,)$$

In general solution of velocity potential listed in Eqs. (2.24) and (2.27), the eigenfunction can be designed as $E_n(k_{0,n}z)$, $Z_n(k_{j,n}z)$ and $\Lambda_n(\lambda_{j,n}z)$ for short, and their formula equations are written as below in Eq. (2.29).

$$E_n(k_{0,n}z) = \frac{\cos k_{0,n}(z+h)}{\cos k_{0,n}h}$$

$$Z_n(k_{j,n}z) = \frac{\cos k_{j,n}(z+d_j)}{\cos k_{j,n}d_j} \quad (\,2.29\,)$$

$$\Lambda_n(\lambda_{j,n}z) = \cos\lambda_{j,n}(z+h)$$

From the general solution of velocity potential, we can obtain the free surface elevation profile based on conventional linear potential wave theory.

$$\eta_{1\ or\ 2,j}(x) = \frac{ig}{\omega}\phi_{1\ or\ 2,j}(x,0) \quad (\,2.30\,)$$

Since the velocity potential, $\Omega_{1,1}$, at $x = -\infty$, and $\Omega_{1,J}$, at $x = +\infty$, is bounded; and it is obvious that the water region in charge of radiation conditions, which means that in the general solution equations, the coefficients satisfy

$$A_{1,0} = 1$$
$$B_{J+1,0} = 0 \quad (\,2.31\,)$$

$$A_{1,1} = A_{1,2} = A_{1,3} = \cdots = A_{1,n} = \cdots = 0$$
$$B_{J+1,1} = B_{J+1,2} = B_{J+1,3} = \cdots = B_{J+1,n} = \cdots = 0 \quad (\,2.32\,)$$

because we can confirm that in the infinite far away, the velocity potential decay in incident and transmission region.

$$\frac{\partial}{\partial x}\left(\phi_{1,j}|_{x=-\infty}\right) = -k_{0,n}e^{-k_{0,n}x} + k_{0,n}B_{1,0}e^{k_{0,n}x} = ik\phi_{1,j}|_{x=-\infty}$$

$$\frac{\partial}{\partial x}\left(\phi_{1,J+1}|_{x=+\infty}\right) = -k_{0,n}A_{J+1,0}e^{-k_{0,n}x} = ik\phi_{1,J+1}|_{x=+\infty}$$

(2.33)

The matching boundary conditions, at $x = x_j - l_j/2$:

$$\phi_{1,j} = \phi_{2,j}, \qquad -d_j < z < 0$$

$$\frac{\partial\phi_{1,j}}{\partial x} = \frac{\partial\phi_{2,j}}{\partial x}, \qquad -d_j < z < 0$$

$$\frac{\partial\phi_{1,j}}{\partial x} = 0, \qquad -d_j - \delta_j < z < -d_j$$

(2.34)

$$\phi_{1,j} = \phi_{3,j}, \qquad -h < z < -d_j - \delta_j$$

$$\frac{\partial\phi_{1,j}}{\partial x} = \frac{\partial\phi_{3,j}}{\partial x}, \qquad -h < z < -d_j - \delta_j$$

and at $x = x_j + l_j/2$:

$$\phi_{1,j+1} = \phi_{2,j}, \qquad -d_j < z < 0$$

$$\frac{\partial\phi_{1,j+1}}{\partial x} = \frac{\partial\phi_{2,j}}{\partial x}, \qquad -d_j < z < 0$$

$$\frac{\partial\phi_{1,j+1}}{\partial x} = 0, \qquad -d_j - \delta_j < z < -d_j$$

(2.35)

$$\phi_{1,j+1} = \phi_{3,j}, \qquad -h < z < -d_j - \delta_j$$

$$\frac{\partial\phi_{1,j+1}}{\partial x} = \frac{\partial\phi_{3,j}}{\partial x}, \qquad -h < z < -d_j - \delta_j$$

Substitute the general solution of velocity potential into Eqs. (2.34) and (2.35), take advantage of orthogonality relation (Lawrie and Abrahams, 1999) in Eqs. (2.36).

$$\int_{-h}^{0} E_{j,n} E_{j,m} \, dz = \frac{1}{2}\left[\frac{sin(2k_{0,n}h)}{2k_{0,n}} - (h)\right] \times \delta_{n,m}$$

$$\int_{-d_j}^{0} Z_{j,n} Z_{j,m} \, dz = \frac{1}{2}\left[\frac{sin(2k_{j,n}d_j)}{2k_{j,n}} - (d_j)\right] \times \delta_{n,m}$$

$$\int_{-h}^{-d_j-\delta_j} \Lambda_{j,n} \Lambda_{j,m} \, dz = \begin{cases} h & m = 0 \\ h/2 & m \neq 0 \end{cases}$$ (2.36)

$$\int_{a}^{b} cos[u(z+h)] \, cos[v(z+d)] \, dz$$

$$= \frac{u[sin\, u(b+h)\, cos\, v(b+d) - sin\, u(a+h)\, cos\, v(a+d)]}{u^2 - v^2}$$

$$- \frac{v[cos\, u(b+h)\, sin\, v(b+d) - cos\, u(a+h)\, sin\, v(a+d)]}{u^2 - v^2}$$

Combining velocity continuity equations into unity and finally do integrals separately from its height range, an equation set can be obtained as below.

$$\left(A_{j,n}X_{j,L}^+ + B_{j,n}X_{j,L}^-\right)\{E_{j,n}:Z_{j,m}\} - \left(C_{j,n}X_{j,L}^+ + D_{j,n}X_{j,L}^-\right)\{Z_{j,n}:Z_{j,m}\} = 0$$

$$\left(A_{j,n}X_{j,L}^+ + B_{j,n}X_{j,L}^-\right)\{E_{j,n}:\Lambda_{j,m}\} - \left(E_{j,n}X_{j,L}^+ + F_{j,n}X_{j,L}^-\right)\{\Lambda_{j,n}:\Lambda_{j,m}\} = 0$$

$$\left(A_{j,n}X_{j,L}^+ + B_{j,n}X_{j,L}^-\right)\{E_{j,n}:E_{j,m}\} - \left(C_{j,n}X_{j,L}^+ + D_{j,n}X_{j,L}^-\right)\{Z_{j,n}:E_{j,m}\}$$
$$- \left(E_{j,n}X_{j,L}^+ + F_{j,n}X_{j,L}^-\right)\{\Lambda_{j,n}:E_{j,m}\} = 0$$

(2.37)

$$\left(A_{j,n}X_{j,L}^+ + B_{j,n}X_{j,L}^-\right)\{E_{j,n}:Z_{j,m}\} - \left(C_{j,n}X_{j,L}^+ + D_{j,n}X_{j,L}^-\right)\{Z_{j,n}:Z_{j,m}\} = 0$$

$$\left(A_{j,n}X_{j,L}^+ + B_{j,n}X_{j,L}^-\right)\{E_{j,n}:\Lambda_{j,m}\} - \left(E_{j,n}X_{j,L}^+ + F_{j,n}X_{j,L}^-\right)\{\Lambda_{j,n}:\Lambda_{j,m}\} = 0$$

$$\left(A_{j,n}X_{j,L}^+ + B_{j,n}X_{j,L}^-\right)\{E_{j,n}:E_{j,m}\} - \left(C_{j,n}X_{j,L}^+ + D_{j,n}X_{j,L}^-\right)\{Z_{j,n}:E_{j,m}\}$$
$$- \left(E_{j,n}X_{j,L}^+ + F_{j,n}X_{j,L}^-\right)\{\Lambda_{j,n}:E_{j,m}\} = 0$$

And some explanations are worth discussed on both symbolic annotations in Eq. (2.38),

$$\{E_{j,n} : Z_{j,m}\} = \int_{-d_j}^{0} E_{j,n} Z_{j,m} \, dz;$$

$$\{Z_{j,n} : Z_{j,m}\} = \int_{-d_j}^{0} Z_{j,n} Z_{j,m} \, dz$$

$$\{E_{j,n} : \Lambda_{j,m}\} = \int_{-h}^{-d_j-\delta_j} E_{j,n} \Lambda_{j,m} \, dz;$$

$$\{\Lambda_{j,n} : \Lambda_{j,m}\} = \int_{-h}^{-d_j-\delta_j} \Lambda_{j,n} \Lambda_{j,m} \, dz \qquad (\,2.38\,)$$

$$\{E_{j,n} : E_{j,m}\} = \int_{-h}^{0} E_{j,n} E_{j,m} \, dz;$$

$$\{Z_{j,m} : E_{j,n}\} = \int_{-d_j}^{0} Z_{j,m} E_{j,n} \, dz;$$

$$\{\Lambda_{j,m} : E_{j,n}\} = \int_{-h}^{-d_j-\delta_j} \Lambda_{j,m} E_{j,n} \, dz$$

and symbol shortage simplify in Eq. (2.37).

$$e^{-k_{0,n}(x_j - l_j/2)} \Longleftrightarrow X_{j,L}^{-k_{0,n}},$$

$$e^{+k_{0,n}(x_j - l_j/2)} \Longleftrightarrow X_{j,L}^{+k_{0,n}};$$

$$e^{-k_{j,n}(x_j - l_j/2)} \Longleftrightarrow X_{j,L}^{-k_{j,n}},$$

$$e^{+k_{j,n}(x_j - l_j/2)} \Longleftrightarrow X_{j,L}^{+k_{j,n}};$$

$$e^{-\lambda_{j,n}(x_j - l_j/2)} \Longleftrightarrow X_{j,L}^{-\lambda_{j,n}},$$

$$e^{+\lambda_{j,n}(x_j - l_j/2)} \Longleftrightarrow X_{j,L}^{+\lambda_{j,n}};$$

$$e^{-k_{0,n}(x_j + l_j/2)} \Longleftrightarrow X_{j,R}^{-k_{0,n}},$$

$$e^{+k_{0,n}(x_j + l_j/2)} \Longleftrightarrow X_{j,R}^{+k_{0,n}};$$

$$e^{-k_{j,n}(x_j + l_j/2)} \Longleftrightarrow X_{j,R}^{-k_{j,n}},$$

$$e^{+k_{j,n}(x_j + l_j/2)} \Longleftrightarrow X_{j,R}^{+k_{j,n}};$$

$$e^{-\lambda_{j,n}(x_j + l_j/2)} \Longleftrightarrow X_{j,R}^{-\lambda_{j,n}},$$

$$e^{+\lambda_{j,n}(x_j + l_j/2)} \Longleftrightarrow X_{j,R}^{+\lambda_{j,n}};$$

(2.39)

The Eqs. (2.37) consist a group of equation set which contain $8(N + 1)$ variables in $8(N + 1)$ linear equations. And considering we have j elements dispersed by inclined plate, so we have $(6J + 2)(N + 1)$ variables in $(6J + 2)(N + 1)$ linear equations, it is more convenient we consider it in a matrix equation form.

2.2.2 Matrix Equations and Its Resolution

For the sake of convenience, we introduce a series of matrix equation for variables, not only for the convenience of analysis, but also for the convenience of computational operation which is attached in appendix C.

The complex root of dispersion relation for free surface water regions and meaningless wave number for compressed flow,

$$\{k_{0,n}\} \equiv \{-ik_0, k_{0,1}, k_{0,2}, k_{0,3}, \dots, k_{0,n}, \dots\}$$

$$\{k_{j,n}\} \equiv \{-ik_j, k_{j,1}, k_{j,2}, k_{j,3}, \dots, k_{j,n}, \dots\} \quad\quad (\,2.40\,)$$

$$\{\lambda_{j,n}\} \equiv \{0, \lambda_{j,1}, \lambda_{j,2}, \lambda_{j,3}, \dots, \lambda_{j,n}, \dots\}$$

and eigenfunctions are speared in matrix form in Eq. (2.41).

$$\{E_n(k_{0,n}z)\} \equiv \left\{\frac{\cos k_{0,0}(z+h)}{\cos k_{0,0}h}, \frac{\cos k_{0,1}(z+h)}{\cos k_{0,1}h}, \dots, \frac{\cos k_{0,n}(z+h)}{\cos k_{0,n}h}, \dots\right\}$$

$$\{Z_n(k_{j,n}z)\} \equiv \left\{\frac{\cos k_{j,0}(z+d_j)}{\cos k_{j,0}d_j}, \frac{\cos k_{j1}(z+d_j)}{\cos k_{j,1}d_j}, \dots, \frac{\cos k_{j,n}(z+d_j)}{\cos k_{j,n}d_j}, \dots\right\} \quad (\,2.41\,)$$

$$\{\Lambda_n(\lambda_{j,n}z)\} \equiv \{1, \cos \lambda_{j,1}(z+h), \dots, \cos \lambda_{j,n}(z+h), \dots\}$$

The final equation for one horizontal-plate element is obtained that,

$$[M_j]_{8(N+1)\times 8(N+1)} \cdot [A_j, B_j, C_j, D_j, E_j, F_j, A_{j+1}, B_{j+1}]^T_{8(N+1)\times 1} = [R]_{8(N+1)\times 1} \quad (\,2.42\,)$$

where, the coefficient matrix of j elements is present below in Eq. (2.43).

$$[M_j]_{6(N+1)\times 8(N+1)} =$$

$$
\begin{bmatrix}
X_{j,L}^+\{E_{j,n}:Z_{j,m}\} & X_{j,L}^-\{E_{j,n}:Z_{j,m}\} & -X_{j,L}^+\{Z_{j,n}:Z_{j,m}\} & -X_{j,L}^-\{Z_{j,n}:Z_{j,m}\} & \square & \square & \square & \square \\[4pt]
X_{j,L}^+\{E_{j,n}:E_{j,m}\} & X_{j,L}^-\{E_{j,n}:E_{j,m}\} & -X_{j,L}^+\{Z_{j,n}:E_{j,m}\} & -X_{j,L}^-\{Z_{j,n}:E_{j,m}\} & -X_{j,L}^+\{\Lambda_{j,n}:\Lambda_{j,m}\} & -X_{j,L}^-\{\Lambda_{j,n}:\Lambda_{j,m}\} & \square & \square \\[4pt]
X_{j,L}^+\{E_{j,n}:\Lambda_{j,m}\} & X_{j,L}^-\{E_{j,n}:\Lambda_{j,m}\} & \square & \square & -X_{j,L}^+\{\Lambda_{j,n}:E_{j,m}\} & -X_{j,L}^-\{\Lambda_{j,n}:E_{j,m}\} & \square & \square \\[4pt]
\square & \square & -X_{j,R}^+\{Z_{j,n}:Z_{j,m}\} & -X_{j,R}^-\{Z_{j,n}:Z_{j,m}\} & \square & \square & X_{j,R}^+\{E_{j,n}:Z_{j,m}\} & X_{j,R}^-\{E_{j,n}:Z_{j,m}\} \\[4pt]
\square & \square & -X_{j,R}^+\{Z_{j,n}:E_{j,m}\} & -X_{j,R}^-\{Z_{j,n}:E_{j,m}\} & -X_{j,R}^+\{\Lambda_{j,n}:\Lambda_{j,m}\} & -X_{j,R}^-\{\Lambda_{j,n}:\Lambda_{j,m}\} & X_{j,R}^+\{E_{j,n}:\Lambda_{j,m}\} & X_{j,R}^-\{E_{j,n}:\Lambda_{j,m}\} \\[4pt]
\square & \square & \square & \square & -X_{j,R}^+\{\Lambda_{j,n}:E_{j,m}\} & -X_{j,R}^-\{\Lambda_{j,n}:E_{j,m}\} & X_{j,R}^+\{E_{j,n}:E_{j,m}\} & X_{j,R}^-\{E_{j,n}:E_{j,m}\}
\end{bmatrix}
$$

$$(2.43)$$

The influence of the selected horizontal plate elements and the other horizontal plate elements is mutual: the transmitted waves of the first sea side horizontal plate will propagate into the second horizontal plate element area as the incident wave; the reflected wave of the second horizontal plate element region will reflected waves into the first horizontal plate element area in the equivalent way. In terms of the velocity potential, generally is, the mutual effect onto coefficient: as shown in Figure 2-5, the incident wave height coefficient $A_{1,n}$ ($n = 0,1,2,3 \dots$) is affected by the first horizontal plate element, and this influence will propagate over the first plate element by the help of coefficient $C_{1,n}$ ($n = 0,1,2,3 \dots$), then the transmission of the coefficient, $A_{2,n}$ ($n = 0,1,2,3 \dots$), will propagate into the second horizontal plate element region, the transmitted wave height coefficient $A_{J+1,n}$ ($n = 0,1,2,3 \dots$) will inherit the final effect, the reflect effect is also *vice versa*.

If the gap between the horizontal plate element is gradually reduced, the transfer effect of wave height coefficient will be more continuous connection; with the gradually fine discrete distance, the effect of wave height coefficient transmission will be closer to the real inclined plate wave deformation. This interaction is mirrored in the calculation of all the horizontal plate elements at the same time, that is: the horizontal plate elements cannot be separated or calculated one by one. For the above reasons, the matrix assembly is intuitively shown in Figure 2-6.

For the model, the coefficient matrix is consisted of two parts: the coefficient matrix of each horizontal element, the radiation boundary conditions of the transmitted wave and the initial incident wave condition. Figure 2-6 shows an inclined plate model which is consisted of or, in another word, discrete $J = 3$ horizontal plate elements, the mode of evanescent wave is $N = 1$.

Matrix of the three horizontal plate element denote by M_j ($j = 1,2,3$) is arranged downwardly from the top, and final rows is the matrix for radiation boundary condition; the dimension of horizontal plate element matrix M_j is

$6(N+1) \times (6J+2)(N+1)$, the dimension of radiation boundary condition matrix $M_{Boundary}$ is $2(N+1) \times (6J+2)(N+1)$, as shown in Figure 2-6, total dimension is $(6J+2)(N+1) \times (6J+2)(N+1)$.

The matrix is Eq. (2.44).

$$[M]_{(6J+2)(N+1)\times(6J+2)(N+1)} \cdot [X]_{(6J+2)(N+1)\times1} = [R]_{(6J+2)(N+1)\times1} \quad (2.44)$$

After the linear set of algebraic equations solved uniquely, the $\mathcal{K}_R$ and $\mathcal{K}_T$ can be calculated form reflection and transmission coefficient in general solution of velocity potential.

$$\mathcal{K}_R = \left| \frac{B_{1,0}}{A_{1,0}} \right|$$

$$\mathcal{K}_T = \left| \frac{A_{J+1,0}}{A_{1,0}} \right| \quad (2.45)$$

The transmission coefficients and the reflection coefficients were calculated from Eq. (2.45) and this solution follows energy conservation equation.

$$\mathcal{K}_R{}^2 + \mathcal{K}_T{}^2 = 1 \quad (2.46)$$
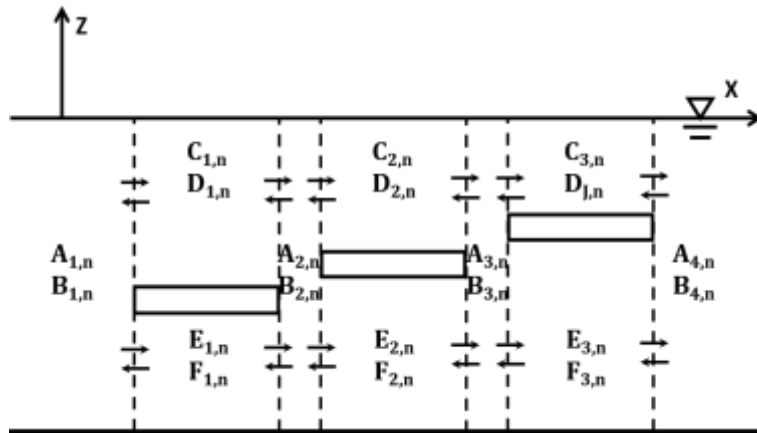
Figure 2-5   Transmission Effect over Plates Elements (n = 0, 1, 2 … N).
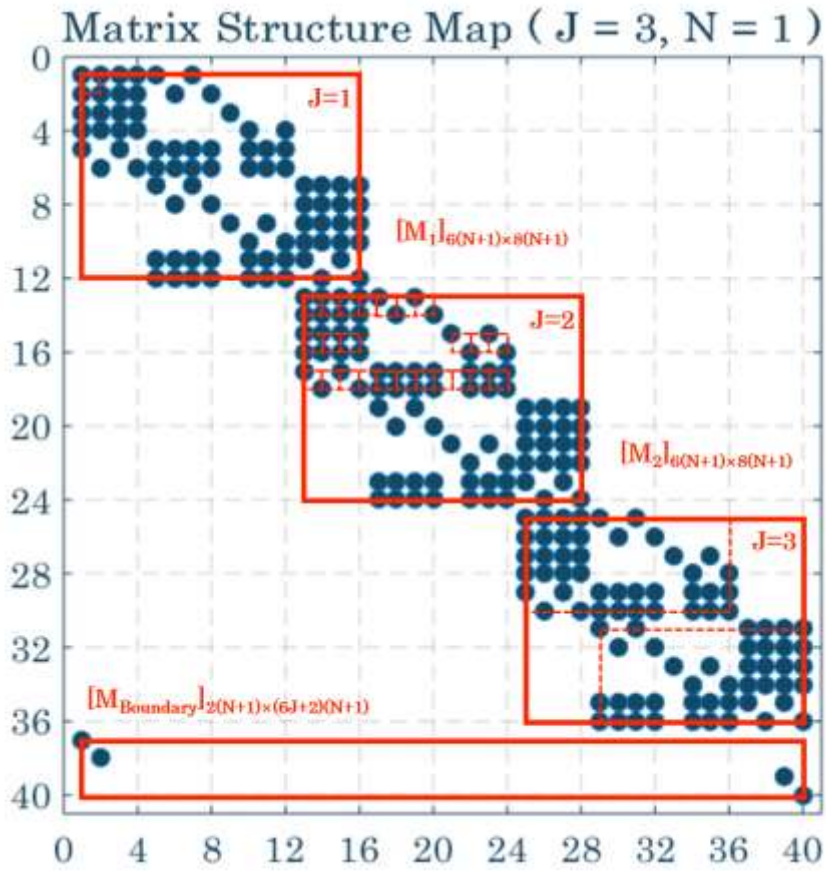
Figure 2-6   Diagram of Matrix Structure (J=3，N=1).

2.3 Applications of Analytical Model

The computed results by model are compared and verified with both numerical and experimental results of preview researchers consequently. A test shows the difference when J, the number of horizontal elements, is increase from 10 to 25 gradually. As the model is developed for submerged inclined-plate based on the linear potential theory with considering the evanescent wave mode, the horizontal-plate element number J is of importance. Gap between each line when increasing J is smaller which indicates J = 25 is satisfactory.
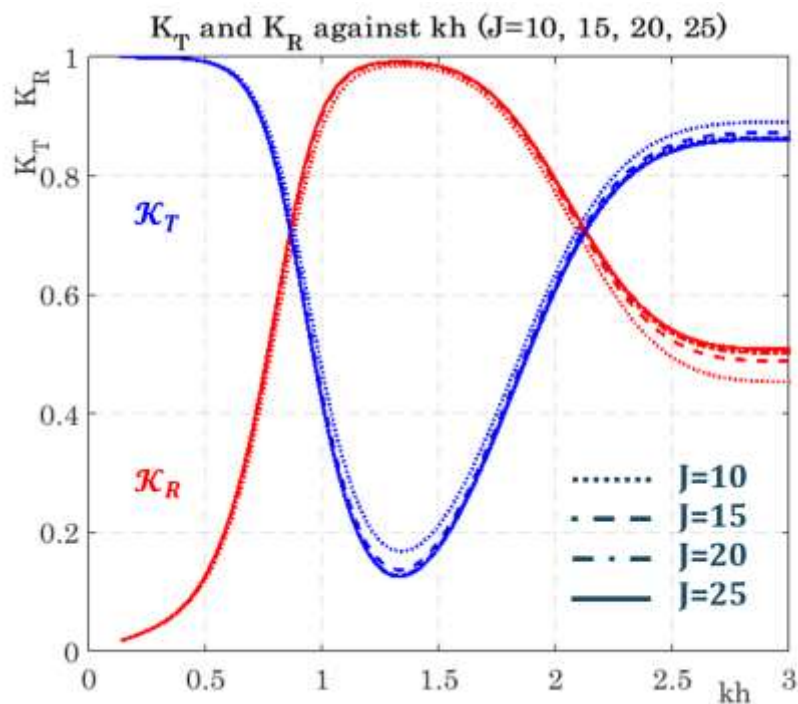
Figure 2-7 $\mathcal{K}_R$ and $\mathcal{K}_T$ against kh (N=20, θ=15°).

It is known that a reasonable value of evanescent wave mode number N is negligible and should satisfy a certain condition for a certain accuracy. And preview study and comparison show N = 20 is a quite satisfactory computational condition.

2.3.1 Verification by Previews Numerical Study

The primary computed results are verified by compared to preview numerical researches which show agreement quite closely with the numerical method of Liu (Liu *et al.*, 2011) and Yu (Yu, 1990) as seen in Figure 2-8 and Figure 2-9.

A boundary element method was used to analyze the submerged inclined plate breakwater, and discussed the influence of the inclination on the reflection coefficient and the transmission coefficient in his research. Figure 2-8 shows the results of present research (finite depth of 30.0 meters, the average water depth of 2.0 meters, plate thickness of 3.0 meters, plate length of 30.0 meters; the horizontal plate number is J = 25, the evanescent wave mode number is N = 20 and the inclination of submerged plate is 15 degree.) and Liu's inclination plate breakwater model based on potential wave theory (plate thickness a = 0.1h, average water depth s = 0.15h, plate length and water depth ratio B / h = 1.0); the results are obvious which curves and dots fit to each other to almost same.

Figure 2-9 shows the results of present calculation (excluding plate thickness; the horizontal plate number is J = 1, the evanescent wave mode number is N = 20 and the inclination of submerged plate is 0 degree.) and results from former research which is based on potential wave theory. The results are almost identical. The same conditions are: depth ratio h / L = 0.5, relative submerged ratio d / h = 0.3. In Figure 2-9, the x axis is the ratio of horizontal plate length to wavelength; due to the depth and wavelength of the fixed, with the increase on x axis, which means of the horizontal plate is gradually increased gradually by the physical meaning: when the wavelength is about 3 to 4 times of horizontal plate length, the reflection coefficient in a higher range, indicates that the plate breakwater can effectively obstruct the waves.
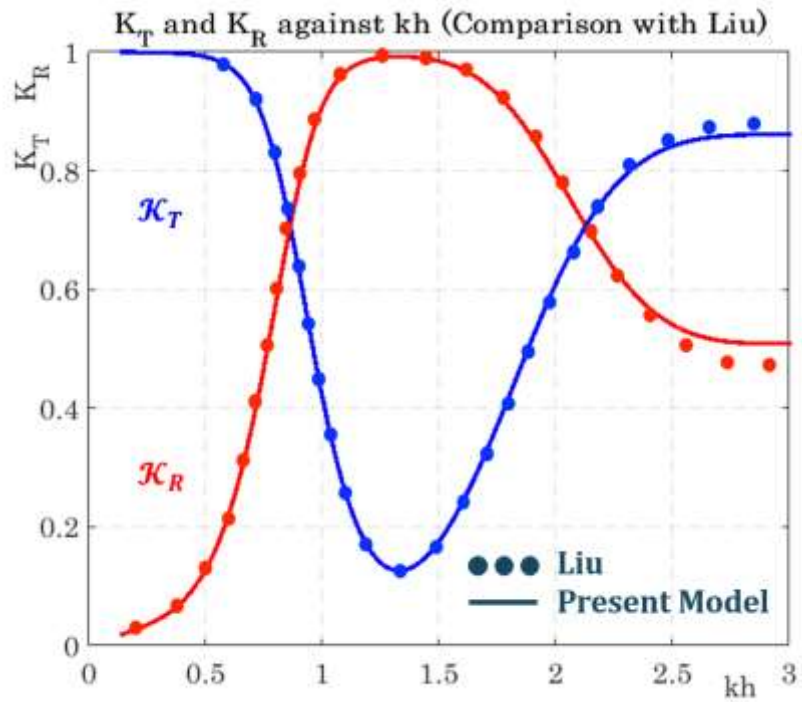
Figure 2-8 $\mathcal{K}_R$ and $\mathcal{K}_T$ against Relative Water Depth (case Liu).
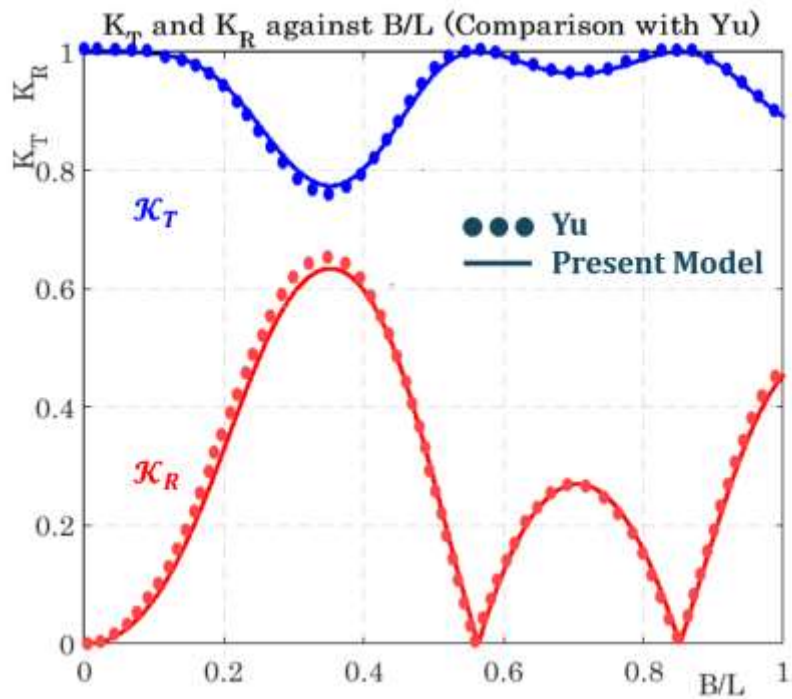
Figure 2-9 $\mathcal{K}_R$ and $\mathcal{K}_T$ against Relative Plate Length (case Yu).

2.3.2 Comparison with Previews Experimental Study

Comparison between the analytical model results and experimental results (Aoyama *et al.*, 1988) indicates that shallow submergence wave breaking is a significant factor for water wave control (Figure 2-10 and Figure 2-11): the disparity between computed curves and measured stars is smaller when the plate submergence is deeper (Case A). It is the reason that shallow submerged plate plays a critical role on wave breaking. It is found from that wave steepness is another principal factor for wave control: red circles, corresponding to lower wave steepness, are close to curve, while blue circles are not (Case B) which gives a brief conclusion that analytical model based velocity potential theory can well describe the wave deformation to a certain content without considering wave breaking.

Table 2-1　　Conditions for Comparison (case Aoyama).

Case	h/L	D/h	θ
A	0.15	0.40	10°
B	0.30	0.20	10°

In addition, these results show the inclined plate breakwater should be quite long (usually 0.25 times wave length, general 20~30 meters long) if this breakwater works effective. So, it is worth trying to improve the submerged inclined plate as a breakwater, and test the validity of breakwater wave controlling performance based on the mechanism which derived from comparison. This become the secondary purpose of research.
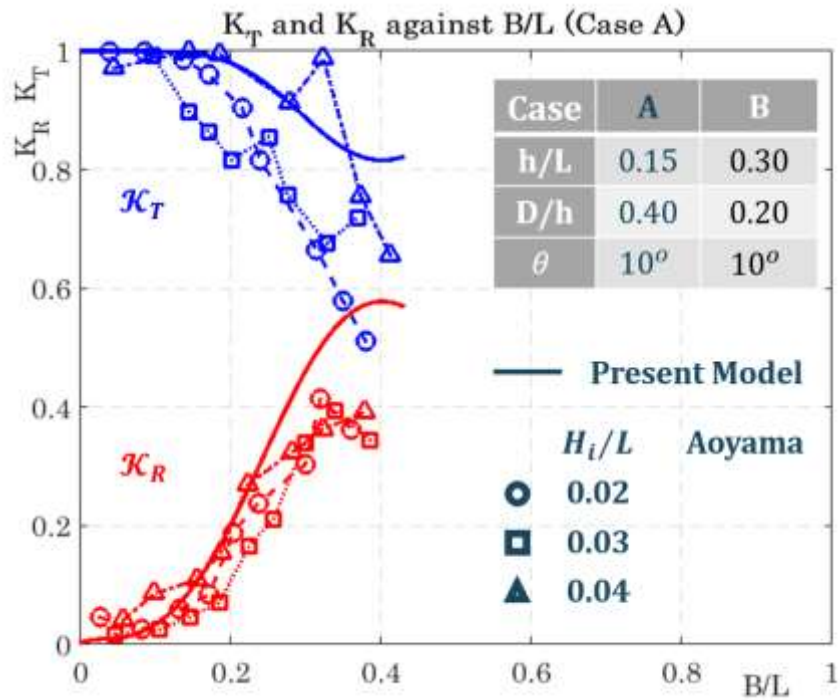
Figure 2-10 Results Comparison of Submerged Inclined Plate (case A).
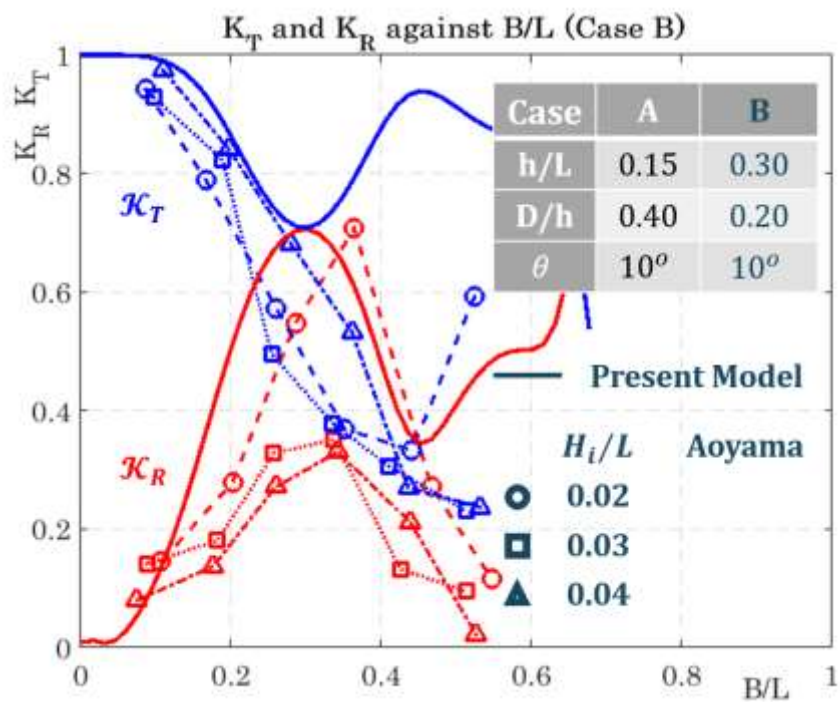
Figure 2-11 Results Comparison of Submerged Inclined Plate (case B).

2.3.3 Study on Several Variables

As relative plate length and plate thickness are researched which also showed influence on wave deformation, the interest of variable study focuses on the plate inclination of submerged plate and relative submergence. The conditions for computational study are listed as below.

Table 2-2　　Conditions for Computational Study.

Case	D/h	δ/h	B/h	θ
IN	0.15	0.10	1.00	--
SU	--	0.10	1.00	$15°$

Figure 2-12 and Figure 2-13 show the effect of the plate inclination and relative plate submergence on the wave-control performance of the submerged inclined plate breakwater (the horizontal plate number is J = 25, the evanescent wave mode number is N = 20.). The curves in Figure 2-12 shows the variation of transmission coeeficient with respect to relative plate length B/L for different plate inclination, respectively. The transmission coefficient of the submerged inclined plate breakwater decreases with the increase of the submerged plate inclination, and the increasing and decreasing trend are similar in the variation of inclination. From the curves' change tendency, the optimal relative plate length for lowest transmission is about 0.15 to 0.30. The curves in Figure 2-12 shows the variation of transmission coefficient with respect to relative plate length B/L for different submergence. The transmission coefficient decreases with the increase of the submergence. The smaller the plate submergence is, the better the barrier effect is, the best effect is less than 0.20 on relative plate length.
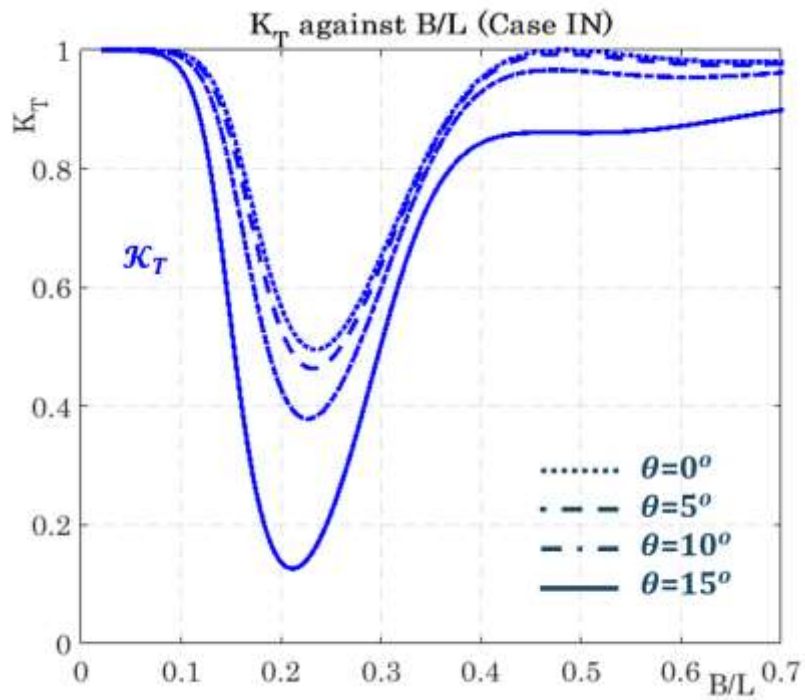
Figure 2-12 Variation of $\mathcal{K}_T$ with Respect to B/L for θ (case IN).
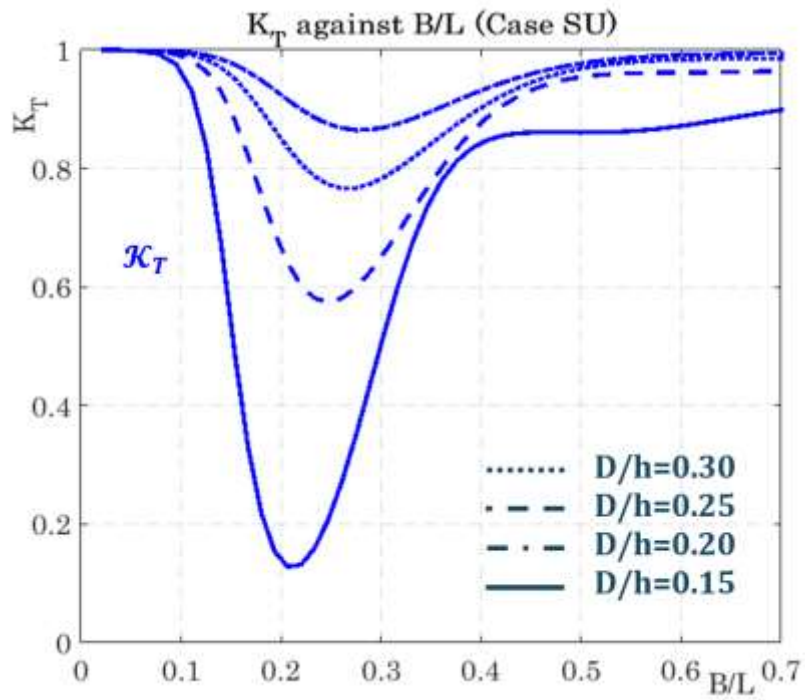
Figure 2-13 Variation of $\mathcal{K}_T$ with Respect to B/L for D/h (case SU).

Chapter 3
Experimental Study

Comparisons between computed and experimental results above inclined plate in last chapter indicate that wave breaking and wave steepness over plate are significant components to water wave controlling. Computed results based on velocity potential theory is almost identical to measured results from wave flume experiments when plate submergence is relative deep and wave steepness is relative low which lead wave propagation over plate in flume is more alike to velocity potential theory. By studying the plate inclination of submerged plate and relative submergence, the transmission coefficient of the submerged inclined plate breakwater decreases with the increase in the submerged plate inclination, and decreases with the increase in the plate submergence which demonstrate that the inclination and submergence are interesting to further study by experiment.

The model experiment described in this chapter was carried out in the wave flume of hydraulic experimental laboratory in Tokyo University of Marine and Science Technology. Two proposals are set for the model experiment, the first proposal is to verify computational results by developed approximation model; the second proposal is to test improved submerged inclined breakwater on their performance of wave deformation, wave transmission and wave reflection. The results are shown in Figure 3-18 to 3-63 in the latter sections.

3.1　Background and Physical Model

In addition to verify computational results, the improvement of submerged inclined plate controlling performance has become to a new mission which aims to enhance the capacity of wave energy dissipation caused by stronger wave breaking.

3.1.1　Background

Rough (serrated) plate breakwater is a less researched topic, the wave transmission of submerged inclined rough plate as a breakwater (Shirlal, 2013) was studied and the research gave innovative idea to improvement. Rectangular and square shapes of roughness is mounted onto inclined plate with zigzag and parallel configurations and experimental comparison shows the zigzag configuration and square shape is more effective in reducing wave transmission.

In terms of fluid mechanics, flow around a submerged object is depended by object shape and fluid Reynolds number. A recumbent short cylinder and a cube has high drag coefficient in fluids with Reynolds number approximately 10^4, while, a recumbent short cylinder is difficult to mount lying or machining on the plate surface; a cube is, in a consequence, appropriate for serrated shape. In this study, the regulation of dimension and distribution of cube is not the proposal, for the sake of convenient, a similar arrangement in scale could refer to Shirlal's case, details see Figure 3-1-b, the side length of cube is $a = 0.4\, cm$, and the interspace is $b = 0.5\, cm$.

Perforated plate breakwater is more researched as a popular topic, a wave absorbing system using inclined perforated plates was studied (Cho and Kim, 2008), research selected the optimal porosity parameter $P = 0.1$ for the

absorption system. It is also difficulty to clarify the different among perforated type which made holes on plate, slitted type which made bar shape space along vertical direction and slotted plate in same porosity parameter without a test. While in this study, the aim is to improve the plate's wave deformation performance. For the sake of convenient, a slotted plate scheme shown in Figure 3-2 is chosen with different porosity rate which the area rate of space to plate ranging from 0 to 0.3.

a   Cylinder Shape Serrated Plate

b   Cube Shape Serrated Plate
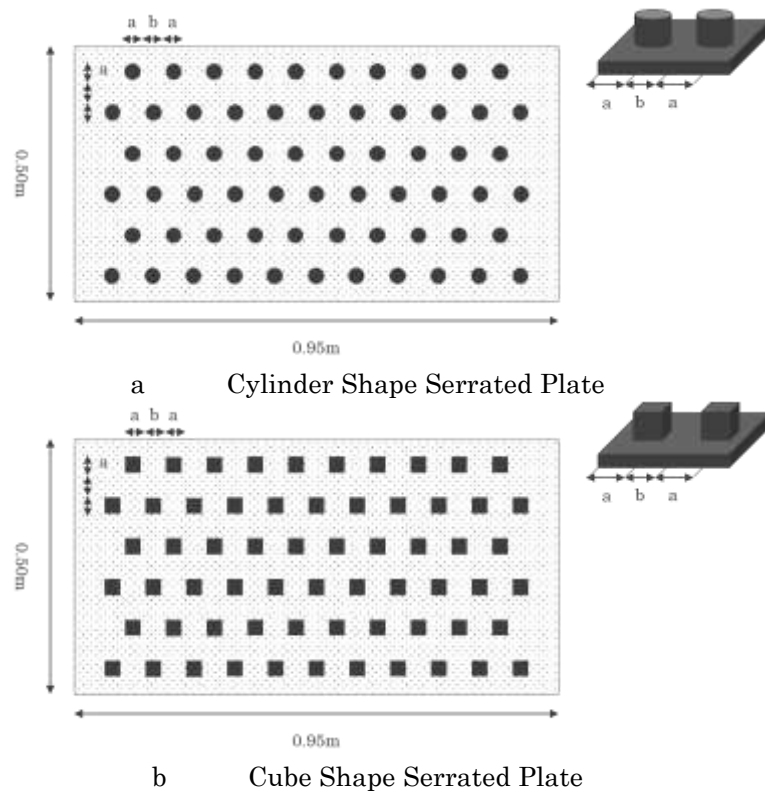
Figure 3-1   Candidate for improvement of breakwater (Roughness).
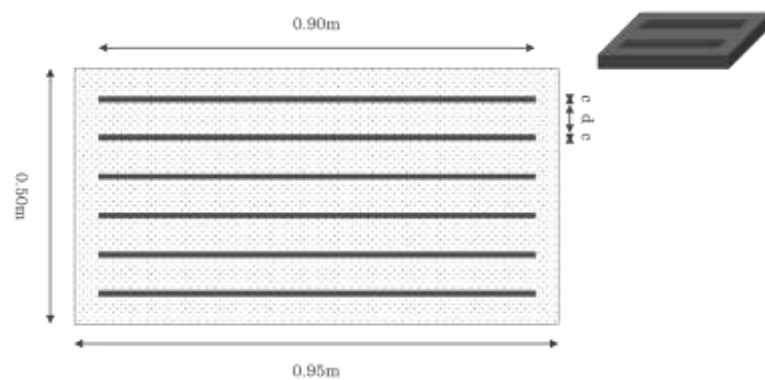
Figure 3-2   Candidate for Improvement of Breakwater (Porosity).

3.1.2 Physical Model

Therefore, a combination improvement scheme is proposed as shown in Figure 3-3 and Figure 3-4. This scheme can be categorized into smooth plate, plate with slots and plate with roughness, each feature can be regarded as a factor to influence the wave deformation over the plate and tested respectively as shown in Table 3-1. Considering the real scale in next wave experiment in flume, the dimension is set to 0.95m × 0.50m. Serrated blocks are arranged in row on the surface of plate, the side length of cube is $a = 0.4\ cm$, and the inter space is $b = 0.5\ cm$. The slotted rate of plate change from 0 to 30 percentage with 10 percentage intervals.
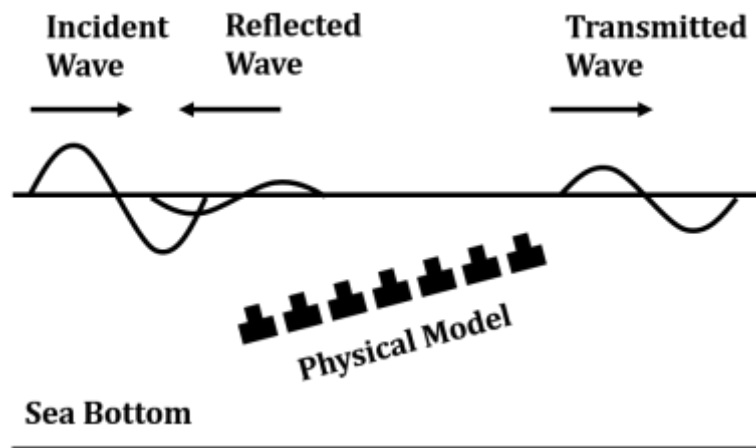
Figure 3-3   Solution Scheme in Front View.
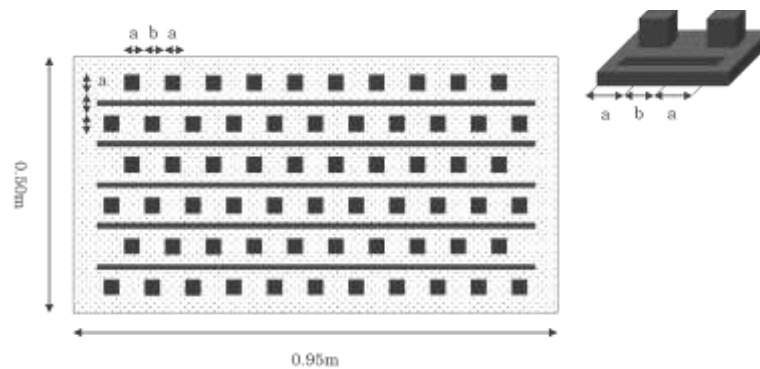
Figure 3-4   Solution Scheme in Vertical View.

Table 3-1   Conditions for Experiment of Plate Arrangement.

Case		Inclination	Roughness	Porosity	Fig.
IN	1*	30°			
	2	15°	×	0.0	
	3	0°			
PO	4			0.0	
	5	15°	√	0.1	
	6			0.2	
	7			0.3	
RO	8	15°	×	0.1	

√: plate with roughness.

×: plate without roughness.

*: slightly water surface piercing.

3.2 Equipment and Physical Model Preparation

3.2.1 Wave Flume and Wave Generator

The wave flume, see Figure 3-5 below, is 29.0 meters long by 1.0-meter-wide; it consists of two 1.5 meters high glass walls on both sides which allow visual observation of experimental phenomenon and equips with a piston-type wave maker at one end and wave energy absorber at the other end. The x-axis is taken positive to the wave energy absorber ward direction with $x = 0$ at the original of the wave paddle. The stainless steel made wave paddle is controlled by a AC servomotor which its output capacity is 3.3 kw with 2000 revolutions per minute (rpm) and the paddle vibrates back and forth along a linear rail. A KENEK Co., Ltd. made CHT4-100BNC 2-line capacitance type wave gauge for detecting wave height is mounted on the wave paddle, it is for controlling the feedback signal when the paddle is making wave with a consideration to absorb the reflected wave (Kawaguchi, 1986), the wave generator is controlled by digital signals from MATLAB software, those signals are then converted to analog format by an ADC, detail can be found in Figure 3-6. The wave energy absorber is fixed by a trapezium shape frame and screw bolts and made of high porous material (ヘチマロン, in Japanese), a polypropylene material molded fibrous net shape plastic block, which permit continuous wave energy dissipation.

After two modifications which show in Figure 3-7, the reflection from wave energy absorber can be controlled by a relative low ratio to incident wave in front of the wave energy absorber. As illustrated, an about 55-centimeter vertical step stands in front of the original absorber which leads significant wave reflection when wave comes; the first-time modification built an arc in front of absorber whose back just connect to original slope part of absorber where the transition corner also reflect wave obviously; the second-time modification extended absorber block to a mild slop with a 1:2 gradient to flume bottom which leads a good regulation to wave reflection ratio shows in Figure 3-8.
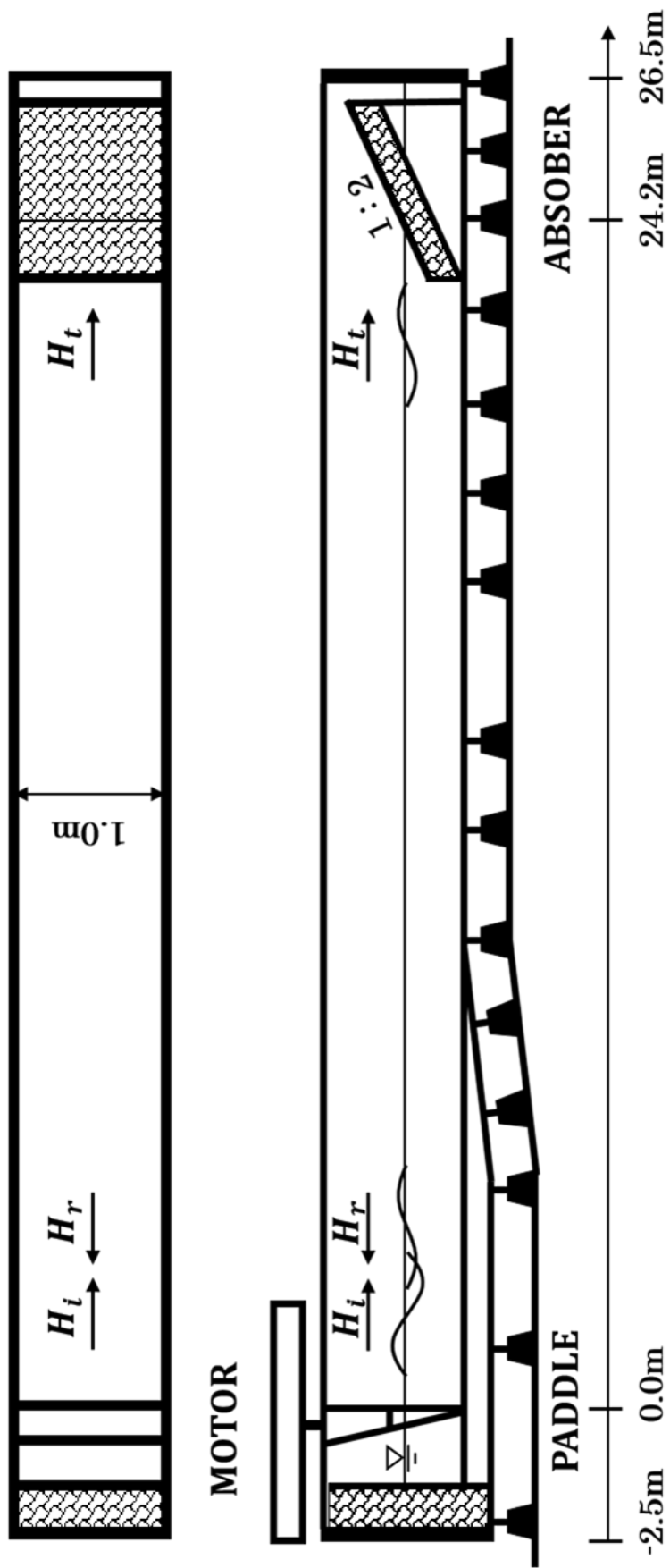
Figure 3-5　Sketch of the 2-dimensional Wave Flume.
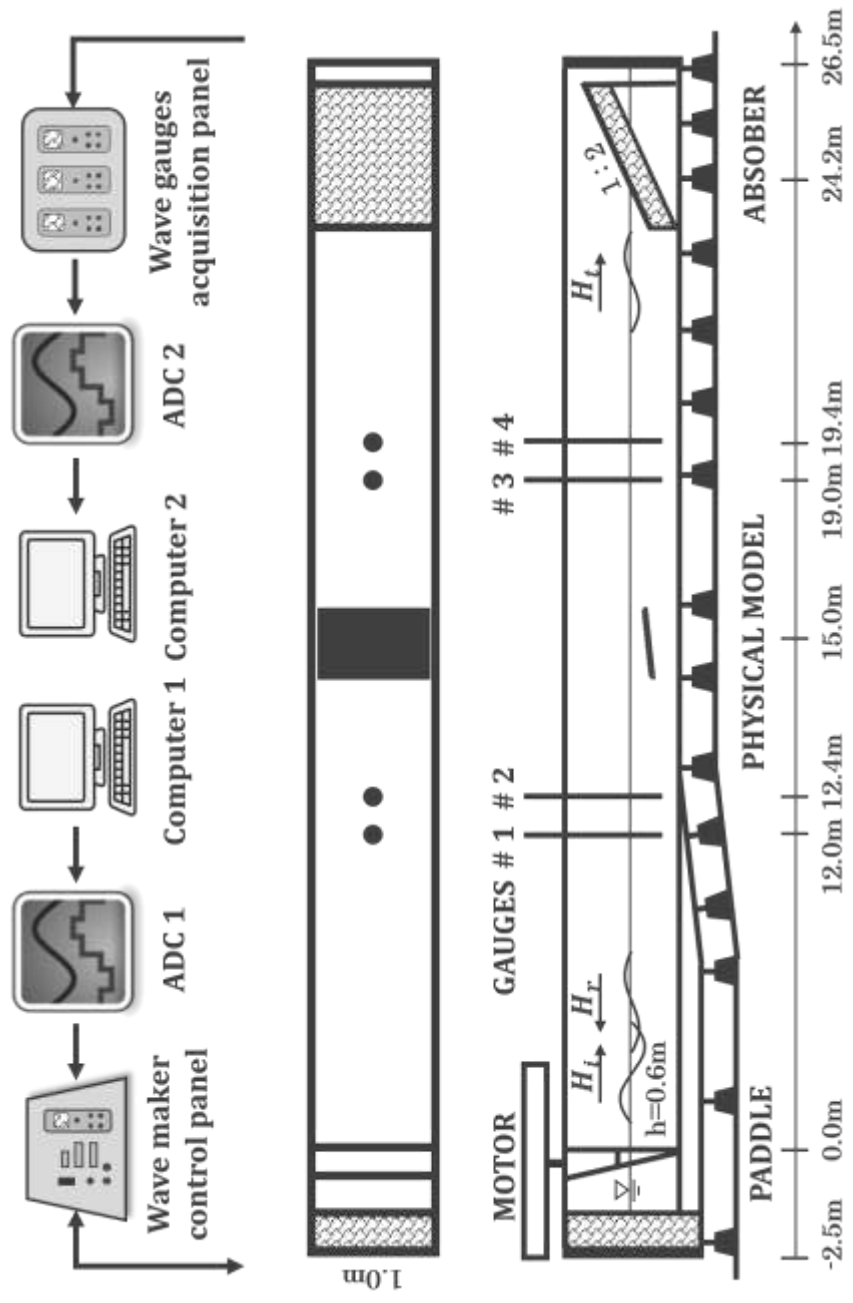
Figure 3-6　Equipment Setup of Controlling and Collection.
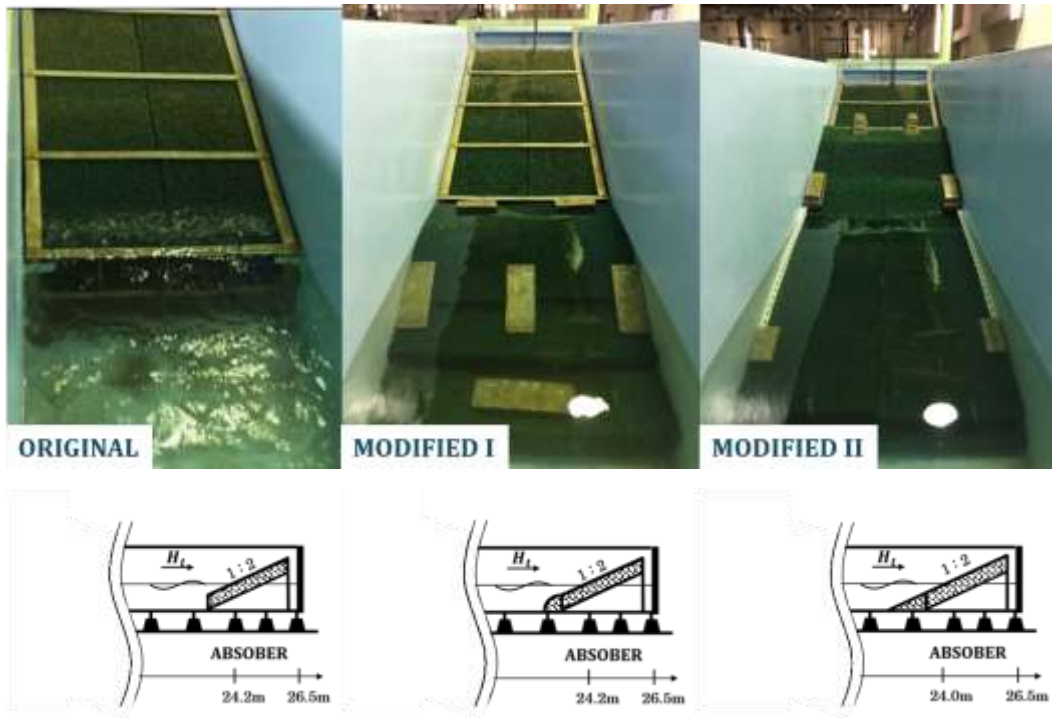
Figure 3-7　　2 Times Wave Absorber Modification for Low Reflection.
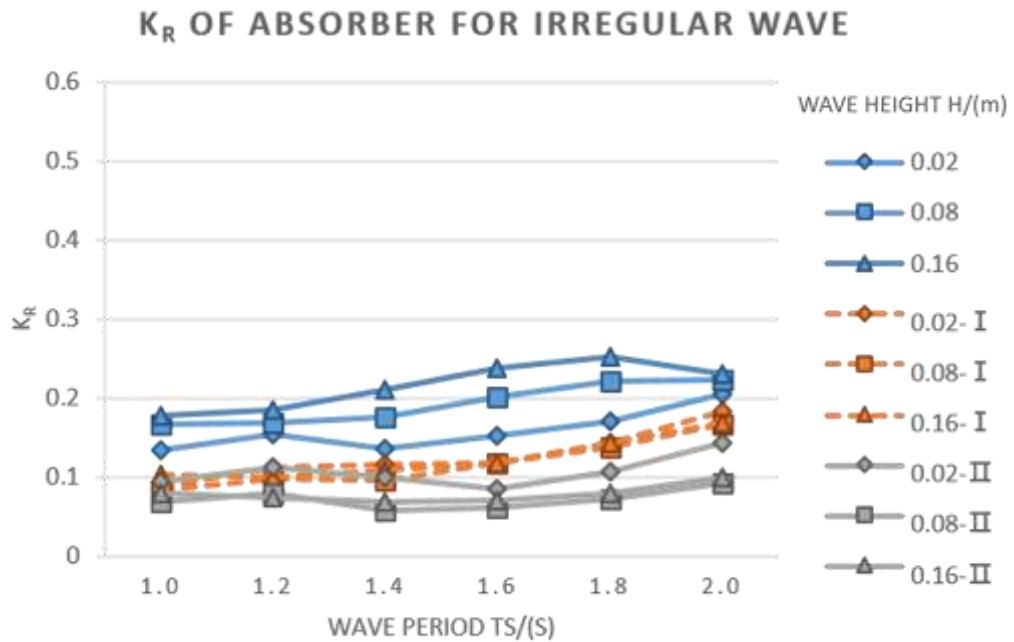
Figure 3-8　　Absorber Reflection Ratio in Irregular Wave Conditions.

3.2.2 Wave Gauge and Data Recording

The measurement of water surface elevation is CHT6-50E 2-line capacitance type wave gauges made by the KENEK Co., Ltd., see Figure 3-9. The sensor part of wave gauge consists a pair of thin Teflon insulation wires tensioned by a thin C-shape round stainless supporting frame. The change of sensor submergence into fluctuating water surface will be detected trough the change of electric capacity which can be described by a linear relation of different electric capacities of insulated wire in water and air. The change of capacity is responded by a change of voltage as output after amplified. The dynamic responsibility frequency of wave gauge is 10 Hz which is accurate enough to measure water wave elevation within 0.3 percentage linearity error. 4 wave gauges mentioned above are used for measure wave surface, and they are aligned along the centerline of the flume.

Figure 3-9   CHT6-50E 2-line Capacitance Type Wave Gauges.

Generation of regular and irregular wave height data is executed by applying MATLAB software and compatible PCI Express board interface with

software "ML-DAQ" released by CONTEC Co., Ltd. "ML-DAQ" has a library software for using analog input-output board with MATLAB, and each function is provided according to the unified interface of MATLAB's Data Acquisition Toolbox. To compose the regular wave height data, the sinusoidal curve function is given with target wave height and period, while for irregular wave height data composing, a famous Mitsuyasu-Bretschneider Spectrum (Bretschneider, 1968; Mitsuyasu, 1970) is used to generate power spectral density, in which significant wave height, significant wave period and frequency is defined. The mean wave height and period of regular wave and $H_{1/3}$, $T_{1/3}$ of irregular wave are obtained respectively in Table 3-2.

Table 3-2   Measured Experimental Wave Conditions.

Case	H_i (H_{mean})	T (T_{mean})	Case	H_i ($H_{1/3}$)	T ($T_{1/3}$)
	2.0cm	1.0s		1.8cm	1.3s
RE1	2.0cm	1.5s	IR1	2.0cm	1.8s
	1.8cm	2.0s		2.1cm	2.4s
	8.2cm	1.0s		6.9cm	1.4s
RE2	7.8cm	1.5s	IR2	8.1cm	1.9s
	7.3cm	2.0s		7.6cm	2.4s
	15.9cm	1.0s		11.8cm	1.5s
RE3	16.0cm	1.5s	IR3	15.2cm	2.0s
	15.2cm	2.0s		16.2cm	2.5s

Wave heights are measured and recorded by a wave-logger software named C-LOGGER released by CONTEC Co., Ltd. simultaneously, the analog data from wave gauges is amplified and converted by wave height meter panel and an Analog-to-digital converter (short for ADC). The converted digitalized signals are shown on monitor and written to hard disk, which can be directly used in further analysis.

Wave gauge calibration should be applied in different still water surface levels before formal making wave. Practical experience indicates that the

voltage responded by change of capacity is not only decided by water surface elevation, and it is believed temperature and environmental conditions also attribute to slightly error. Usually, calibration is applied before each case of experiment during a certain period of work time. An example of calibration curve is shown in Figure 3-10, the calibration procedure is performed manually in the -8 ~ +8 cm location range. which implies that the linearity of the device is quite satisfactory.
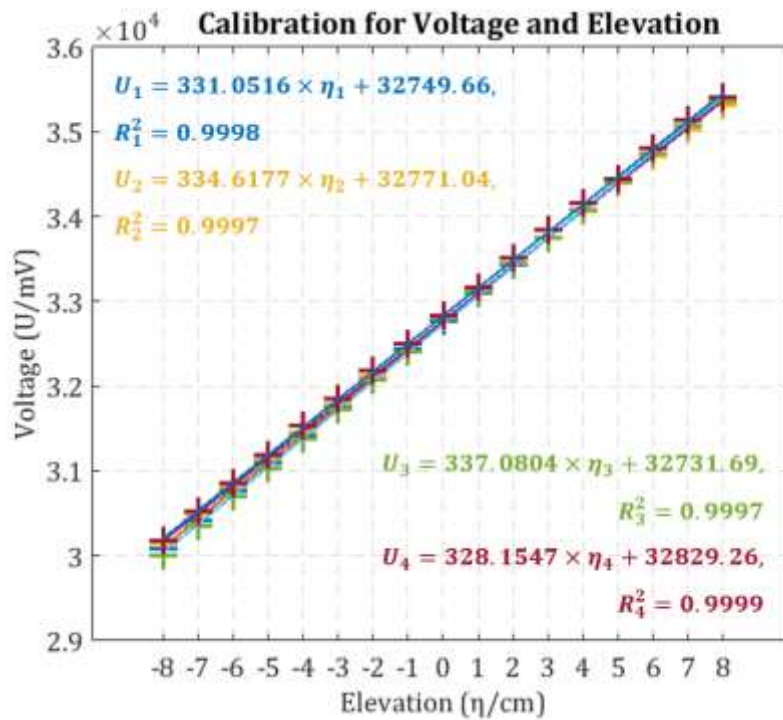
Figure 3-10 Example of Calibration Curve and Coefficients.

3.2.3 Physical Model Preparation

As introduced, models are categorized into smooth plate, plate with slots and plate with serrated blocks. For the convenient of adjustment and installation, the wood plate and steel frame are chosen to assemble the model.

Plate models are machined, drilled, painted and repainted as shown in Figure 3-11., finally made into 500×15×990mm size plate model with or without slots or serrated blocks. 4 large white pine wood plates with a 300×15×1820mm size are cut into 20 wood bars with a 50×15×990mm size and 4 pieces of 300×15×800mm offcuts. 5 spruce-pine-fir (SPF) wood square columns with a 40×40×910mm size are cut into cubes as serrated blocks on plate. 8 to 10 pieces of wood bars with or without serrated blocks are lined as a group and assembled by steel angles and steel bars to make a plate model; as shown in Figure 3-12, the models are comprised of different pieces of wood bar with serrated blocks to make different slots.

A plate model with changeable inclination and fixed submergence will be mounted on a steel frame system which consists of steel angles above water and flat bars below water for regular and irregular wave tests. Steel frame system is fixed on its head and toe, fix points locations as shown in Figure 3-13 by red and blue cycles. Upside fix points where red cycles noted are fixed by clip screws and bottom fix points are fixed by U-bolts to anchored rings on flume bottom. Plate fixed on the steel frame can be firm with no concussion under wave induced force as shown in Figure 3-14.

Figure 3-11   Physical Model Making Process.
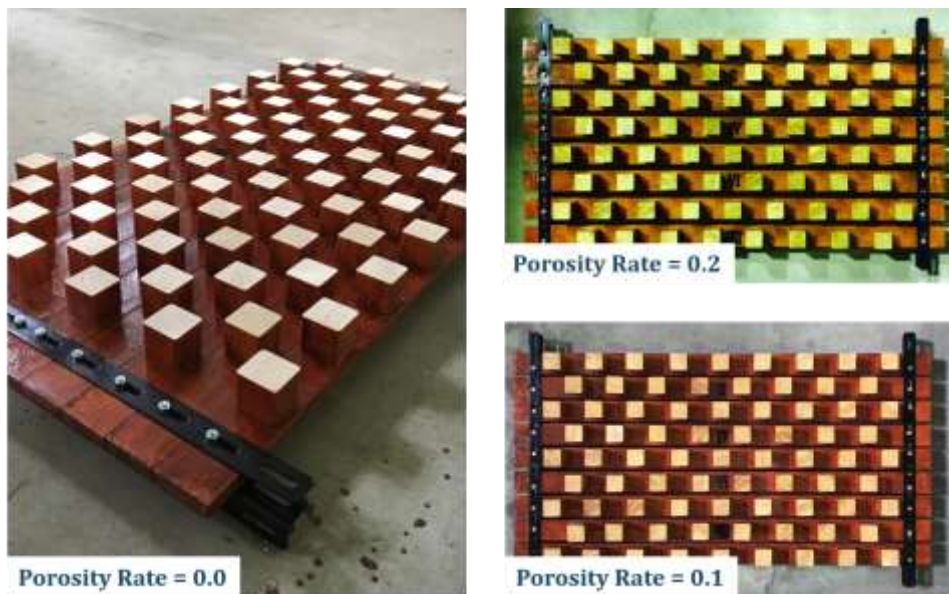
Figure 3-12   Physical Model of Plate with both Roughness and Porosity
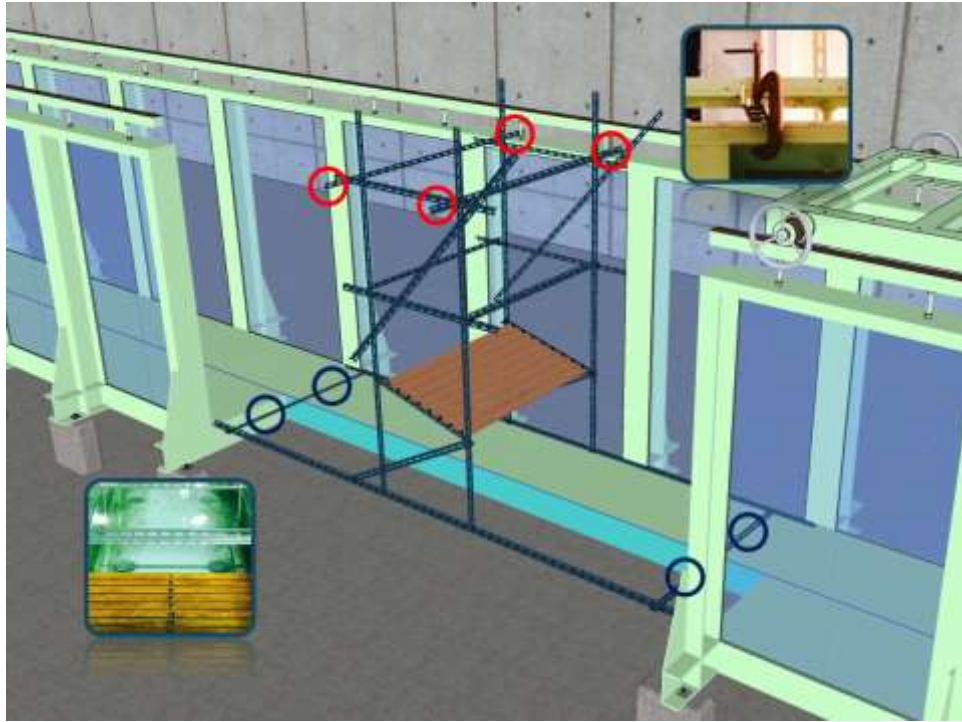
Figure 3-13　Steel Frame System for Physical Model Arrangement.
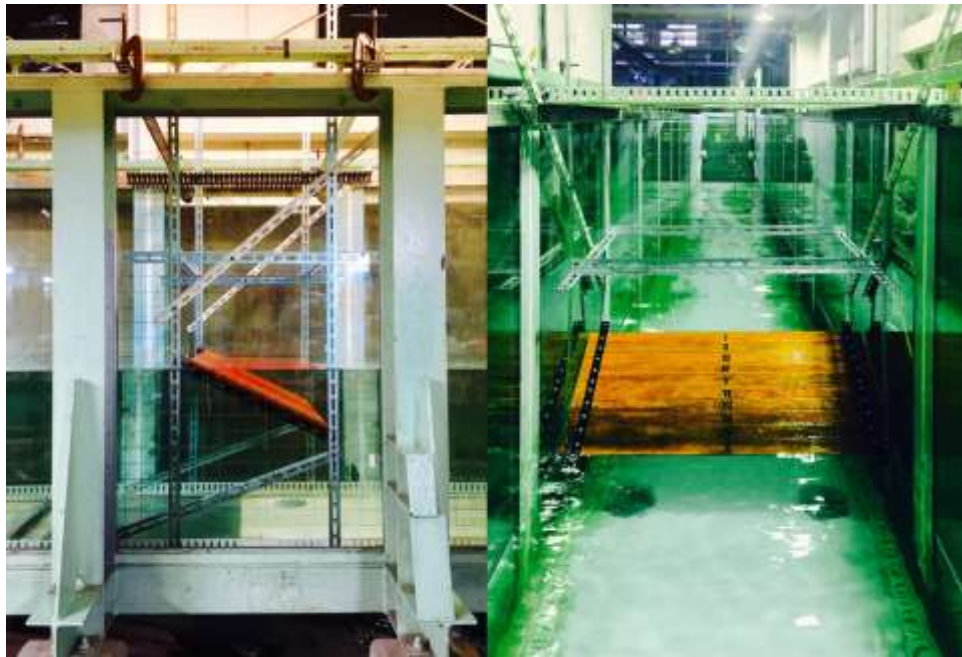
Figure 3-14　Fixed Oil Painted Wood Plate Mounted on Steel Frame.

3.3 Measurement and Data Processing

3.3.1 Wave Height Measurement

Measurement of wave transformation in terms of wave height means to measure how the plate breakwater in the center of flume influence incident wave and the transmission wave which deformed by the interaction of wave and plate during the propagating of wave over plate. While, the water surface elevation measured directly by wave gauges are superposed by incident wave and multiple reflection wave which much differ from that wave propagates in wave flume without an obstacle.

To decompose the measured waves including the components propagating in the two directions, two wave gauges are located 0.4 meter apart in front of plate where in the reflection region and in behind of pate at the far end of wave flume.

The location of the wave gauges is decided on the two-following consideration except spacing distance between 2 wave gauges: the wave gauges in front of plate where in the reflection region are as far as possible from paddle so that the wave may well developed to a steady state and the wave gauges in behind on plate where in the transmission region are as far as possible from plate to avoid influence from the end of plate.

The sampling frequency is selected by 20Hz whose frequency is higher 2 times than gravity wave and differ from local power supply in Kanto region to avoid influence. Since the test wave periods vary from 1.0 second to 2.0 second, we have more than 20-point values to determine the wave profile in a period. To make more reliable data, a record is taken for 300 seconds to include at least 150 periods.

3.3.2 Decomposition of Incident and Reflected Wave

Different methods have been developed for separating the incident and reflected waves. A method (Healy, 1952; Horikawa *et al.*, 1988) by moving wave gauges to measuring the maximum and minimum wave heights of superposed partial repetitive waves in regular wave condition. In the present case, regular wave profiles are recorded by fixed wave gauges, which the method is introduced below; for the irregular wave condition, since the measurement of instantaneous water level elevation simultaneously at different stations is possible, the method (Goda and Suzuki, 1987) based on the principle is utilized.

When analysis experiment data in regular wave cases, a method by fitting the measurement curves manually was used. Specifically speaking, the measured wave profile was assumed as η, and the fitted wave profile function was described by η^* which shows in equation below.

$$\eta^* = \frac{1}{2}\bar{H}^* \cos\left(\frac{2\pi}{\bar{T}^*} \times t + \varphi^*\right) + M^* \qquad (\,3.1\,)$$

where, $\bar{H}^*$ and $\bar{T}^*$ are obtained by using zero crossing method, M^* is average water level of measured profile, φ^* is measured and calculated by phase lag, for the sake of convenience in coding, a trying method is used for the convenient of computational calculation.

$$f: \varphi^* \to \int |\eta - \eta^*|$$
$$\varphi^* = \varphi\left[min\left(\int |\eta - \eta^*|\right)\right] \qquad (\,3.2\,)$$

As the function relation show between the assumed initial phase φ^* and the relative error of wave profiles show, the minimum relative error corresponding the approximate initial phase which can be coded by trying the initial phase in 0 to 2π to examine the minimum relative error.

In the wave flume where regular wave is generated, the free surface elevation superposed by the incident and reflected waves which follow the linear superposition and dispersion relation.

$$\eta_I = a_I \cos(kx - \sigma t + \varepsilon_I) \tag{3.3}$$

$$\eta_R = a_R \cos(kx + \sigma t + \varepsilon_R) \tag{3.4}$$

where a is the wave amplitude, k is the wave number, σ is the angular frequency and the phase lag; the subscripts I and R denote the incident and reflected waves respectively. Thus, the superposed water surface elevation is

$$\eta = \eta_I + \eta_R \tag{3.5}$$

At two measuring points 1 and 2, we use Eq. (4.5) to express the water surface elevation.

$$\eta_1 = (\eta_I + \eta_R)_{x=x_1} = A_1 \cos \sigma t + B_1 \sin \sigma t \tag{3.6}$$

$$\eta_2 = (\eta_I + \eta_R)_{x=x_2} = A_2 \cos \sigma t + B_2 \sin \sigma t \tag{3.7}$$

in which

$$A_1 = a_I \cos \varphi_I + a_R \cos \varphi_R \tag{3.8}$$

$$B_1 = a_I \sin \varphi_I + a_R \sin \varphi_R \tag{3.9}$$

$$A_2 = a_I \cos(\varphi_I + k\Delta l) + a_R \cos(\varphi_R + k\Delta l) \tag{3.10}$$

$$B_2 = a_I \sin(\varphi_I + k\Delta l) + a_R \sin(\varphi_R + k\Delta l) \tag{3.11}$$

and φ denotes the phase and Δl denotes the distance between the two wave gauges. Therefore, the incident and reflected wave parameters can be obtained.

$$a_I = \frac{\sqrt{(A_2 - A_1 \cos k\Delta l - B_1 \sin k\Delta l)^2 + (B_2 + A_1 \cos k\Delta l - B_1 \sin k\Delta l)^2}}{2|\sin k\Delta l|} \tag{3.12}$$

$$a_R = \frac{\sqrt{(A_2 - A_1 \cos k\Delta l + B_1 \sin k\Delta l)^2 + (B_2 - A_1 \cos k\Delta l - B_1 \sin k\Delta l)^2}}{2|\sin k\Delta l|} \tag{3.13}$$

$$\tan \varphi_I = -\frac{A_2 - A_1 \cos k\Delta l - B_1 \sin k\Delta l}{B_2 + A_1 \cos k\Delta l - B_1 \sin k\Delta l} \qquad (3.14)$$

$$\tan \varphi_R = \frac{A_2 - A_1 \cos k\Delta l + B_1 \sin k\Delta l}{B_2 - A_1 \cos k\Delta l - B_1 \sin k\Delta l} \qquad (3.15)$$

in which A_1, A_2, B_1 and B_2 are determined by the fitting wave surface profile η_1^* and η_2^* at the measuring points 1 and 2, detail process is explained in the appendix D.

$$A_1 = \frac{2}{n\pi} \int_0^{nT} \eta_1^* \cos \sigma t \, dt \qquad (3.16)$$

$$B_1 = \frac{2}{n\pi} \int_0^{nT} \eta_1^* \sin \sigma t \, dt \qquad (3.17)$$

$$A_2 = \frac{2}{n\pi} \int_0^{nT} \eta_2^* \cos \sigma t \, dt \qquad (3.18)$$

$$B_2 = \frac{2}{n\pi} \int_0^{nT} \eta_2^* \sin \sigma t \, dt \qquad (3.19)$$

The wave energy dissipation of submerged inclined plate $\mathcal{K}_D$ is quantified by the separated wave characteristics, reflection coefficient $\mathcal{K}_R$ and transmission coefficient $\mathcal{K}_T$, which are defined by Eq. (3-20) to Eq. (3-22).

$$\mathcal{K}_R = \frac{H_r}{H_i} \qquad (3.20)$$

$$\mathcal{K}_T = \frac{H_t}{H_i} \qquad (3.21)$$

$$\mathcal{K}_R{}^2 + \mathcal{K}_T{}^2 + \mathcal{K}_D{}^2 = 1 \qquad (3.22)$$

H_i, H_r, and H_t denote the height of incident, reflected and transmitted of regular wave. For irregular wave $\mathcal{K}_R$ can be obtained in a separate way, while for regular wave, $\mathcal{K}_R$ and $\mathcal{K}_T$ are calculated from Eq. (3.20) and Eq. (3.21).

3.4 Results and Discussion

To demonstrate the validity of model and to investigate the relationship among plate inclination degree, plate roughness and plate porosity, the variation of transmission and reflection coefficients against relative plate length are discussed by the semi-analytical method model and by conducting wave flume experiments, results are plotted by lines and dots from Figure 3-18 to Figure 3-25.

3.4.1 Wave Breaking over Plate

To verify the effect of wave breaking over plate to wave deformation in regular wave experiments, video under various wave condition and plate cases for overtopping, breaking and none breaking is recorded. As we found in each case of experiment, the results are listed in Table 3-3. Wave keeps continuity over various kinds of plate without any break when the wave height is small. For all the cases with 0.02-meter wave height (case RE1), wave propagates over plate expect in the case 1 due to the penetration water surface of inclined plate.

Non-wave breaking phenomenon is observed in case 5, case 6 and case 7 when wave height is 0.08 meters (case RE2) which corresponds different porosities rate of plate range from 0.10 to 0.30. It is obvious that bigger rate of plate porosity obstructs wave propagation in weaker way, which shows that the experimental result is reasonable. The comparison of regular wave experiments in case 4 to case 7 indicates that slots on plate help water mass exchange from the region beneath plate to the region above plate before wave crest travelling to plate; in other words, solid plate attributes to prevent water particles to orbiting by its original way which cause phase lag of wave on both side of plate

and wave breaking over plate, see Figure 3-15.

In addition, controlling the horizontal component of velocity is studied and compared by case 2 and case 4 shown in Figure 3-16, whose difference is serrated cube blocks on the surface of plate. Plate with surface roughness causes more disturbance of water wave to generate more chaos which does not allow movement or propagation of wave profile, in other words, roughness attributes to cause wave propagation lag above plate, which makes it easy to break over plate, this effect will significant when incident wave height become higher and *vice versa*.

Horizontal plate test which corresponds to case 3 shows different tendency with case 1 and case 2 when incident wave height is 0.08 meters (case RE2), as the wave breaking position is quite uniform at the end of number 1 plate bar. Propagation process over submerged horizontal plate is consist of two interactions: at the beginning edge of plate, wave profile deformed because of sudden water depth change with a visible wave reflection transmit to incident direction; and the deformed wave crest travels without breaking to the end edge of plate and finally broken until wave over topping to the region behind plate, wave reflection also takes place when wave broken. This reflection phenomenon is obviously observed in experiments when incident wave height is 0.16 meters (case RE3), and a supernumerary wave break by reflected wave may also take place above plate.

This phenomenon was researched in some former studies (Yu *et al.*, 1995) and it is believed the wave breaking is caused by disturbance on water surface due to water mass exchange between two layers of water above and beneath plate and the wave surface deformation is a presence of flow phase dis-synchronized which leads to a significant vertical velocity component, even the wave height is quite small.

Table 3-3　　Wave Breaking Observation Results in Experiments.

RE	Case (H_i)	RE1 (0.02m)			RE2 (0.08m)			RE3 (0.16m)		
	T	1.0s	1.5s	2.0s	1.0s	1.5s	2.0s	1.0s	1.5s	2.0s
RE	case 1	●▲	●▲	●▲	⑤	⑥	⑦	⑥	⑧	⑨
IN	case 2	●	●	●	②	③	④	⑤	⑥	⑥
	case 3	●	●	●	①	①	①	⑦	④	④
	case 4	●	●	●	③	④	⑤	⑤	⑦	⑦
PO	case 5	●	●	●	③	③	●	?	⑤	⑤
	case 6	●	●	●	②	●	●	③	④	④
	case 7	●	●	●	●	●	●	③	④	④
RO	case 8	●	●	●	②	④	④	⑤	⑥	⑥

▲ : non - wave overtopping;

● : non - wave breaking;

⊙ : wave breaking at the plate which sign with number;

? : data record failed.
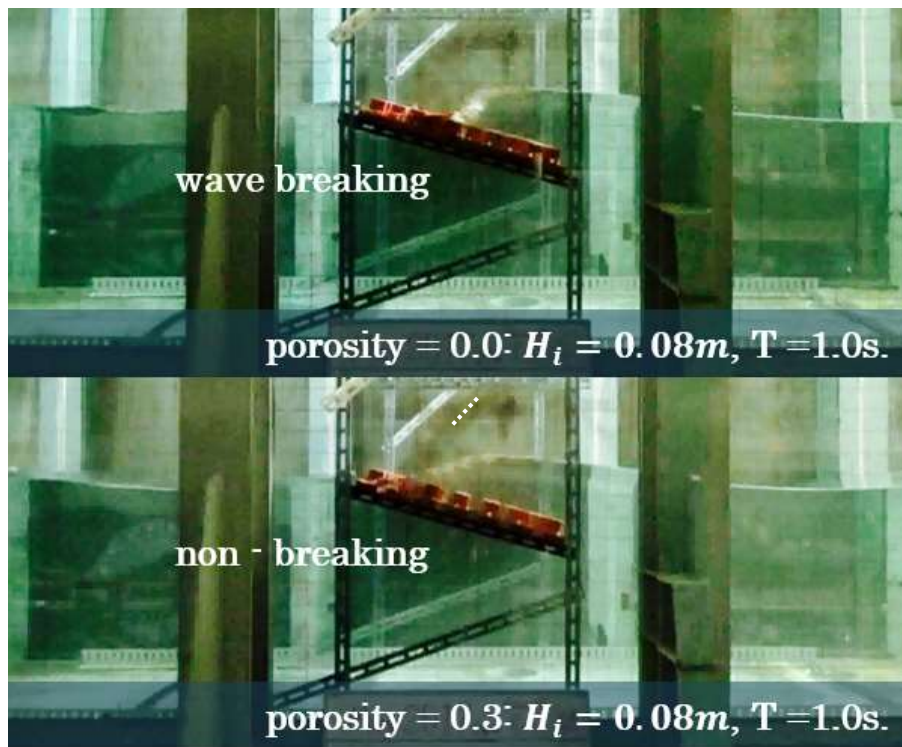
Figure 3-15 Water Mass Exchange Effect on Wave Breaking.
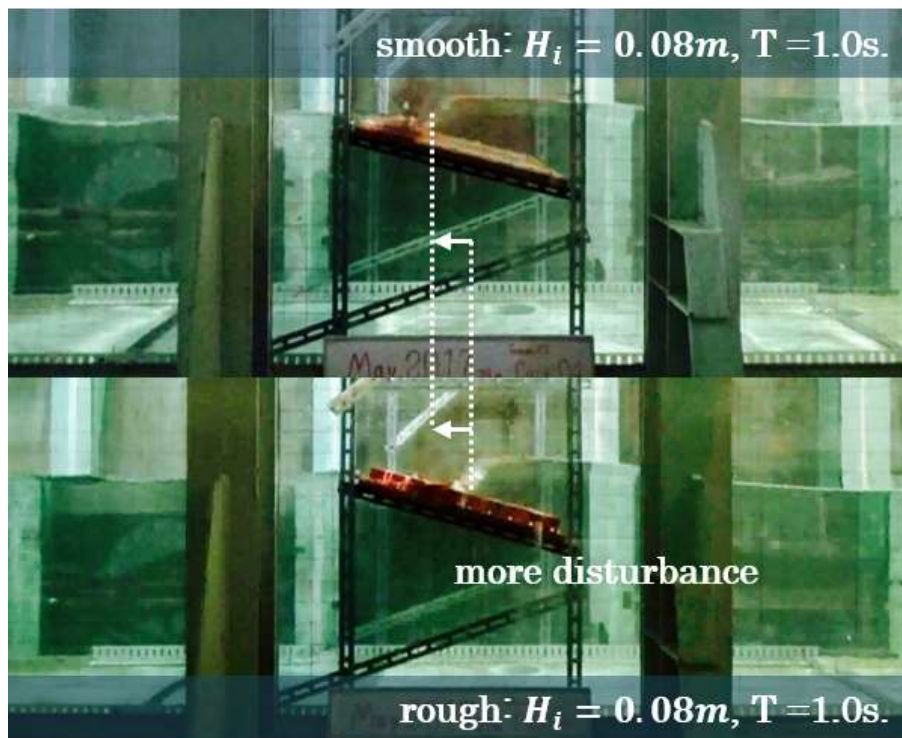
Figure 3-16 Disturbance Effect on Wave Breaking.

3.4.2 Inclination θ

To conduct the investigation of inclination influence with the purpose of validity, computational and wave conditions for comparing the wave flume experiment IN case is listed in Table 3-5 and Table 3-6.

Table 3-4   Computational Conditions for Comparison (case IN).

Case	B/h	D/h	δ/h	θ	roughness	porosity
1	0.83			30°	×	0.00
2	0.80	1/6	1/30	15°	×	0.00
3	0.72			0°	×	0.00

Table 3-5   Experimental Conditions for Comparison (case IN).

Case	H_i	θ	roughness	porosity
1	RE1 (0.02) RE2 (0.08) RE3 (0.16)	30°		
2	RE1 (0.02) RE2 (0.08) RE3 (0.16)	15°	×	0.00
3	RE1 (0.02) RE2 (0.08) RE3 (0.16)	0°		
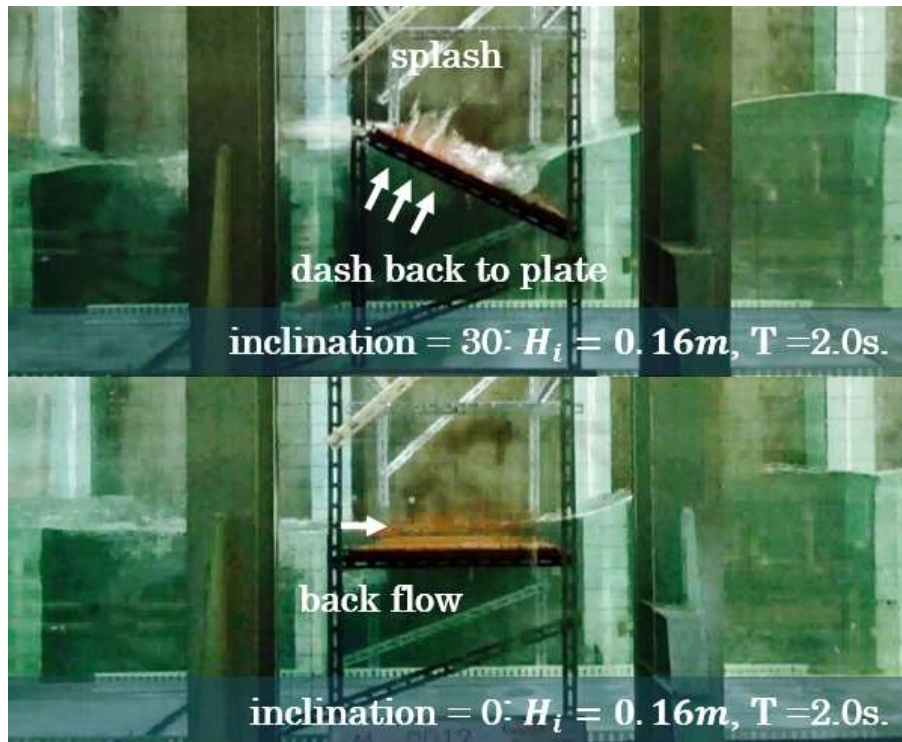
Figure 3-17 Water splash Caused by Water Dash on Inclined Plate.

As following Figure 3-18 to Figure 3-20 show, the computed transmission and reflection coefficients described by solid line is independent on incident wave height, while dots plotted from measurement of experiment are influenced by variety incident wave height. It can be found that the influence of the plate inclination become a significant variable both in computed and measured result. The transmission coefficient tends to increase remarkably when the plate inclination decrease, and the scattering dots which fluctuate around solid lines also shift upward with the plate inclination decrease. It is believed that inclined plate breakwater makes wave break more easily when climb the plate as we can image, and the observation also give a clue that inclined plate obstruct wave to move back when wave crest is going to climb the plate and the water particle transmitting waveform, from the Figure 3-17 large mass of water dash back side of inclined plate which cause big splash periodically, and backward flow will cause visible wave breaking and reflection towards incident wave direction.

Solid curves of case 1 and case 2 in Figures 3-18 and 3-19 show that reflection and transmission coefficients of different inclinations appear to be identical both analytically and experimentally, this implies submerged plate inclination affects transmission to a little extend when relative plate length is smaller than 0.2. For instance, 30-degree inclined plate is more effective than 15-degree which shows lower transmission coefficient just when relative plate length larger than 0.2. On the contrary, analytical curves of horizontal plate does not show better performance due to its height transmission and relative identical reflection compared to inclined plate, experimental dots also proof it.

In addition, in Figures 3-18 and 3-19, 2-cm incident wave height is significant obstructed which corresponds dots of case 1-1 and case 2-1 both regular and irregular, their transmission curves are lower than 8-cm and 16-cm and reflection curves are higher than 8-cm and 16-cm case in general. What's more, transmission and reflection of 8-cm and 16-cm wave height seem to be identical which corresponds dots of case 1-2, 1-3 and case 2-2, 2-3. By surveying experimental video record in Table 3-4, it is found that the phenomenon is consequence by wave overtopping which is heavily depending on incident wave height, plate in case 1 is a slightly water surface piercing case which prevent wave propagation, lower reflection dots in case 2 and case 3 also confirm this fact.

A brief discussion on steeper plate inclination give a clear conclusion that plate inclination attributes to lower wave transmission meanwhile higher reflection as Figure 3-22 shows; it is worth to note that reflection from horizontal is different on mechanism to inclined plate, which is caused by back flow and plate obstruction respectively; higher incident wave height can propagate over submerged inclined plate easier to a certain extent, because of amount of wave overtopping, while no evidence shows higher incident wave height leads to higher reflection coefficient. Figures 3-23 and 3-24 show that inclined plate cause larger wave energy dissipation.

Comparison of computed and measured K_T (case 1)

Comparison of computed and measured K_R (case 1)
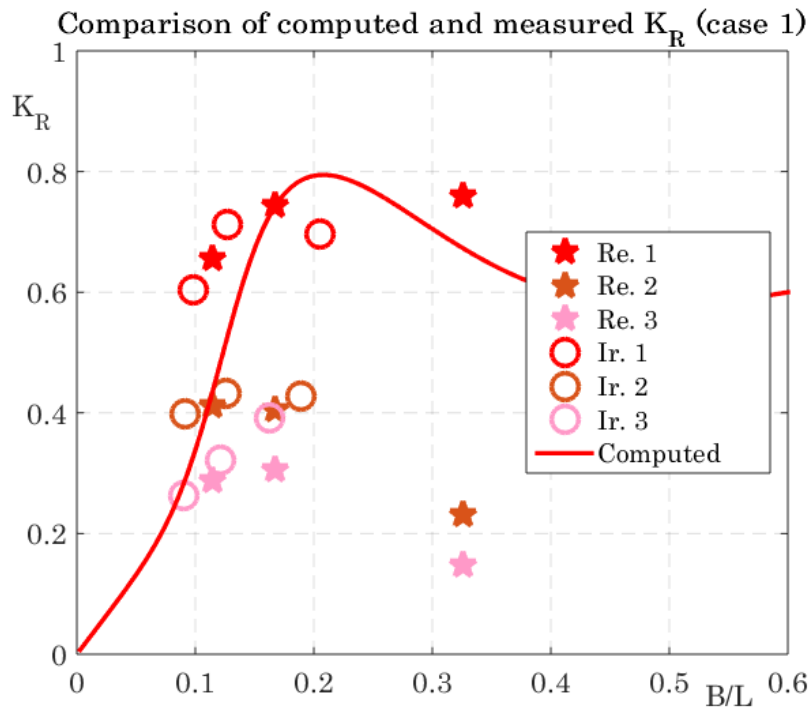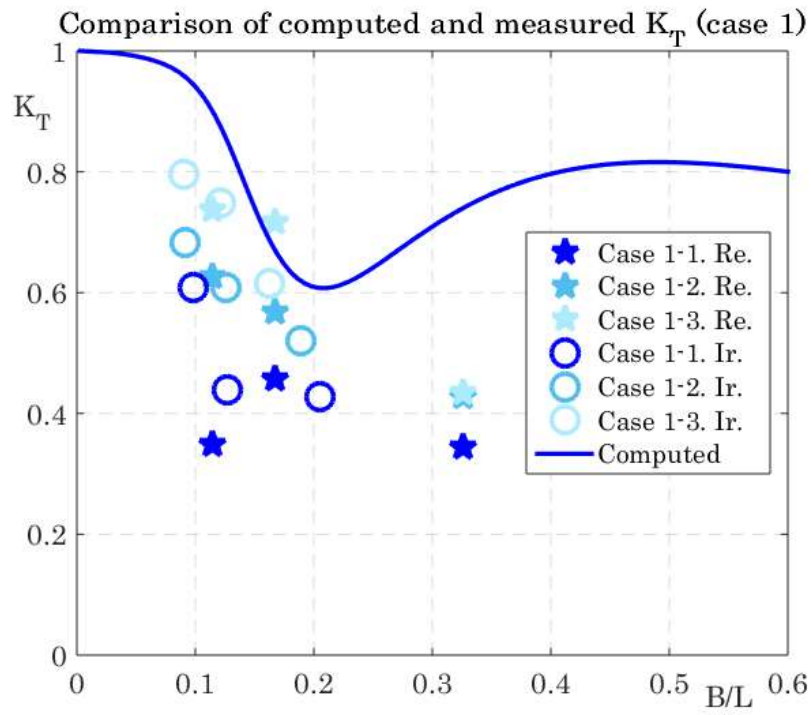
Figure 3-18 $\mathcal{K}_R$ and $\mathcal{K}_T$ against B/L (case 1).
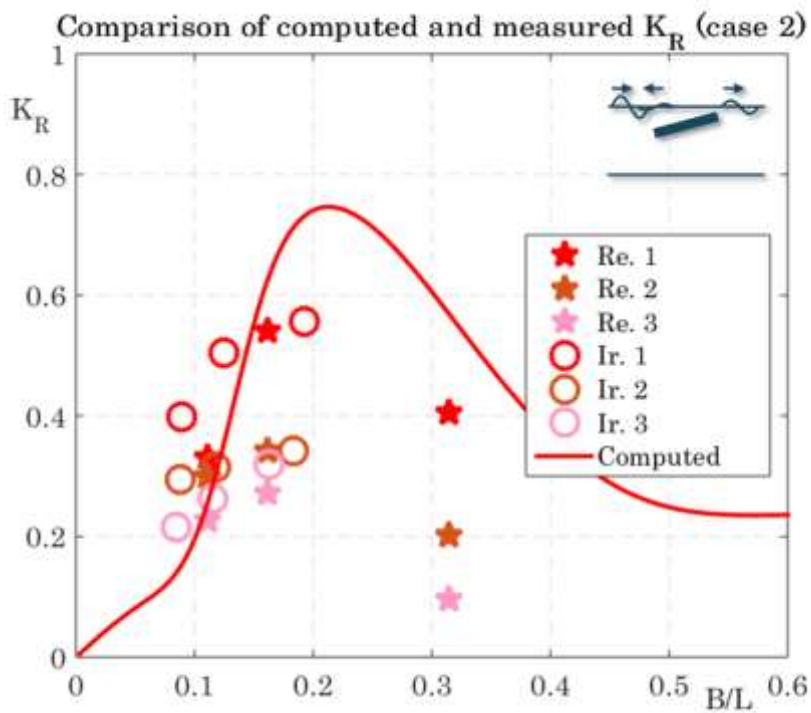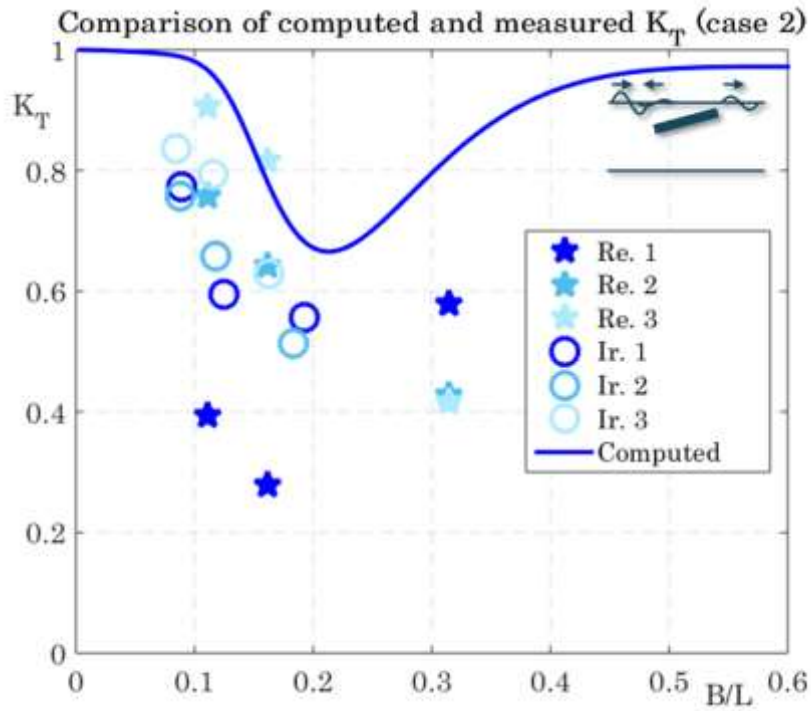
Figure 3-19 $\mathcal{K}_R$ and $\mathcal{K}_T$ against B/L (case 2).

Comparison of computed and measured K_T (case 3)

Comparison of computed and measured K_R (case 3)
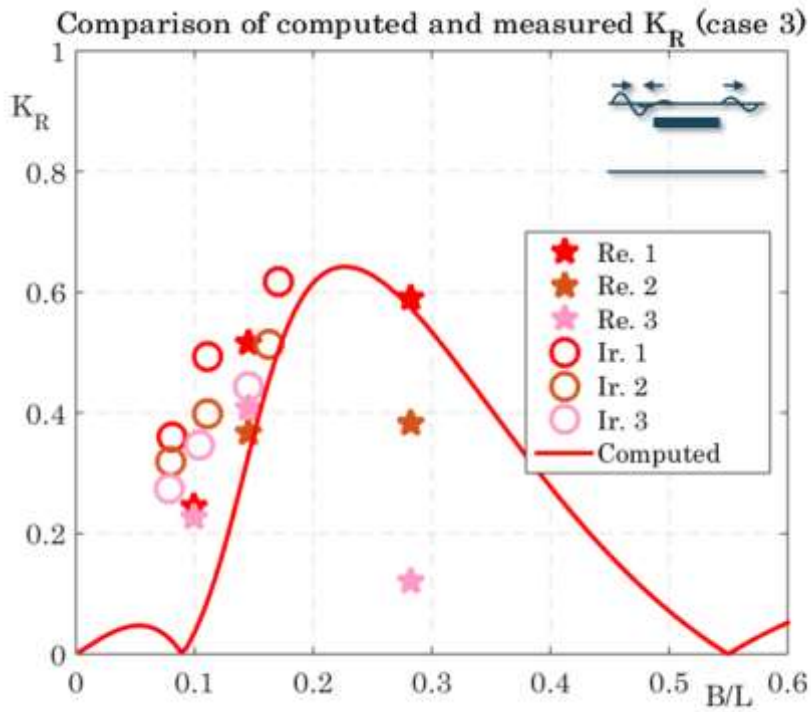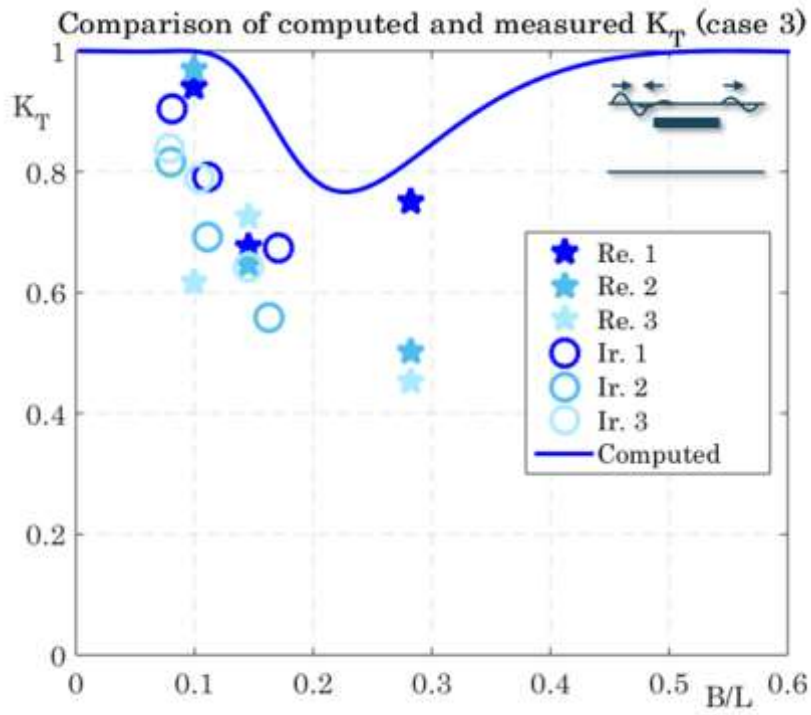
Figure 3-20 $\mathcal{K}_R$ and $\mathcal{K}_T$ against B/L (case 3).
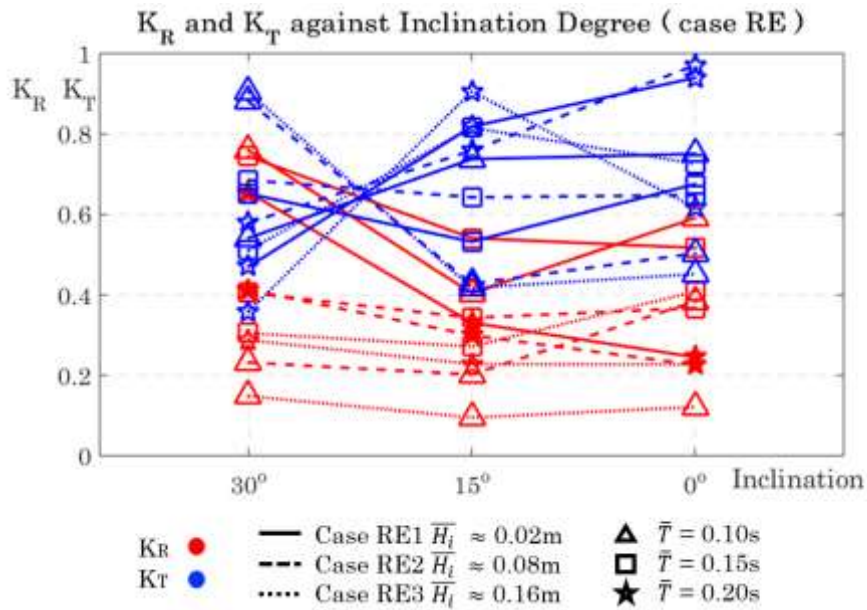
Figure 3-21 $\mathcal{K}_R$ and $\mathcal{K}_T$ against Plate Inclination (case RE).
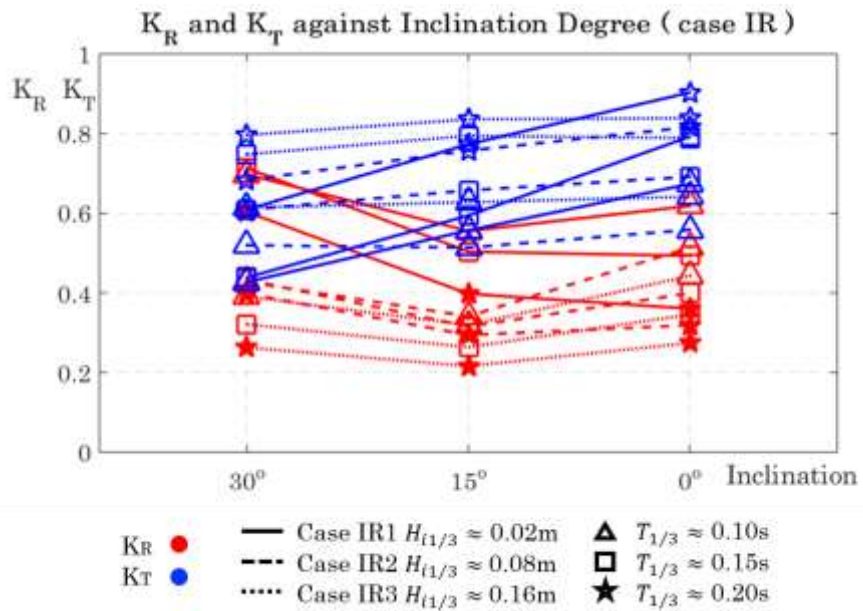
Figure 3-22 $\mathcal{K}_R$ and $\mathcal{K}_T$ against Plate Inclination (case IR).
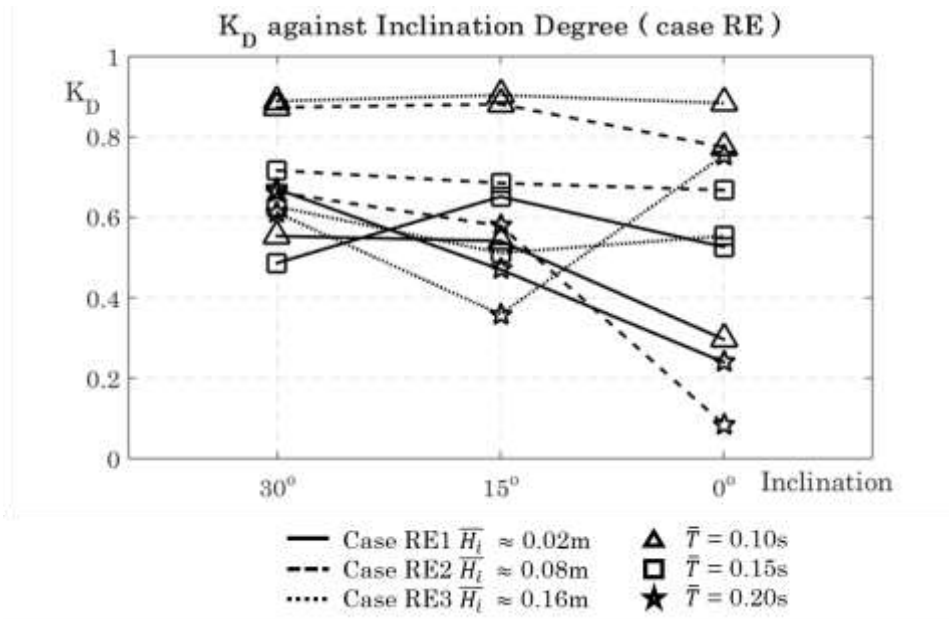
Figure 3-23 $\mathcal{K}_D$ against Porosity Ratio (case RE).
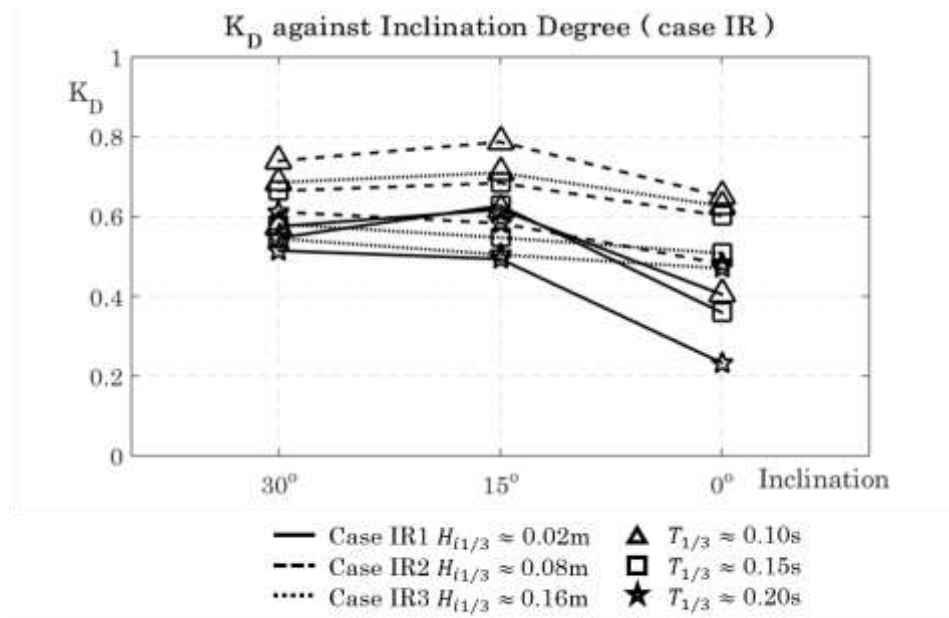
Figure 3-24 $\mathcal{K}_D$ against Porosity Ratio (case IR).

3.4.3 Roughness and Porosity

In roughness and porosity influence investigation, experimental conditions for RO case and PO case are listed in Table 3-7 and Table 3-8. For the sake of convenience, only when the wave height is 0.08 m case is presented.

Comparisons between case 4, case 7 and case 2, case 8 investigate the porosity influence which correspond plate conditions as Table 3-7 shows, their results are presented below, which illustrated as the following Figure 3-25 to Figure 3-26, it can be found that the influence of the plate porosity is significant. The transmission coefficient tends to increase remarkably when the plate porosity increasing from 0.0 to 0.3, and the reflection coefficient tends to decrease remarkably when the plate porosity increasing. It can be expected from where discussing the wave breaking over plate in wave breaking section and Table 3-4, with the increasing of slots on plate, water mass exchange across plate can be regarded as kind of transmission when wave propagating as Figure 3-15 illustrated. Another case, showed in Figure 3-26, also tells identical tendency that 0.1 porosity slot plate is slightly weak on the transmission, and weak on reflection. While it is worth to mention that, due to relative small porosity rate, wave in case 8 is broken over plate, this lead a result that the transmission coefficient is closed to solid plate but a lower reflection.

Comparisons between case 2, case 4 and case 5, case 8 investigates the roughness influence which correspond solid plate with and without roughness situation, slotted plate with and without roughness situation. It is found in Figure 3-27 and 3-28 that the roughness decreases both the transmission coefficient and the reflection coefficient which implies plate with roughness lead more wave energy dissipation. It also can be expected once when discussing the wave breaking over plate in wave breaking section and Table 3-4, with the adding roughness on plate, roughness attributes to cause wave propagation lag above plate, which makes it easy to break over plate as Figure 3-16 illustrated.

Table 3-6   Experimental Conditions Detail (case PO).

Case	H_i	θ	roughness	porosity
4	RE2 (0.08)		√	0.00
7	RE2 (0.08)	15°	√	0.30
2	RE2 (0.08)		×	0.00
8	RE2 (0.08)	15°	×	0.10

Table 3-7   Experimental Conditions Detail (case RO).

Case	H_i	θ	roughness	porosity
2	RE2 (0.08)		×	0.00
4	RE2 (0.08)	15°	√	0.00
8	RE2 (0.08)		×	0.10
5	RE2 (0.08)	15°	√	0.10
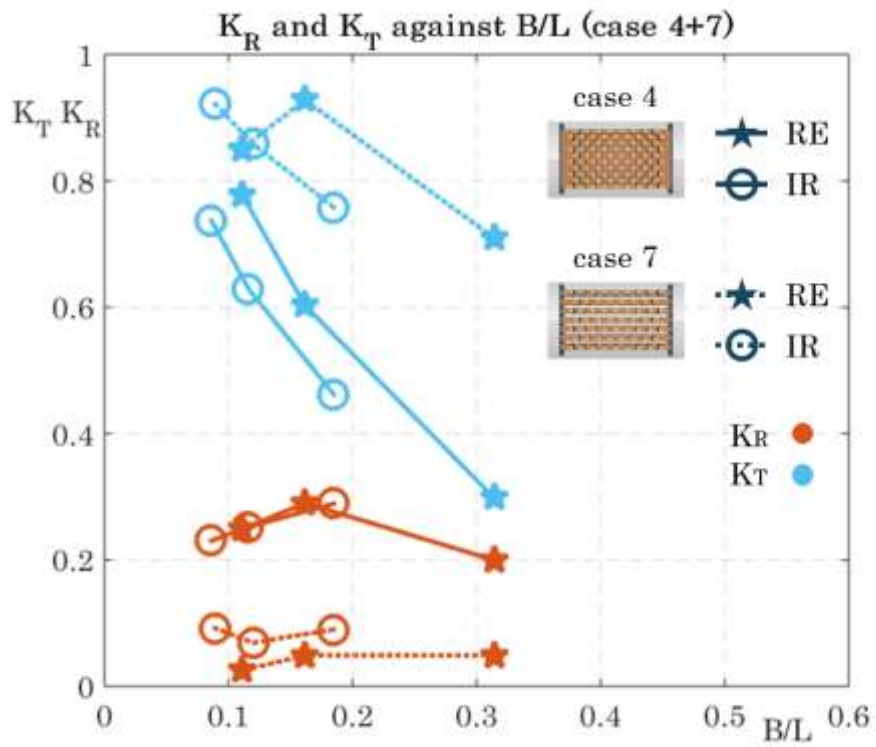
Figure 3-25 $\mathcal{K}_R$ and $\mathcal{K}_T$ against B/L (case 4+7).
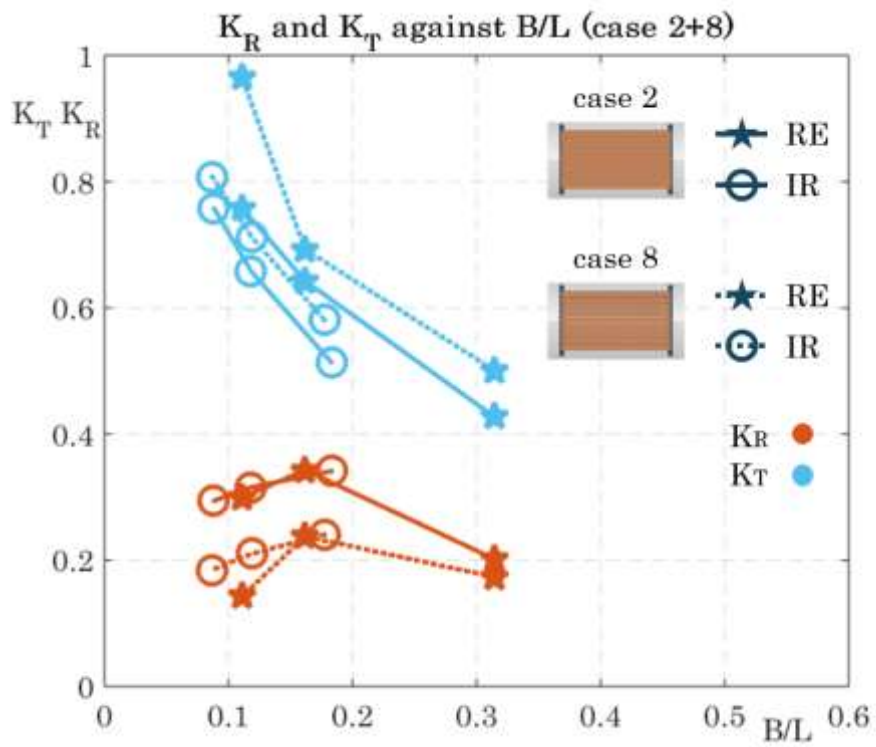
Figure 3-26 $\mathcal{K}_R$ and $\mathcal{K}_T$ against B/L (case 2+8).
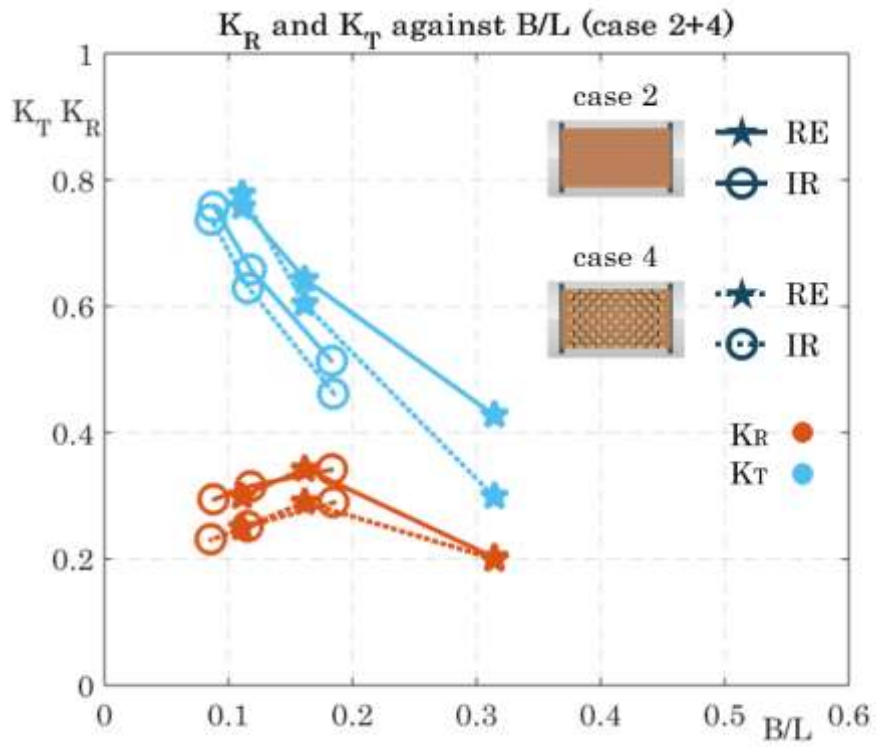
Figure 3-27 $\mathcal{K}_R$ and $\mathcal{K}_T$ against B/L (case 2+4).
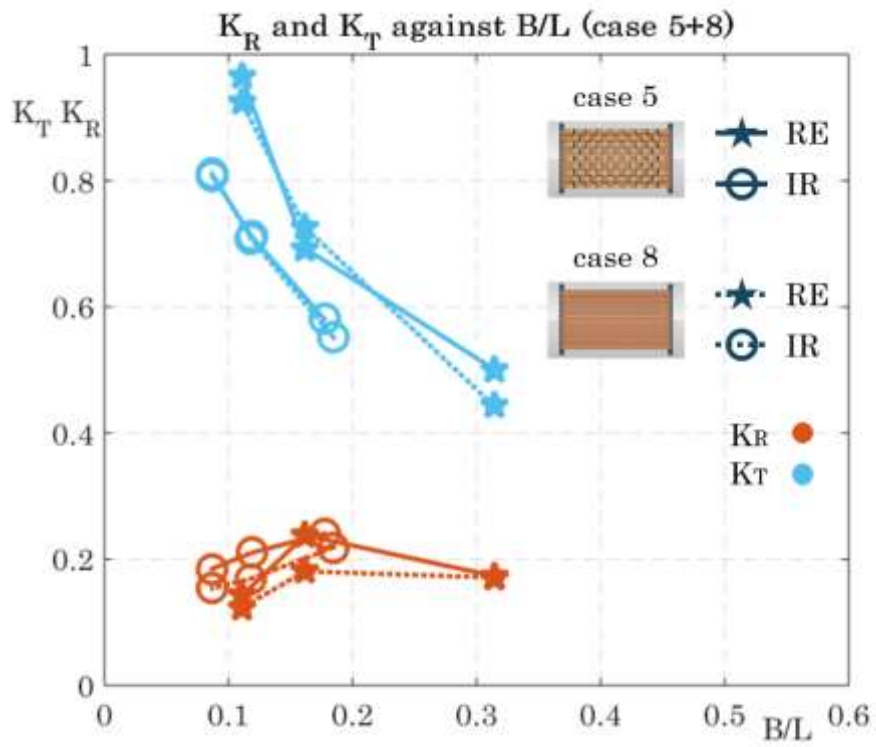
Figure 3-28 $\mathcal{K}_R$ and $\mathcal{K}_T$ against B/L (case 5+8).

Combining the transmission coefficient, reflection coefficient comparison with the wave breaking phenomenon analysis introduces an abstract impression that cube roughness on plate promotes wave breaking over plate, while on the contrary, slot gap on plate promotes wave flow exchange, which lead high wave transmission and low reflection that weaken the performance of submerged inclined plate breakwater.

To further ensure the wave flow exchange promoting property, variation of reflection, transmission and energy dissipation with respect to plate porosity ratio are illustrated from Figure 3-29 to 3-32, in which case 4, case 5 case 6 and case 7 are surveyed in different wave conditions of both regular and irregular. Reflection and transmission values are dyed in red and blue, wave energy dissipation remains to be black; wave conditions are presented in groups, types of line and dot represent types of wave condition.

Start with the irregular cases, dots and curves show high degree uniform distribution, indicating that porosity ratio affects wave in different contend. Generally speaking, wave transmission $\mathcal{K}_T$ and wave energy dissipation $\mathcal{K}_D$ change significant against plate porosity changing, wave reflection $\mathcal{K}_R$ keeps relative stable around 0.2. Small wave height wave seems sensitive to plate porosity changing, the reason may be that small wave is prone to prevented by obstruction while big wave is easily transmitted over plate. Wave period is relative not sensitive to porosity changing, longer wave is easily transmitted and enery maintaned when propogating over submerged inclined plate breakwater.

As for regular cases which phenomenon and results show more extreme, differences among periods are active, short period wave is deeply affected especially when plate porosity is small which wave may be absolutly absorbed by plate, and long period wave is more affected when porosity approximate to 0.2 which may be special geometric relation that cause wave concentration.
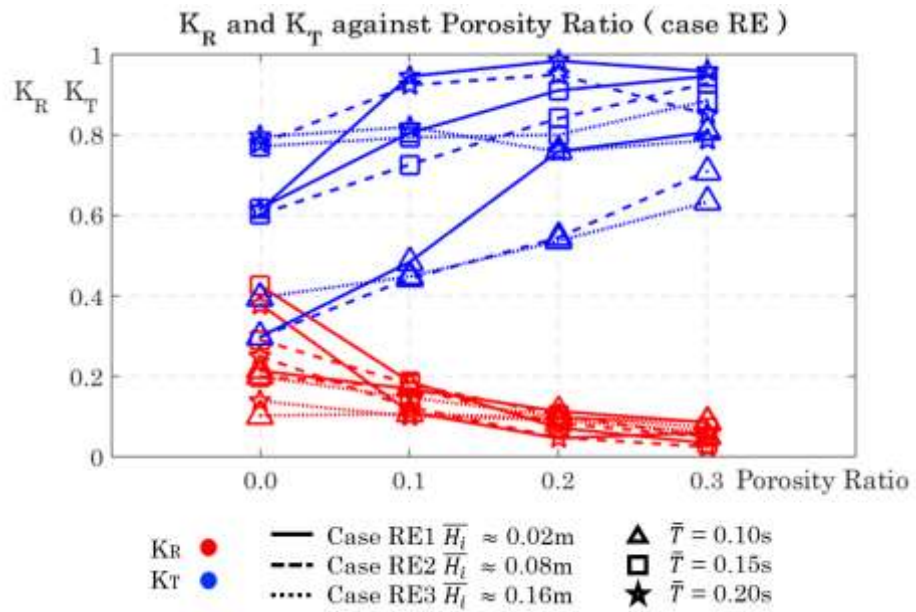
Figure 3-29 $\mathcal{K}_R$ and $\mathcal{K}_T$ against Porosity Ratio (case RE).
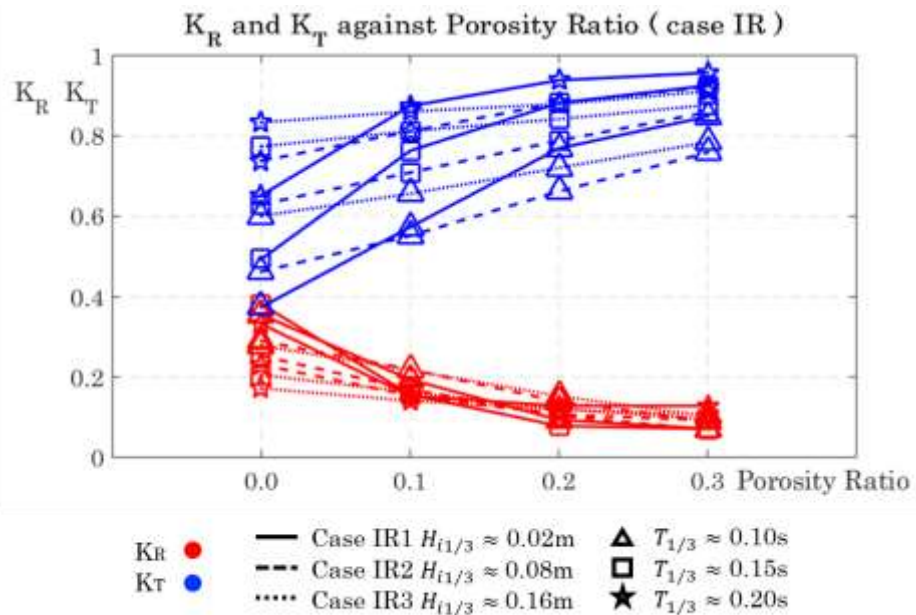
Figure 3-30 $\mathcal{K}_R$ and $\mathcal{K}_T$ against Porosity Ratio (case IR).
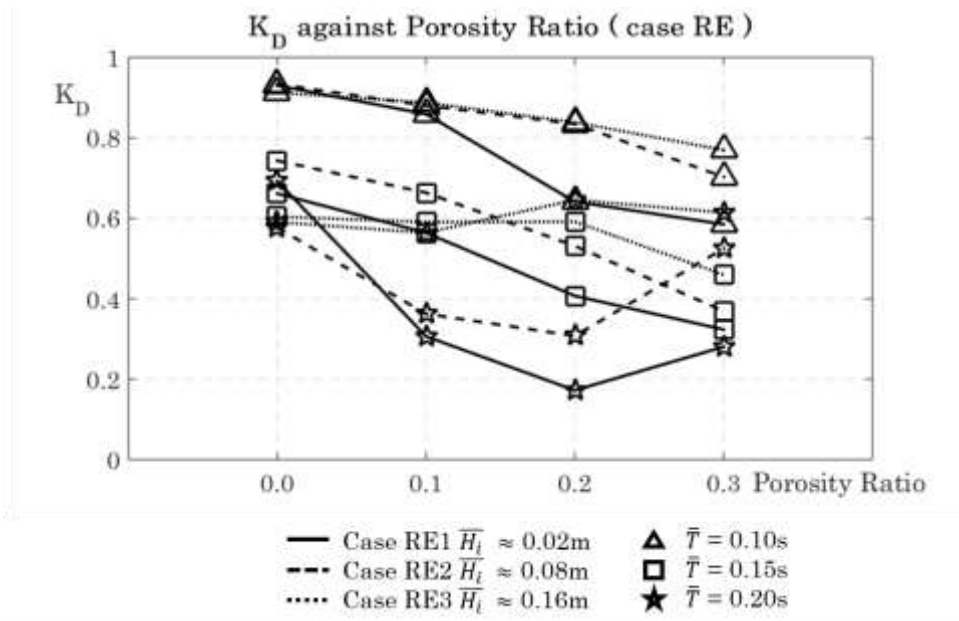
Figure 3-31 $\mathcal{K}_D$ against Porosity Ratio (case RE).
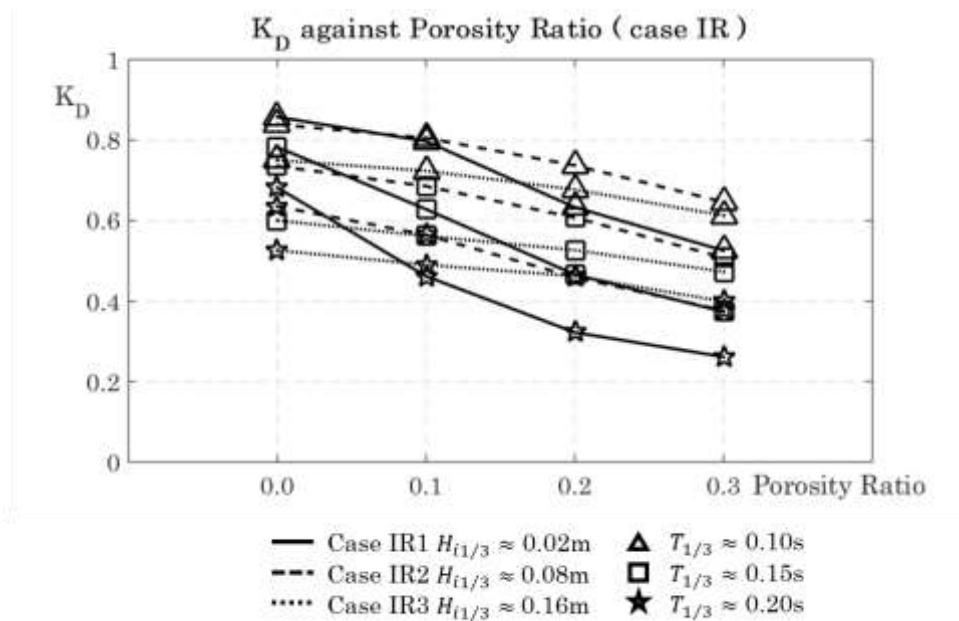
Figure 3-32 $\mathcal{K}_D$ against Porosity Ratio (case IR).

3.4.4 Water Depth to Wave Length Ratio *h/L*

As informed wave length is an important variable may affect transmission and dissipation performance especially when wave length is longer, wave length L will be discussed. Because in the present research, water depth, submergence and plate length are constant, it is an appropriate choice to dimensionless wave length L by using an incident wave parameter, water depth d. From Figure 3-33 to 3-50 the wave length L represents mean wave length for regular wave and represents significant wave length for irregular wave which we can regard L as representative wave length. Solid curves are fitted manually. As concluded in section 3.4.2 that reflection from horizontal is different on mechanism to inclined plate, which is caused by back flow and plate obstruction respectively. It is no wonder that reflection horizontal plate which corresponds case 3 in Figure 3-33 is relative small.
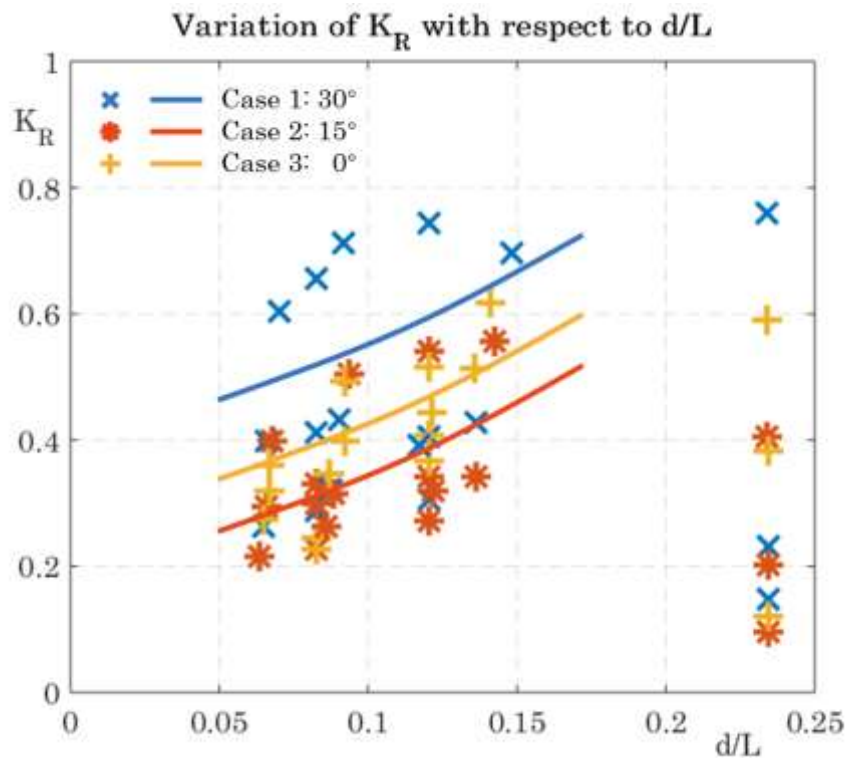
Figure 3-33 Variation of $\mathcal{K}_R$ with Respect to *d/L* (case 1, 2, 3).
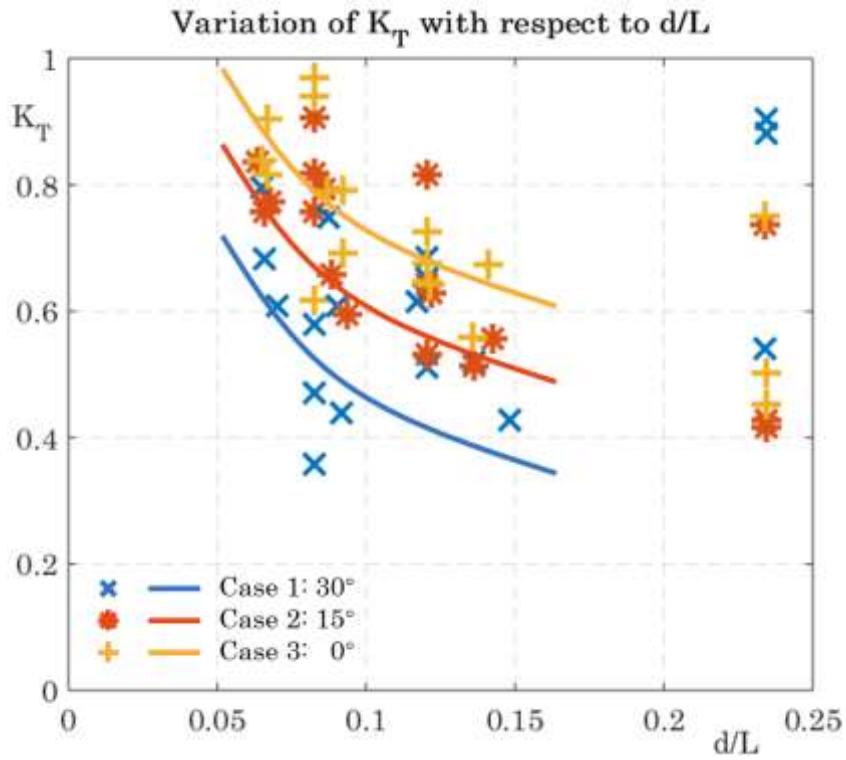
Figure 3-34 Variation of $\mathcal{K}_T$ with Respect to d/L (case 1, 2, 3).
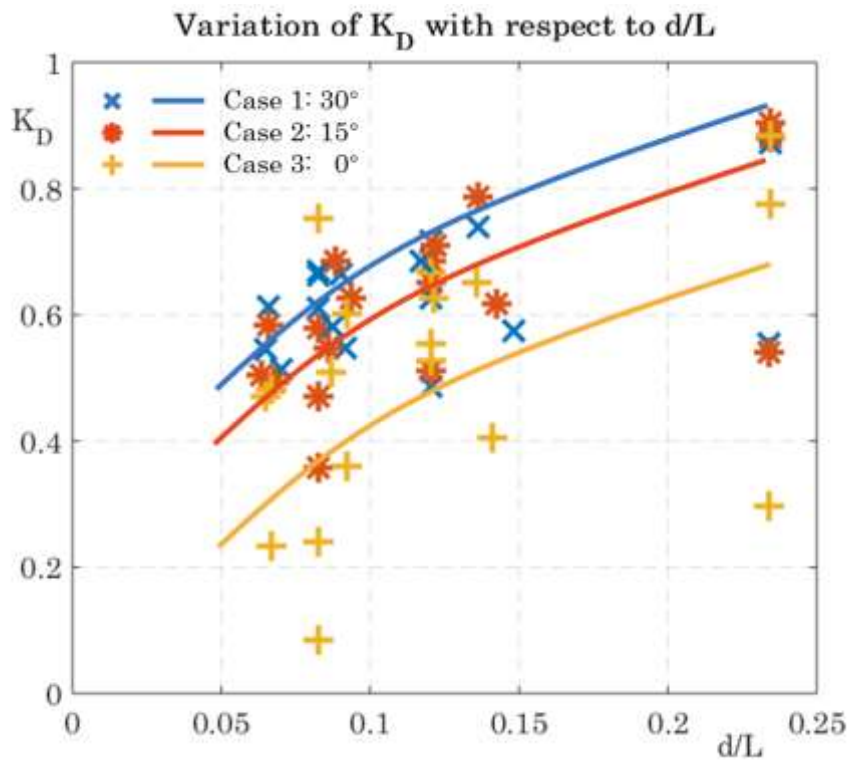
Figure 3-35 Variation of $\mathcal{K}_D$ with Respect to d/L (case 1, 2, 3).

Figure 3-36 to 3-38 illustrate variation of coefficients with respect to d/L for different cases correspond to different plate porosity, these Figures fit well with preview conclusions. Additional discovery is that solid plate of case 4 remains higher reflection coefficient and reflection among cases.

Dots and curves scatter in a satisfy pattern, in other words, variation with respect to d/L screen each case off so that it is clear to make a speculation that water depth to wave length ratio is an important parameter to performance of submerged inclined plate water. Specifically speaking, in experiment which water depth is constant, we can give an inference that wave length is of critical variable may affect breakwater performance.

Additional discovery on case 4 which corresponds solid plate with cubes roughness shows it is a good improvement scheme because it transmit wave and reflect wave in low contend but keep relative high wave energy dissipation in both regular and irregular wave condition. It is an appreciating feature.
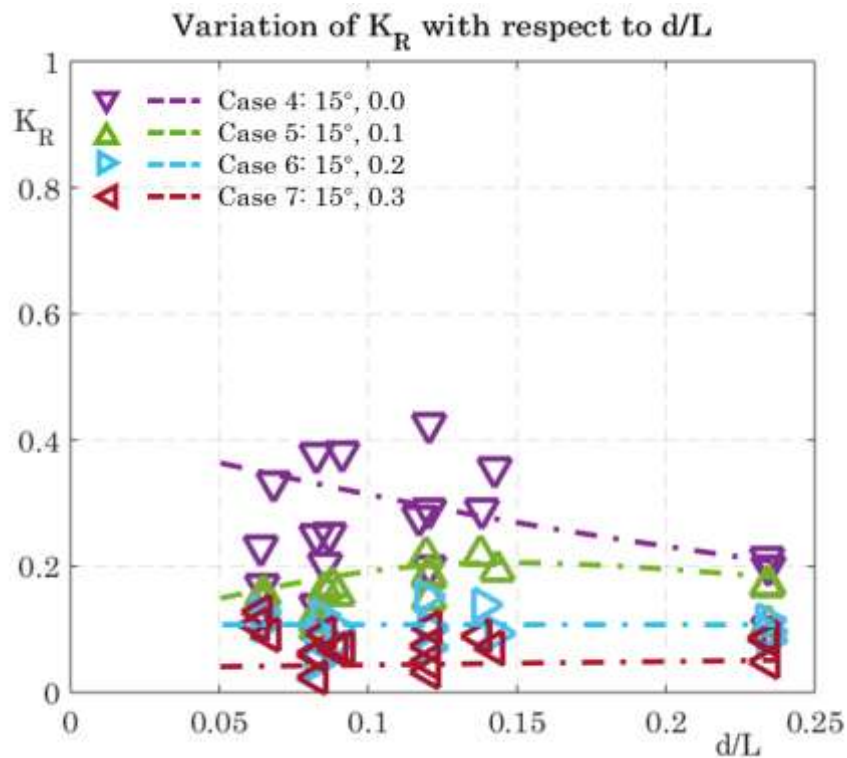
Figure 3-36 Variation of $\mathcal{K}_R$ with Respect to d/L (case 4, 5, 6, 7).
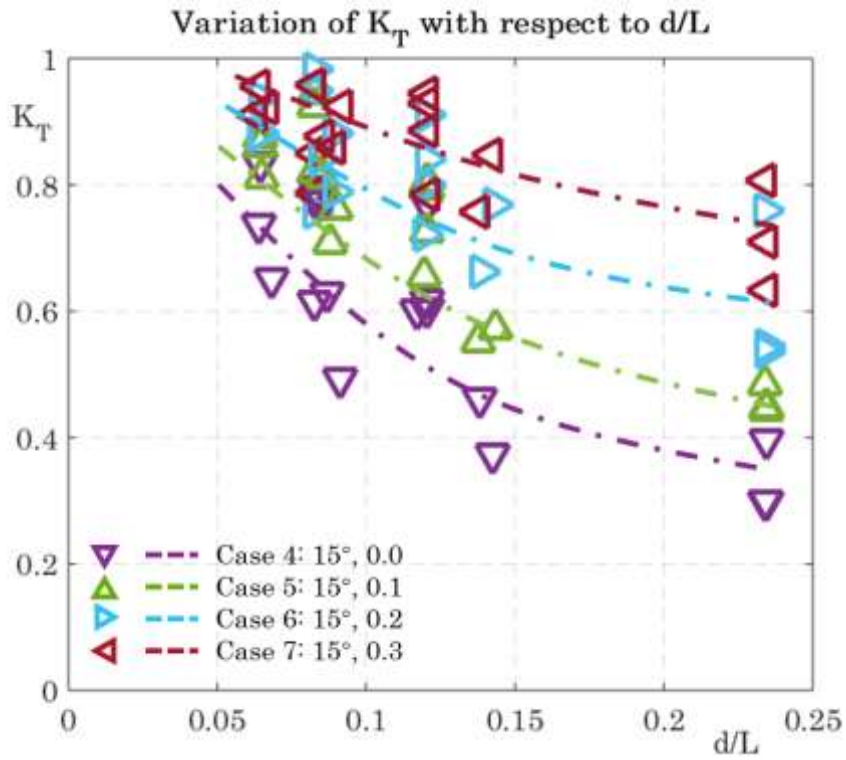
Figure 3-37 Variation of $\mathcal{K}_T$ with Respect to d/L (case 4, 5, 6, 7).
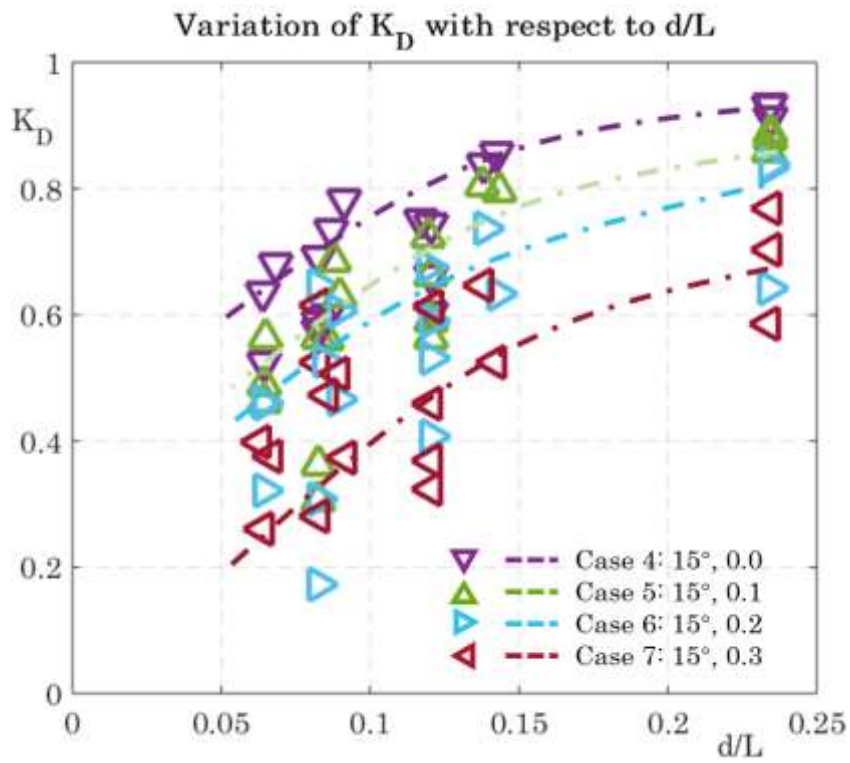
Figure 3-38 Variation of $\mathcal{K}_D$ with Respect to d/L (case 4, 5, 6, 7).

Figure 3-39 to 3-41 make parallel contrast on plate roughness between plates with and without slot gap. It is found that plate with cubes roughness shows roughness on plate make performance better with lower wave reflection, lower transmission and higher wave energy dissipation.

In conclusion, reflection with respect to d/L keep a stable range from 0.1 to 0.5 averagely in all cases of plate model, the fact can lead a clue that the reflection of submerged inclined plate breakwater is not sensitive to d/L, in other words, they keep low correlation to each other. All Figures about transmission and dissipation coefficient show a relationship of a certain function, so it is a promise attempt developing a multi-parameter model for transmission or dissipation coefficient. The tentative model for transmission coefficient will be discussed in the next part.
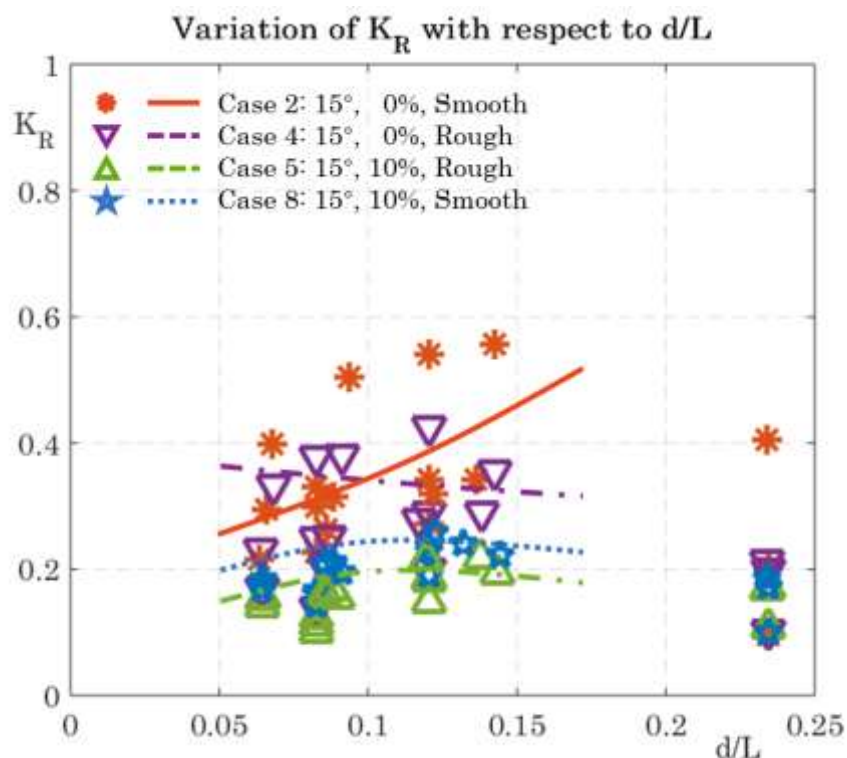
Figure 3-39 Variation of $\mathcal{K}_R$ with Respect to d/L (case 2, 4, 8, 5).
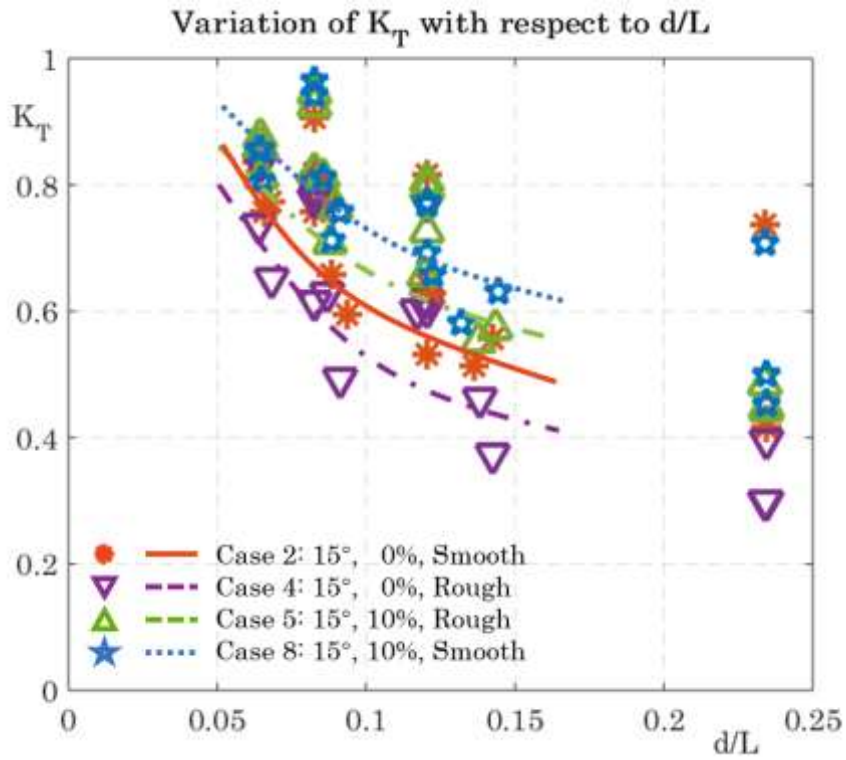
Figure 3-40 Variation of $\mathcal{K}_T$ with Respect to d/L (case 2, 4, 8, 5).
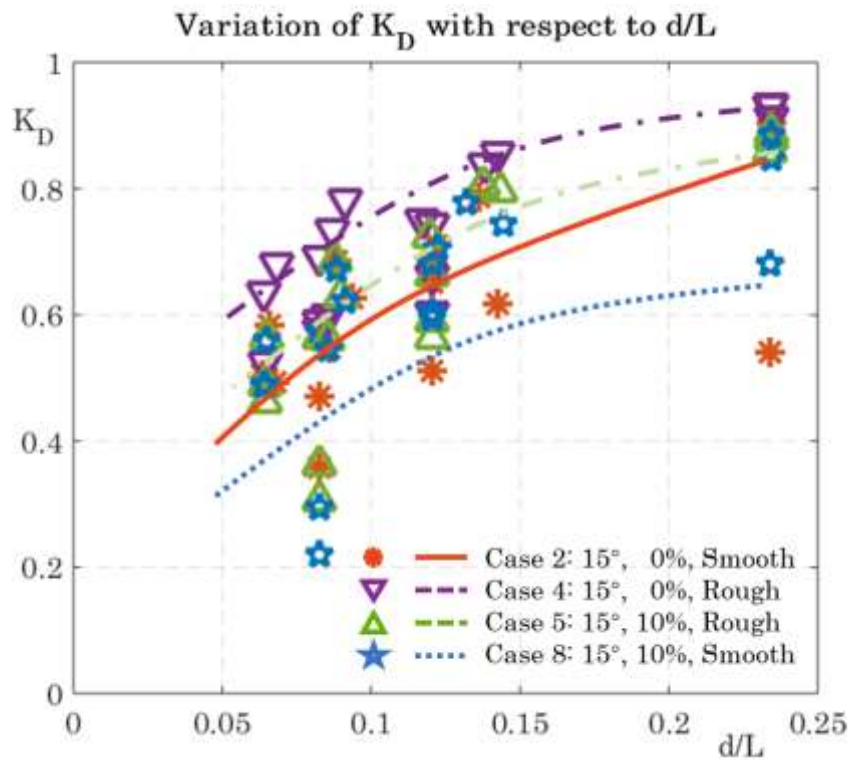
Figure 3-41 Variation of $\mathcal{K}_D$ with Respect to d/L (case 2, 4, 8, 5).

3.4.5 Wave Steepness H_i/L

Wave breaking over plate observation in last section and comparison study above indicate that incident wave height plays a critical role in influencing the wave controlling performance. The former comparison between computed result and experiment results of Aoyama also points to wave breaking due to wave steepness. In this section, wave energy dissipation is estimated with respect to wave steepness, both regular and irregular wave.

With additional purposes considering comparison of different configurations. In the dissipation analysis which shows, the coefficient become convergence when wave steepness become lager. Compared with results in last section which discuss variation of coefficients with respect to d/L, the dissipation of each case in Figure 3-47 shows that wave breaking is enhanced by increasing wave steepness. Fully wave breaking observation in 0.08m and 0.16m incident wave height conditions are scattering in region where wave steepness bigger than the fully-broken red line.
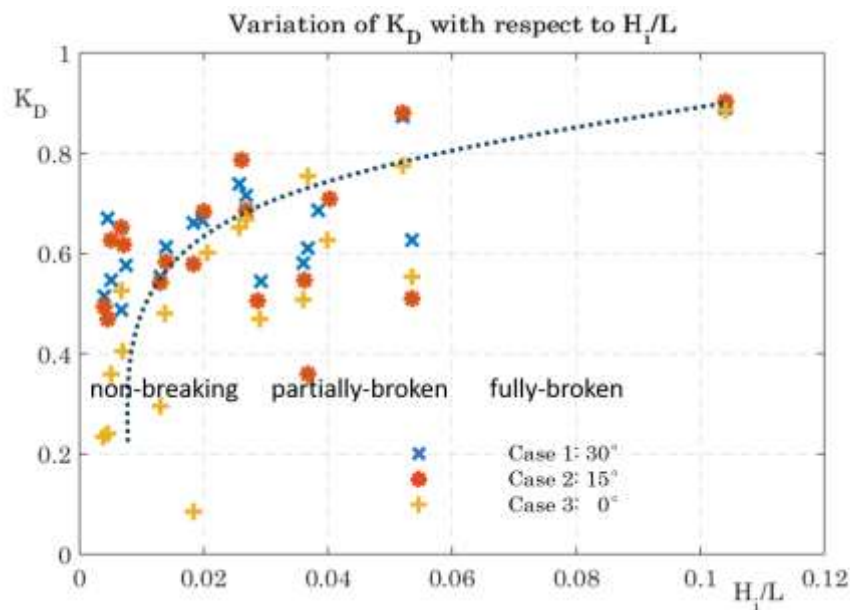
Figure 3-42 Variation of $\mathcal{K}_D$ with Respect to H_i/L (case 1, 2, 3).
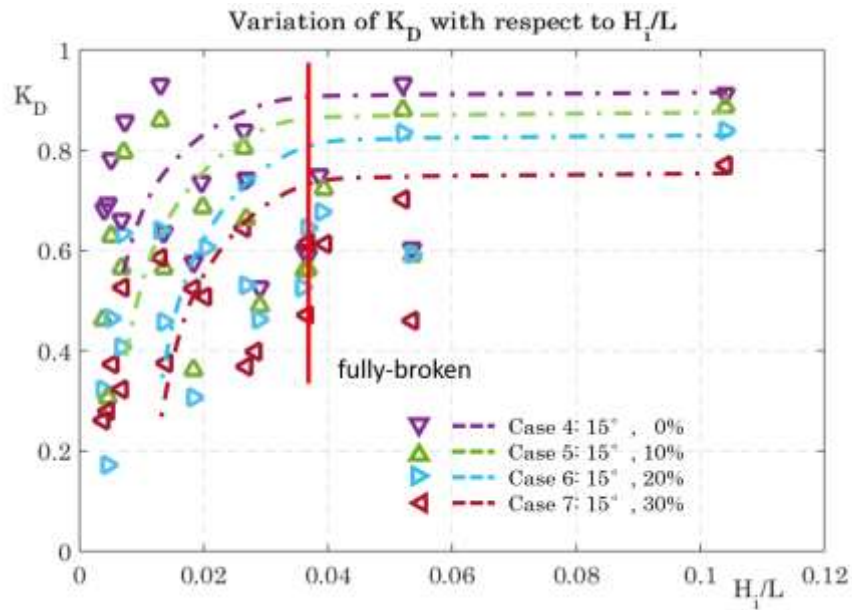
Figure 3-43 Variation of $\mathcal{K}_D$ with Respect to H_i/L (case 4, 5, 6, 7).
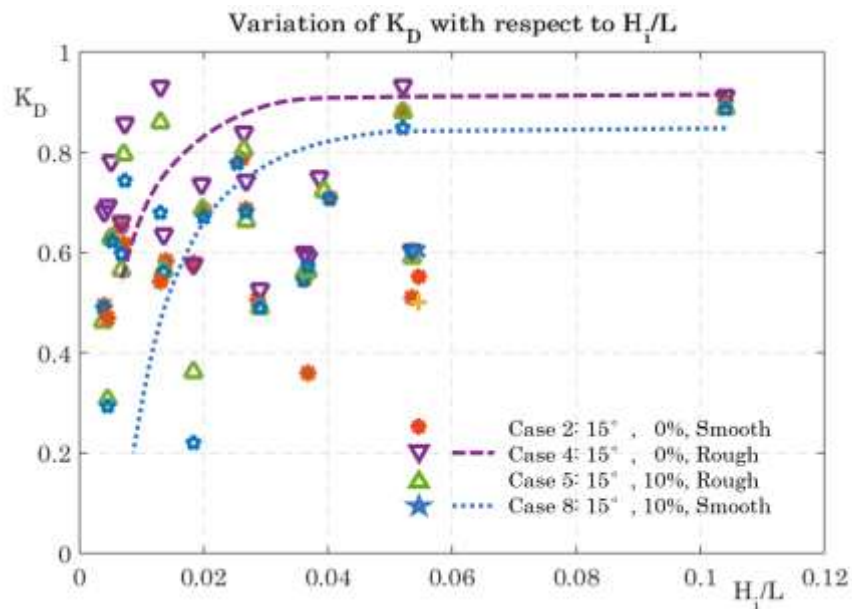
Figure 3-44 Variation of $\mathcal{K}_D$ with Respect to H_i/L (case 2, 4, 8, 5).

3.4.6 Wave Height to Submergence Ratio H_i/D

It is believed that both incident wave height H_i and plate submergence D are important parameters to performance of submerged inclined plate breakwater. Coupled effect of these two parameters is studied below. As plate submergence is constant, wave propagation and their deformation on plate should governed by incident wave height.

While results from Figure 3-45 to 3-47 scatters without a clear pattern, further manually plotted curves show litter information neither. Conclusion is that wave height to submergence ratio H_i/D affect submerged inclined plate breakwater in a very little contend.
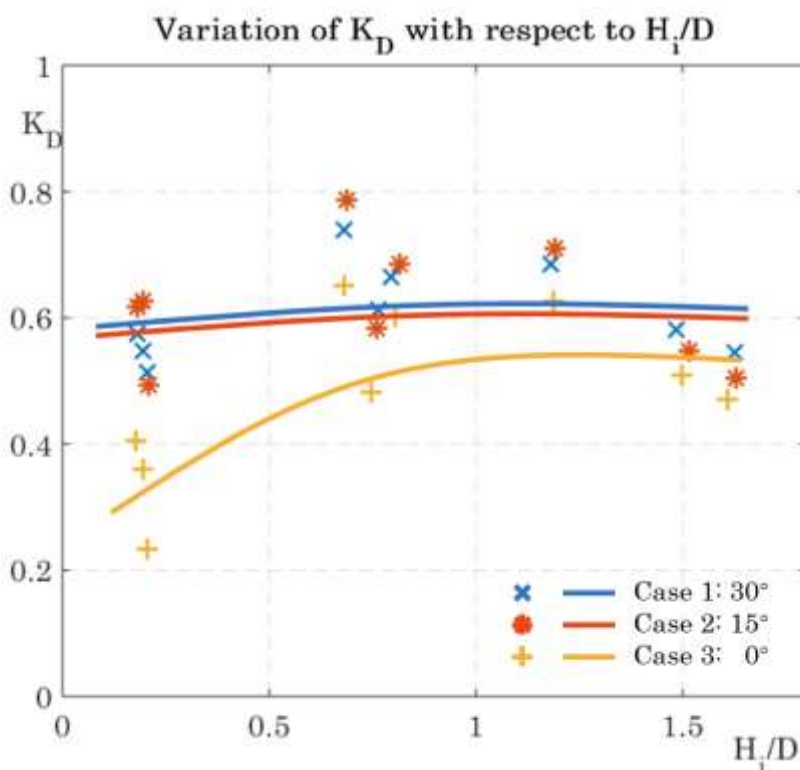
Figure 3-45 Variation of $\mathcal{K}_D$ with Respect to H_i/D (case 1, 2, 3).
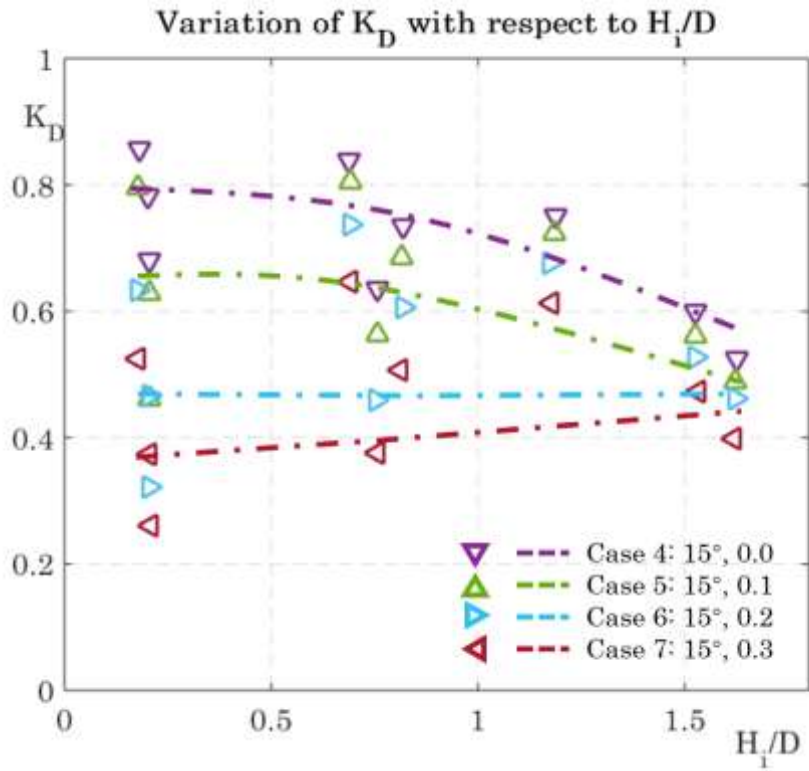
Figure 3-46 Variation of $\mathcal{K}_D$ with Respect to H_i/D (case 4, 5, 6, 7).
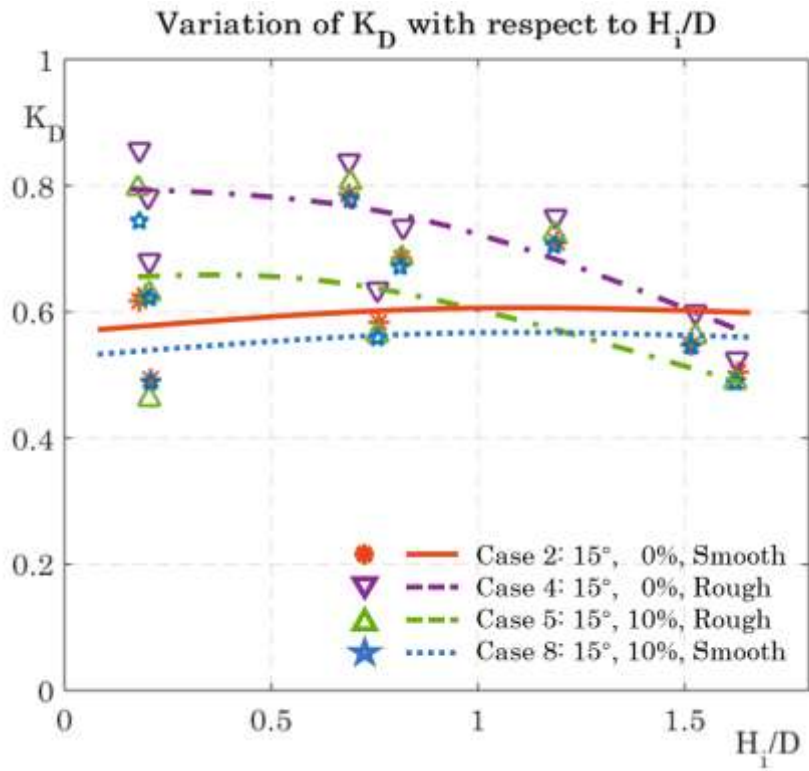
Figure 3-47 Variation of $\mathcal{K}_D$ with Respect to H_i/D (case 2, 4, 8, 5).

3.5 A Tentative Model for Qualitative Analysis

As discussed in preview sections, the wave control performance of submerged inclined plate breakwater is affected by variety of factors, among which, plate inclination θ, roughness $Coef._R$ and porosity $Coef._P$ are discussed as present of configuration of plate; B/L, d/L, H_i/L and H_i/D are also discussed which mainly focus on wave height, wave length and submergence influence. These parameters are, generally speaking, dependent on incident wave and plate geometry. Based on variation tendency with respect to those parameters, a regression analysis of transmission coefficient $\mathcal{K}_T$ and dissipation coefficient $\mathcal{K}_D$ with six non-dimensional parameters was obtained as below formulations in Eq. (3.23).

This regression analysis is based on 72 groups measured data out of total 144 cases, in which all the irregular wave data are utilized as they show good stability for an estimation model. As can be found in Figure 3-22, 3-24, 3-27, 3-30 and 3-32, change of variables will cause predictable changes on transmission and dissipation coefficient, also found on reflection. Meanwhile, circumstance also apply to incident wave characters, especially when discussing the wave steepness and wave depth to wave length ratio.

The estimation orientation formulas which we can call them tentative models for transmission and dissipation estimation show perfect agreement with the measured $\mathcal{K}_T$ and $\mathcal{K}_D$, plots are presented in Figure 3-48 and 3-49. The R squared are 0.82 and 0.66 which mean the square of correlation coefficient between the measured and estimated values, and the absolute root mean square error in the estimation regression analysis are $\pm6.43\%$ and $\pm9.69\%$.

There some points worth mentioning for the application of the tentative models. Constant coefficients of variables tell that wave height and wave length are predominant factors to wave control performance of a submerged inclined
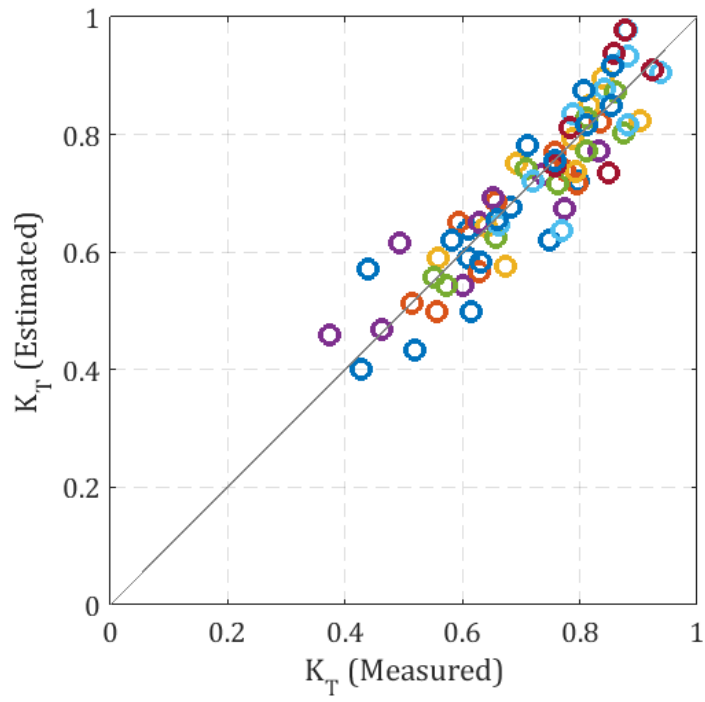
Figure 3-48 Measured $\mathcal{K}_T$ versus Estimated $\mathcal{K}_T$.
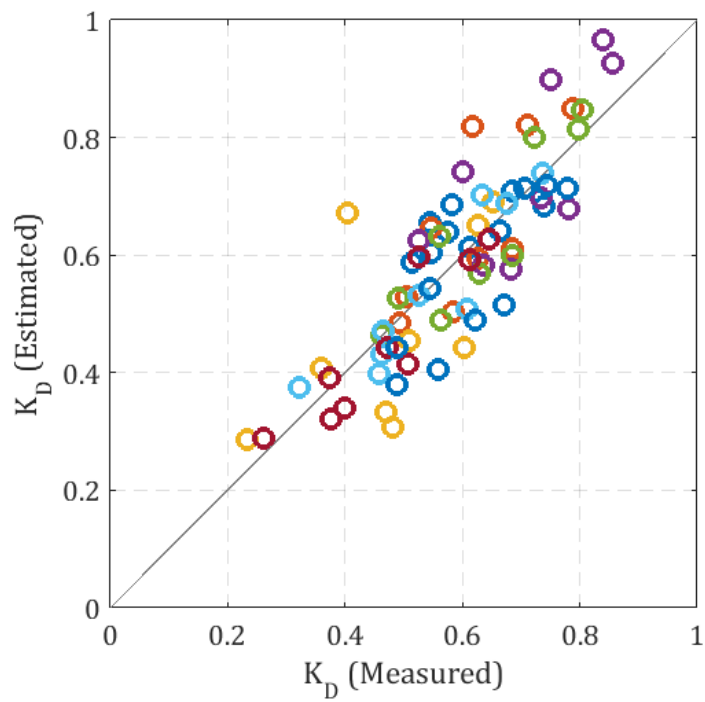
Figure 3-49 Measured $\mathcal{K}_D$ versus Estimated $\mathcal{K}_D$.

plate breakwater when water depth is uniform, it is obvious that the submerged inclined plate breakwater will be more popular in a higher incident wave height and shorter wave length condition. Comparing with incident wave characters, plate geometry is minor on influnence, among variables the plate inclination is dominated variable when plate is solid, as higher porosity does not attribute lower transmission. Plate roughness is helpful on decreasing the transmission coefficient but just in a limit contend, on the contrary roughness will cause more wave breaking so that it can be assumed that plate roughness is more helpful on increasing wave energy dissipation.

The tentative model shows valuable property, coefficients in regression formulas can mirror significant parameters. The most significant is water depth to wave length ratio d/L, the second is the wave steepness H_i/L, as their corresponding coefficients are far bigger than the other one, the wave height to submergence ratio H_i/D. The coefficients in formulas verify experimental results well.

$$\mathcal{K}_T = 2.889 \times \exp\left\{-0.118 \times \tan\theta - 0.017 \times Coef._R + 0.378 \times Coef._P - 0.688 \times \left(\frac{h}{L}\right) - 1.020 \times \left(\frac{H_i}{L}\right)\right.$$

$$\left. -0.078 \times \left(\frac{B}{L}\right) + 0.036 \times \left(\frac{H_i}{D}\right)\right\} - 1.843$$

$$\mathcal{K}_D = 1.074 \times \exp\left\{+0.695 \times \tan\theta + 0.055 \times Coef._R - 0.604 \times Coef._P - 11.417 \times \left(\frac{h}{L}\right) + 1.605 \times \left(\frac{H_i}{L}\right)\right.$$

$$\left. +16.086 \times \left(\frac{B}{L}\right) + 0.001 \times \left(\frac{H_i}{D}\right)\right\} - 1.062$$

$$Coef._R = \begin{cases} 0, & smooth\ plate \\ 1, & rough\ plate \end{cases}$$

$$Coef._P = \begin{cases} 0.0, & solid\ plate\ without\ slot \\ 0.1, & 0.1\ slot\ porosity\ ratio \\ 0.2, & 0.2\ slot\ porosity\ ratio \\ 0.3, & 0.3\ slot\ porosity\ ratio \end{cases}$$

(3.23)

Note: The regression function is only used for tendency analysis in this experiment, not for designing.

Chapter 4
Conclusion

To evaluate the wave deformation over the inclined plate breakwater, analytical model is established and employed for the analysis and the experiment was carried out.

Because the eigenfuction matching method can merely resolve horizontal plate with horizontal and vertical transboundaries, a step-like approximate method is integrated and the reflection and transmission coefficients were obtained to describe wave deformation over plate.

Main results from application of analytical show some conculsions.

- The analytical model shows good agreement on accuracy camparing to the boundary element method and the finite element method, in addition this model also calculate less elements with efficiency.

- Analytical result show inclination and plate submergence dominate performance of submerged inclined plate. Transmission coefficient of the submerged inclined plate breakwater decreases with increase of the submerged plate inclination, and the increasing and decreasing trend are similar in the variation of inclination. And the smaller the plate submergence is, the better the plate deforme incident wave.

- Primery comparisons indicated wave steepness may be another importance vatiable which is important to wave control.

For purpose of discovering dissipation mechanisms, submerged inclined plate breakwater with different cinlination were studied with wave breaking analysis.

- Plate inclination attributes to lower wave transmission meanwhile higher reflection which fits the results of analytical model.

- Propagation process over submerged horizontal plate is consist of two interactions: at the beginning edge of plate, wave profile deformed because of sudden water depth change with a visible wave reflection transmit to incident direction; and the deformed wave crest travels without breaking to the end edge of plate and finally broken until wave over topping to the region behind plate, wave reflection also takes place when wave broken.

- Reflection from the submerged horizontal plateis is different on mechanism compared with the submerged inclined plate, as reflection from horizontal plate is mainly due to partial obstruction of plate foreward edge and the back flow from backward edge.

For purpose of improving submerged inclined plate breakwater, roughness and pososity were studied to increase wave energy dissipation.

- Slots on plate help water mass exchange from the region beneath plate to the region above plate before wave crest travelling to plate; in other words, solid plate attributes to prevent water particles to orbiting by its original way which cause phase lag of wave on both side of plate and wave breaking over plate.

- Plate with roughness causes more disturbance of water wave to generate more chaos which does not allow movement or propagation of wave profile, in other words, roughness attributes to cause wave propagation lag above plate, which makes it easy to break over plate, this effect will significant when incident wave height become higher.

Reference

Alonzo D.,. Q., 1971. Design and construction of ports and marine structures. McGraw-Hill Companies.

Aoyama, K., Kamada, A., Tamaoki, J., and Hayashi, K., 1997. The Design of Breakwater by "PSR" at YOBITO Fishery Harbor. Proceedings of Civil Engineering in the Ocean, 13: 931-936.

Aoyama, T., Isobe, M., Izumiya, S., and Watanabe, A., 1988. Fundamental Study on Wave Control Method by Submerged Horizontal Plate. Proceedings of Japanese Conference on Coastal Engineering.35: 507-511.

Bretschneider, C. L., 1968. Significant waves and wave spectrum. Ocean Industry, 3(2): 44-46.

Cho, I.H. and M.H. Kim, 2008. Wave absorbing system using inclined perforated plates. Journal of Fluid Mechanics, 608: 1-20.

Fujita, R., Higoto, Y., Akiyama, Y., Yoshihara, H., and Ueda, M., 1992. Proceedings of Coastal Engineering, JSCE., 39: 561-565.

Goda, Y., and Suzuki T., 1977. Estimation of incident and reflected waves in random wave experiments." Coastal Engineering 1976. 828-845.

Healy, J.J., 1952. Wave damping effect of beaches. Proc. Int. Hydraulics Convention, 213-220.

Horikawa, K., ed., 1988. Nearshore dynamics and coastal processes: Theory, measurement, and predictive models. University of Tokyo press.

Ijima, T., Ozaki, S., Eguchi Y. and Kobayashi, A., 1970. Breakwater and quay wall by horizontal plates. pp: 1537-1556.

Kawaguchi T., 1986. Nonreflective wave making method using wavefront detection and speed control, Mitsui Zosen Technical Report, No. 128, pp. 20 - 24.

Kimura, H., Nemoto, K., Yamamoto, M., Takagi, N. and Horikoshi, N., 1991.

Construction of inclined plate type wave elimination structure and local wave observation. Proceedings of Coastal Engineering, JSCE., 38: 571-575.

Koraim, A.S., 2013. Hydrodynamic efficiency of suspended horizontal rows of half pipes used as a new type breakwater. Ocean Engineering, 64: 1-22.

Lawrie, J.B. and I.D. Abrahams, 1999. An orthogonality condition for a class of problems with high order boundary conditions: Applications in sound/structure interaction. Q J Mechanics Appl Math, 52(2): 161-181.

Linton, C.M. and P. McIver, 2001. Handbook of mathematical techniques for wave/structure interactions. CRC Press.

Liu, Y., Yao, Z. and Xie, L., 2011. Analysis on the hydrodynamic performance of a submerged Inclined plate breakwater. Sciencepaper Online.

Meylan, M.H. and M.A. Peter, 2009. Water-wave scattering by submerged elastic plates. Q J Mechanics Appl Math: hbp008.

Midya, C., M. Kanoria and B.N. Mandal, 2001. Scattering of water waves by inclined thin plate submerged in finite-depth water. Archive of Applied Mechanics, 71(12): 827-840.

Mitsuyasu, H., 1970. Development of spectra of wind waves (2). The shape of the spectrum of wind waves at a finite blast distance. Proceedings of Japanese Conference on Coastal Engineering.17: 1-7.

Murakami, H., S. Itoh, Y. Hosoi and Y. Sawamura, 1995. Wave induced flow around submerged sloping plates. ASCE American Society Of Civil Engineers, pp: 1454-1454.

Neelamani, S. and R. Rajendran, 2002. Wave interaction with '⊥'-type breakwaters. Ocean Engineering, 29(5): 561-589.

Neelamani, S. and R. Rajendran, 2002. Wave interaction with T-type breakwaters. Ocean Engineering, 29(2): 151-175.

Okubo, H., I. Kojima, Y. Takahashi and H. Moritaka, 1994. Development of new types of breakwaters. Nippon Steel Technical Report. 1994.

Parsons, N.F. and P.A. Martin, 1995. Trapping of water waves by submerged plates using hypersingular integral equations. Journal of Fluid Mechanics, 284: 359-375.

Raichlen, F. and J.-J. Lee, 1978. An inclined-plate wave generator. Coastal Engineering 1978. 388-399.

Rao, S., K.G. Shirlal, R.V. Varghese and K.R. Govindaraja, 2009. Physical model

studies on wave transmission of a submerged inclined plate breakwater. Ocean Engineering, 36(15–16): 1199-1207.

Shirlal, K.G., 2013. Wave transmission of submerged inclined serrated plate breakwater. International Journal of Chemical, Environment Biology Science(1): 657-660.

Sundar, V., R. Sundaravadivelu and S. Purushotham, 2003. Hydrodynamic characteristics of moored floating pipe breakwaters in random waves. Proceedings of the Institution of Mechanical Engineers, Part M: Journal of Engineering for the Maritime Environment, 217(2): 95-110.

Teh, H.M. and H. Ismail, 2013. Performance evaluation of arrays of stepped-slope floating breakwater. In: 2013 IEEE Business Engineering and Industrial Applications Colloquium (BEIAC). pp: 279-283.

Wang, K.-H. and Q. Shen, 1999. Wave motion over a group of submerged horizontal plates. International journal of engineering science, 37(6): 703-715.

Wu, Y.C., 1988. Waves generated by an inclined-plate wave generator. International journal for numerical methods in fluids, 8(7): 803-811.

Yagci, O., V.S.O. Kirca and L. Acanal, 2014. Wave attenuation and flow kinematics of an inclined thin plate acting as an alternative coastal protection structure. Applied Ocean Research, 48: 214-226.

Yu, X., 1990. Study on wave transformation over submerged plate. University of Tokyo, Tokyo, Japan.

Yu, X., 1995. Patching methods for the analysis of wave motion over a submerged plate. Nagasaki University Faculty of Engineering Research Report, 25(44): 35-42.

Yu, X., 2002. Functional performance of a submerged and essentially horizontal plate for offshore wave control: A review. Coastal Engineering Journal, 44(02): 127-147.

Yu, X., M. Isobe and A. Watanabe, 1995. Wave breaking over submerged horizontal plate. Journal of waterway, port, coastal, and ocean engineering, 121(2): 105-113.

Appendix

Appendix A The Solution to Complex Linear Dispersion

In free surface water regions, the linear dispersion relation can be described as below in Eq. A.1.

$$\alpha + k_n \tan k_n h = 0 \quad n = 0, 1, 2 \cdots \tag{A.1}$$

where the k_n is roots of dispersion relation equation; $\{\pm k_0;\}$ are a pair of imaginary roots; $\{\pm k_n; n = 1, 2, 3 \cdots\}$ are positive real roots and negative roots.

In addition, the real root of linear dispersion relation distribution can be confirmed that $k_n h \in \left((n - 1/2\,\pi), n\pi\right)$, which means the real roots uniformly lie on the x-axis in nearly each $1/2\,\pi$ distance.

For convenience, we give a form of a function as

$$\mathcal{D}(\alpha, k_n, h) = (\alpha h) + (k_n h)\,\tan(k_n h) \quad n = 0, 1, 2 \cdots \tag{A.2}$$

where $k_n h$ can be regarded as a dimensionless wavenumber.

Then Eq. A.2 becomes a none dimensional equation.

$$\mathcal{D}(\hat{\alpha}, \hat{k}_n) = (\hat{\alpha}) + (\hat{k}_n)\,\tan(\hat{k}_n) \quad 0, 1, 2 \cdots \tag{A.3}$$

It is a circumstance of roots approximations, and the Newton-Raphson method are a successively tool to the approach.

The idea of method is starting an initial guess which is close enough to the root, then by re-approximating the x-intercepts of tangent line of the function, the value of x when then tangent line cross to x-axis, and the new x-intercept is then used as the new guess.

Solving for $\hat{k}_{n+1}$, when $\hat{k}_1$ is an initial guess, then gives one root approximately.

$$\hat{k}_{n+1} = \hat{k}_n - \frac{\hat{k}_n \tan \hat{k}_n + \hat{\alpha}}{\tan \hat{k}_n + \hat{k}_n \sec^2 \hat{k}_n} \qquad (A.4)$$

While it is worth to say that finding a good initial guess value is another very important issue and the dispersion relation tells that $k_n h \in \left((n - 1/2\,\pi), n\pi\right)$ are reasonable guess for this method. It is very worth to note that the value of $\hat{\alpha}$ affect the difficulty of approximate when processing on computer, as when $\hat{\alpha}$ is enough, for example, the roots $k_n h$ lie much closer to $n\pi$ when $\hat{\alpha}$ is 0.01 than 1.00.
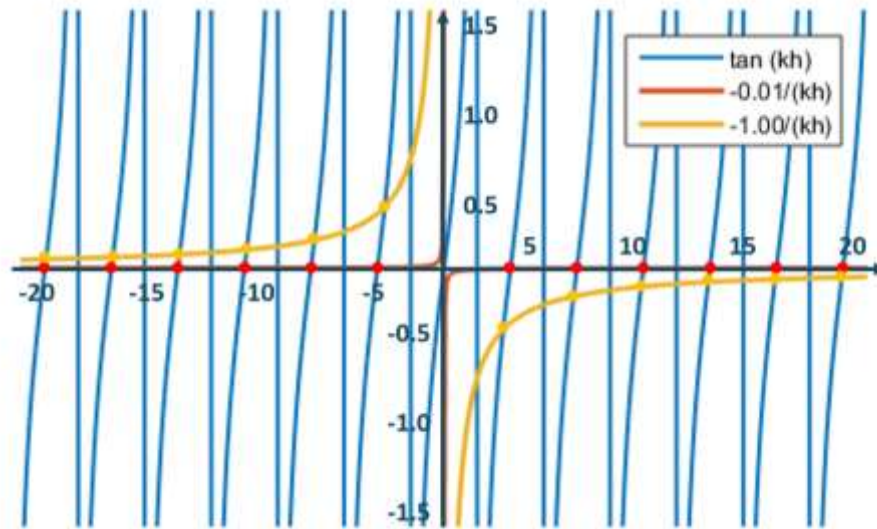
Figure A-1   Locations of Dispersion Real Roots for Different $\hat{\alpha}$
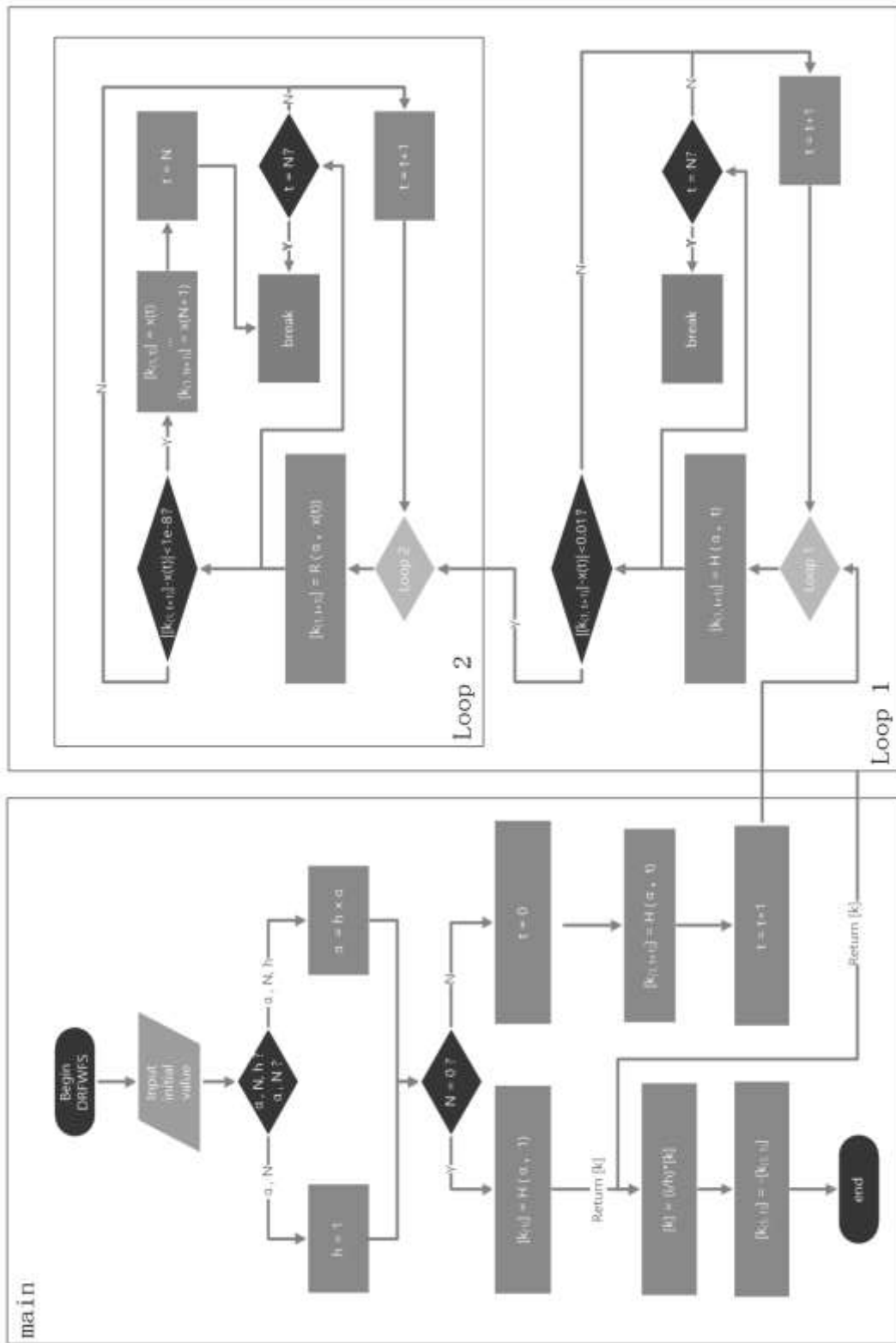
Figure A-2 Outline of Dispersion Relation for Free Water Surface.

Appendix B   The Application of Eigenfunctions Orthogonality

Substituting the matching boundary conditions into general expressions of velocity potential and replace the infinity of the upper limits of summation by a finite number N, which means the amount of evanescent wave we chose and follows to $N = N_A + N_B + 1$, and one should notice that $N_A / N_B = d / (h - d)$, then we have Eq. (A. 5),

$$\mathcal{A}_0 Z(k_0^h z) + \sum_{n=0}^{N} \mathcal{B}_n Z(k_n^h z) = \begin{cases} \displaystyle\sum_{n=0}^{N_A} \left(\mathcal{C}_n + \mathcal{D}_n e^{-2k_n^d L} \right) Z(k_n^d z), & -d < z < 0 \\ \displaystyle\sum_{n=0}^{N_B} (\mathcal{E}_n + \mathcal{F}_n e^{-2\lambda_n L}) Z(\lambda_n z), & -h < z < -d \end{cases}$$

$$-k_0^h \mathcal{A}_0 Z(k_0^h z) + \sum_{n=0}^{N} k_n^h \mathcal{B}_n Z(k_n^h z) = \begin{cases} \displaystyle\sum_{n=0}^{N_A} k_n^d \left(-\mathcal{C}_n + \mathcal{D}_n e^{-2k_n^d L} \right) Z(k_n^d z), & -d < z < 0 \\ \displaystyle\sum_{n=0}^{N_B} \lambda_n(-\mathcal{E}_n + \mathcal{F}_n e^{-2\lambda_n L}) Z(\lambda_n z), & -h < z < -d \end{cases}$$

(A.5)

$$\sum_{n=0}^{N} \mathcal{G}_n Z(k_n^h z) = \begin{cases} \displaystyle\sum_{n=0}^{N_A} \left(\mathcal{C}_n e^{-2k_n^d L} + \mathcal{D}_n \right) Z(k_n^d z), & -d < z < 0 \\ \displaystyle\sum_{n=0}^{N_B} (\mathcal{E}_n e^{-2\lambda_n L} + \mathcal{F}_n) Z(\lambda_n z), & -h < z < -d \end{cases}$$

$$\sum_{n=0}^{N} -k_n^h \mathcal{G}_n Z(k_n^h z) = \begin{cases} \displaystyle\sum_{n=0}^{N_A} k_n^d \left(-\mathcal{C}_n e^{-2k_n^d L} + \mathcal{D}_n \right) Z(k_n^d z), & -d < z < 0 \\ \displaystyle\sum_{n=0}^{N_B} k_n^d(-\mathcal{E}_n e^{-2\lambda_n L} + \mathcal{F}_n) Z(\lambda_n z), & -h < z < -d \end{cases}$$

Expanding all expressions, we can multiply each equation by $Z(k_m^h z)$ and integrate them from $-d$ to 0 or $-h$ to $-d$ separately, and m is a coefficient of height mode.

for $-d < z < 0$ and $m = 0, 1, 2, \cdots, N_A$,

$$\int_{-d}^{0}\left[\mathcal{A}_0 Z(k_0^h z) + \sum_{n=0}^{N_A} \mathcal{B}_n Z(k_n^h z)\right] Z(k_m^h z)\mathrm{d}z = \int_{-d}^{0}\left[\sum_{n=0}^{N_A}(\mathcal{C}_n + \mathcal{D}_n e^{-2k_n^d L}) Z(k_n^d z)\right] Z(k_m^h z)\mathrm{d}z$$

$$\int_{-d}^{0}\left[-k_0^h \mathcal{A}_0 Z(k_0^h z) + \sum_{n=0}^{N_A} k_n^h \mathcal{B}_n Z(k_n^h z)\right] Z(k_m^h z)\mathrm{d}z = \int_{-d}^{0}\left[\sum_{n=0}^{N_A} k_n^d\big(-\mathcal{C}_n + \mathcal{D}_n e^{-2k_n^d L}\big) Z(k_n^d z)\right] Z(k_m^h z)dz$$

$$\int_{-d}^{0}\left[\sum_{n=0}^{N_A} \mathcal{G}_n Z(k_n^h z)\right] Z(k_m^h z)\mathrm{d}z = \int_{-d}^{0}\left[\sum_{n=0}^{N_A}(\mathcal{C}_n e^{-2k_n^d L} + \mathcal{D}_n) Z(k_n^d z)\right] Z(k_m^h z)\mathrm{d}z$$

$$\int_{-d}^{0}\left[\sum_{n=0}^{N_A} -k_n^h \mathcal{G}_n Z(k_n^h z)\right] Z(k_m^h z)\mathrm{d}z = \int_{-d}^{0}\left[\sum_{n=0}^{N_A} k_n^d(-\mathcal{C}_n e^{-2k_n^d L} + \mathcal{D}_n) Z(k_n^d z)\right] Z(k_m^h z)dz$$

(A.6)

and for $-h < z < -d$ and $m = N_A + 1, N_A + 2, N_A + 3, \cdots, N$.

$$\int_{-h}^{-d}\left[\mathcal{A}_0 Z(k_0^h z) + \sum_{n=0}^{N_B} \mathcal{B}_n Z(k_n^h z)\right] Z(k_m^h z)\mathrm{d}z = \int_{-h}^{-d}\left[\sum_{n=0}^{N_B}(\mathcal{E}_n + \mathcal{F}_n e^{-2\lambda_n L}) Z(\lambda_n z)\right] Z(k_m^h z)dz$$

$$\int_{-h}^{-d}\left[-k_0^h \mathcal{A}_0 Z(k_0^h z) + \sum_{n=0}^{N_B} k_n^h \mathcal{B}_n Z(k_n^h z)\right] Z(k_m^h z)\mathrm{d}z = \int_{-d}^{0}\left[\sum_{n=0}^{N_B} \lambda_n\big(-\mathcal{E}_n + \mathcal{F}_n e^{-2\lambda_n L}\big) Z(\lambda_n z)\right] Z(k_m^h z)dz$$

(A.7)

$$\int_{-h}^{-d}\left[\sum_{n=0}^{N_B} \mathcal{G}_n Z(k_n^h z)\right] Z(k_m^h z)\mathrm{d}z = \int_{-h}^{-d}\left[\sum_{n=0}^{N_B}(\mathcal{E}_n e^{-2\lambda_n L} + \mathcal{F}_n) Z(\lambda_n z)\right] Z(k_m^h z)dz$$

$$\int_{-h}^{-d}\left[\sum_{n=0}^{N_B} -k_n^h \mathcal{G}_n Z(k_n^h z)\right] Z(k_m^h z)\mathrm{d}z = \int_{-h}^{-d}\left[\sum_{n=0}^{N_B} k_n^d(-\mathcal{E}_n e^{-2\lambda_n L} + \mathcal{F}_n) Z(\lambda_n z)\right] Z(k_m^h z)dz$$

We can combine the Eq. (A. 6) and Eq. (A. 7), which have similar forms in two different ranges, into a new equation by defining the eigenfunctions as the Eq. (A. 8) shows,

$$\mathrm{E}(\kappa_n z) = \begin{cases} \mathrm{Z}(k_n^d z), & -d < z < 0 \\[2mm] \mathrm{Z}(\lambda_n z), & -h < z \le d \end{cases}$$

(A.8)

where,

$$\kappa_n = \begin{cases} k_n^d, & -d < z < 0 \\[2mm] \lambda_n, & -h < z \leq d \end{cases} \tag{A.9}$$

the equation set can be rewrite as Eq. (A. 10),

$$\int_{-h}^{0}\left[\mathcal{A}_0 Z(k_0^h z) + \sum_{n=0}^{N}\mathcal{B}_n Z(k_n^h z)\right]Z(k_m^h z)\mathrm{d}z = \int_{-h}^{0}\left[\sum_{n=0}^{N}(\mathcal{S}_n^{\mathcal{CE}} + \mathcal{T}_n^{\mathcal{DF}}e^{-2\kappa_n L})\mathrm{E}(\kappa_n z)\right]Z(k_m^h z)\mathrm{d}z$$

$$\int_{-h}^{0}\left[-k_0^h\mathcal{A}_0 Z(k_0^h z) + \sum_{n=0}^{N}k_n^h\mathcal{B}_n Z(k_n^h z)\right]Z(k_m^h z)\mathrm{d}z = \int_{-h}^{0}\left[\sum_{n=0}^{N}\kappa_n(-\mathcal{S}_n^{\mathcal{CE}} + \mathcal{T}_n^{\mathcal{DF}}e^{-2\kappa_n L})\mathrm{E}(\kappa_n z)\right]Z(k_m^h z)dz$$

$$\tag{A.10}$$

$$\int_{-h}^{0}\left[\sum_{n=0}^{N}\mathcal{G}_n Z(k_n^h z)\right]Z(k_m^h z)\mathrm{d}z = \int_{-h}^{0}\left[\sum_{n=0}^{N}(\mathcal{S}_n^{\mathcal{CE}}e^{-2\kappa_n L} + \mathcal{T}_n^{\mathcal{DF}})\mathrm{E}(\kappa_n z)\right]Z(k_m^h z)dz$$

$$\int_{-h}^{0}\left[\sum_{n=0}^{N}-k_n^h\mathcal{G}_n Z(k_n^h z)\right]Z(k_m^h z)\mathrm{d}z = \int_{-h}^{0}\left[\sum_{n=0}^{N}\kappa_n(-\mathcal{S}_n^{\mathcal{CE}}e^{-2\kappa_n L} + \mathcal{T}_n^{\mathcal{DF}})\mathrm{E}(\kappa_n z)\right]Z(k_m^h z)dz$$

where,

$$\sum_{n=0}^{N}\mathcal{S}_n^{\mathcal{CE}} = \begin{cases} \displaystyle\sum_{n=0}^{N_A}\mathcal{C}_n, & -d < z < 0 \\[4mm] \displaystyle\sum_{n=0}^{N_B}\mathcal{E}_n, & -h < z \leq d \end{cases}$$

$$\tag{A.11}$$

$$\sum_{n=0}^{N}\mathcal{T}_n^{\mathcal{DF}} = \begin{cases} \displaystyle\sum_{n=0}^{N_A}\mathcal{D}_n, & -d < z < 0 \\[4mm] \displaystyle\sum_{n=0}^{N_B}\mathcal{F}_n, & -h < z \leq d \end{cases}$$

Here one key point should note that the eigenfunctions are orthogonal, this can be used to simplify the result of integration.

$$\int_{-h}^{0} Z(k_n z)\, Z(k_m z)\mathrm{d}z = \mathcal{X}_n \delta_{nm}$$

$$\int_{-h}^{-d} Z(\lambda_n z)\, Z(\lambda_m z)\mathrm{d}z = \mathcal{Z}_n \delta_{nm}$$

(A.12)

$$\int_{-h}^{0} E(\kappa_n z)\, Z(k_m^h z)\mathrm{d}z = \mathcal{Y}_{nm} = \begin{cases} \displaystyle\int_{-d}^{0} Z(k_m^d z)\, Z(k_m^h z)\mathrm{d}z, & -d < z < 0 \\[4mm] \displaystyle\int_{-h}^{-d} Z(\lambda_n z)\, Z(k_m^h z)\mathrm{d}z, & -h < z \le d \end{cases}$$

where,

$$\mathcal{X}_n = \frac{h}{2\cos^2 k_n h}\left(\frac{\sin 2k_n h}{2k_n h} + 1\right)$$

(A.13)

$$\mathcal{Z}_n = \begin{cases} h - d, & n = 0 \\ \dfrac{1}{2}(h - d), & n \neq 0 \end{cases}$$

and δ_{mn} is called 'Kronecker delta' defined by $\delta_{nm} = 1$ if $n = m$, and $\delta_{nm} = 0$ if $n \neq m$.

Appendix C   General Approach to Submerged Inclined Plate Model

Process of computation based on frequency domain analysis of wave and plate interaction in the assumption of linear wave potential theory can be explained through several initial variables definition which refer to plate state conditions, wave state conditions and the discrete number of inclined plate. In addition to the normal signal horizontal plate modelling problem, coupled consideration for inclined plate is applied in model and accomplished for further observation of velocity and wave profile deformation.
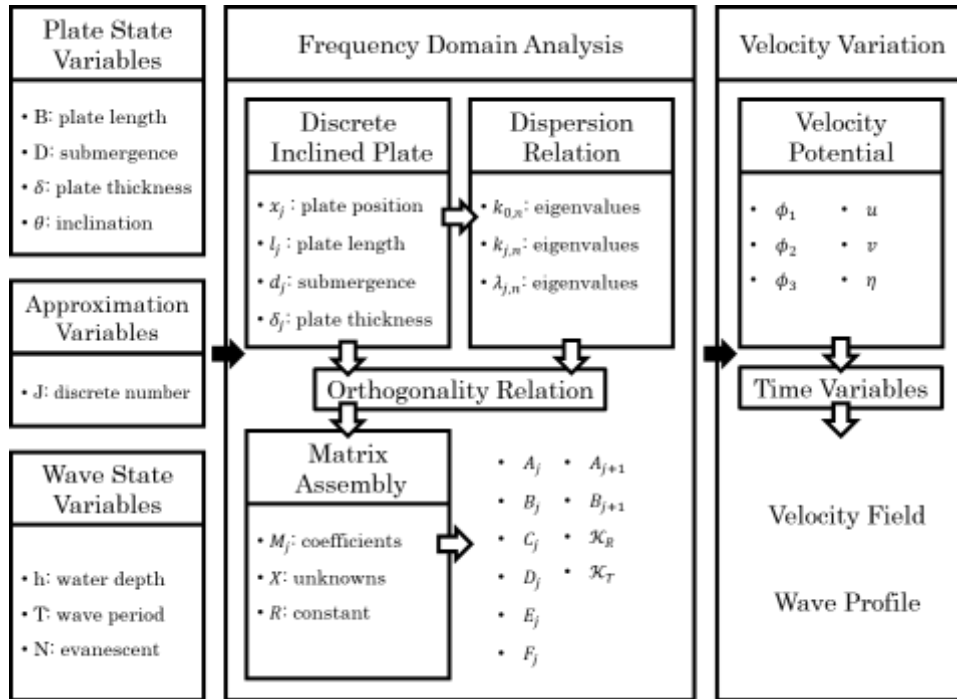
Figure A-3   Schematic Diagram of Modelling Processes.

The codes for computational comprise several main modules and the logical relation for variables and their results are shown in diagram in Figure A-3.

decreat.m

```matlab
function P = decreat(L,hm,th,in,J,r)

% By Y. WANG @TUMSAT Jan.2017.

% INPUTs
% L: The total length of plate.
% hm: The submergence of the middle point of plate.
% th: The thickness of each part of plates, assuming uniform.
% in: The slope of the plate, denote by %% in = tan alpha %%.
% J: The number of plate.
% r: Mean Porosity when considering gap between plates.
% q: (length of 1st gap)/(length of 1st plate).
% q=(r/(J-1))*(J/(1-r))
% r=(q*(J-1))/(J+q*(J-1))

% OUTPUTs
% P:  The patameters of plates.
% P = [submergence, plate length, plate thickness, midpoint coordinate]

if nargin == 5
    r = 0;
end
counts = J - 1;
hestep = L * in / J;
if counts == 0;
    lestep = 0;
else
    lestep = L * (1-r) / J + L * r / counts;
end
leinit = L * (1-r) / J /2;
if (mod(counts,2) == 0)
    heinit = hm - hestep * (counts / 2);
    else
        heinit = hm - hestep * ((J / 2 - 1) + 0.5);
end
dj = zeros(J,1);
xj = zeros(J,1);
for i=1:J;
    dj(i,1) = heinit + (i-1) * hestep;
    xj(i,1) = leinit + (i-1) * lestep;
end
lj = ones(J,1) * L * (1-r) / J;
tj = ones(J,1) *th;
P(:,1) = dj;
P(:,2) = lj;
P(:,3) = tj;
P(:,4) = xj;
```

dispersion_free_surface.m

```matlab
function mroots = dispersion_free_surface(alpha,N,h)

% calculates positive imaginary and N first positive real solutions of
alpha = k*tanh(k h)
% Modified by Y. WANG @TUMSAT @June, 2016.
% Codes from
https://www.math.auckland.ac.nz/~meylan/code/dispersion/dispersion_free_s
urface.m
% guess with linear expansion and a linear expansion.
% The first roots are positive imaginary and the next are the first N
positive real ordered from smallest.

% maincode
% If the value for h is not given the default value is h = 1; it would be
easy to write a much faster program for only real alpha
if nargin == 2
    h = 1;
else
    alpha = h*alpha;
end
mroots = zeros(1,N+1);
if N ==0;
    count = 0;
    mroots(count+1) = homotopy(alpha,count);
else
    count = 0;
    mroots(count+1) = homotopy(alpha,count);
    count = count + 1;
    while 0 <= 1
        mroots(count+1) = homotopy(alpha,count);
        if abs(mroots(count + 1) - (1i*count*pi + alpha/(1i*count*pi))) <
0.01
            while 0 <=1
                mroots(count + 1) = oneroot(alpha,1i*count*pi +
alpha/(1i*count*pi));
                if abs(mroots(count + 1) - (1i*count*pi +
alpha/(1i*count*pi))) < 1e-8
                    mroots(count+1:N+1) = 1i*(count:N)*pi +
alpha./(1i*(count:N)*pi);
                    count = N;
                    break
                end
                if count ==N
                    break
                end
                count = count + 1;
            end
        end
        if count == N
            break
        end
        count = count +1;
    end

end
mroots = -1i/h*mroots;
```

```matlab
% subcode 01
function mroot = homotopy(alpha,N)
if N == 0;
   mroot = oneroot(1,1);
else
   mroot = oneroot(1,1i*N*pi);
end
step =0.05;
if abs(alpha) < 1
    alphastep = ([1:-step:abs(alpha),abs(alpha)]);
else
    alphastep = ([1:step:abs(alpha),abs(alpha)]);
end

for k=2:length(alphastep)
        mroot = oneroot(alphastep(k),mroot);
end

if angle(alpha) > 0
    alphastep = abs(alpha)*exp(1i*[0:pi/30:angle(alpha),angle(alpha)]);
else
    alphastep = abs(alpha)*exp(1i*[0:-pi/30:angle(alpha),angle(alpha)]);
end

for k=2:length(alphastep)
   mroot = oneroot(alphastep(k),mroot);
end

% subcode 02
function out = oneroot(alpha,guess)

ans1 = guess+1;
out = guess;
while abs(ans1 - out) > 1e-9
    ans1 = out;
    out = ans1 - f(ans1,alpha)/difff(ans1);
end

% subcode 03
function out = f(z,alpha)
out = z*tanh(z) - alpha;

% subcode 04
function out = difff(z)
out = tanh(z) + z*sech(z).^2;
```

big_matrix.m

```matlab
function M = big_matrix(J,N,ka0,kaj,laj,xl,xr,iz,il,ie,ez,el,ze,le)

% By Y. WANG @TUMSAT Oct.2016.

% INPUTs
% J:     The number of plate.
% N:     The number of evanescent wave modes.
% ka0:   Wavenumber for free water which depth is h.
% kaj:   Wavenumber for free water which depth is dj.
% laj:   Wavenumber for water beneath plate.
% xl:    Boundary calculate coordinate in left side of plate.
% xr:    Boundary calculate coordinate in right side of plate.

% OUTPUTs
% M: Matrix for Aj_n, Bj_n, Cj_n, Dj_n, Ej_n, Fj_n, Aj+1_n and Bj_n+1.

kayser0 = ka0;
kayserj = kaj;
lambdaj = laj;
xjl = xl;
xjr = xr;
IZ = iz;
IL = il;
IE = ie;
EZ = ez;
EL = el;
ZE = ze;
LE = le;
M = zeros((6*J+2)*(N+1),(6*J+2)*(N+1)+1);

% In M, values are arranged below, for example J = 1.
%%%%%%%%%%%%%%%%%%%%%%%%%%%%%%%%%%%%%%%%%%%%%%%%%%%%%%%%%%%%%%%%%%%%%%%
%      Aj_0-N  Bj_0-N  Cj_0-N  Dj_0-N  Ej_0-N  Fj_0-N  Aj+1_0-N  Bj+1_0-N
%%%%%%%%%%%%%%%%%%%%%%%%%%%%%%%%%%%%%%%%%%%%%%%%%%%%%%%%%%%%%%%%%%%%%%%
% Eqs 1   M21     M22     M23     M24     0.0     0.0     0.0       0.0
% Eqs 2   M31     M32     0.0     0.0     M35     M36     0.0       0.0
% Eqs 3   M11     M12     M13     M14     M15     M16     0.0       0.0
% Eqs 4   0.0     0.0     M43     M44     0.0     0.0     M47       M48
% Eqs 5   0.0     0.0     0.0     0.0     M55     M56     M67       M58
% Eqs 6   0.0     0.0     M63     M64     M65     M66     M67       M68
% incid   M71     0.0     0.0     0.0     0.0     0.0     0.0       0.0
% refle   0.0     0.0     0.0     0.0     0.0     0.0     0.0       M88
%%%%%%%%%%%%%%%%%%%%%%%%%%%%%%%%%%%%%%%%%%%%%%%%%%%%%%%%%%%%%%%%%%%%%%%
zero = zeros(N+1,N+1,J);
% In matrix Mxx values are in this table.
%%%%%%%%%%%%%%%%%%%%%%%%%%%%%%%%%%%%%%%%%%%%%%%%%%%
%          n=0   n=1   n=2   n=3    ...    n=N
%%%%%%%%%%%%%%%%%%%%%%%%%%%%%%%%%%%%%%%%%%%%%%%%%%%
%   m=0
%   m=1
%   m=2
%   m=3
%   ...
%   m=M
%%%%%%%%%%%%%%%%%%%%%%%%%%%%%%%%%%%%%%%%%%%%%%%%%%%
% Mxx is consist of R, S or T which are consist of r, s or t.
% rr, ss or tt are eigenfunctions results which is decided by j, m and n.
```

```matlab
R1 = zero;   R2 = zero;   R3 = zero;
S1 = zero;   S2 = zero;
T1 = zero;   T3 = zero;
for j = 1:J;
    for n =1:N+1;
        R1(:,n,j) = IE(:,n,j)*kayser0(1,n);
        R2(:,n,j) = ZE(:,n,j)*kayserj(j,n);
        R3(:,n,j) = LE(:,n,j)*lambdaj(j,n);

        S1(:,n,j) = EZ(:,n,j);
        S2(:,n,j) = IZ(:,n,j);

        T1(:,n,j) = EL(:,n,j);
        T3(:,n,j) = IL(:,n,j);
    end
end

for j = 1:J;
    for m = 0:N;
        for n = 0:N;
            % For left potential matching equation in region 1 2.
            % They will in the 1st row.
            M((6*j-6)*(N+1)+(m+1),(6*j-6)*(N+1)+(n+1)) =
S1(m+1,n+1,j)*(exp(-1*kayser0(1,n+1)*xjl(j)))                    *(-1);%A
            M((6*j-6)*(N+1)+(m+1),(6*j-5)*(N+1)+(n+1)) =
S1(m+1,n+1,j)*(exp(+1*kayser0(1,n+1)*xjl(j)))                    *(-1);%B
            M((6*j-6)*(N+1)+(m+1),(6*j-4)*(N+1)+(n+1)) =
S2(m+1,n+1,j)*(exp(-1*kayserj(j,n+1)*xjl(j)))  *(-1)             *(-1);%C
            M((6*j-6)*(N+1)+(m+1),(6*j-3)*(N+1)+(n+1)) =
S2(m+1,n+1,j)*(exp(+1*kayserj(j,n+1)*xjl(j)))  *(-1)             *(-1);%D

            % For left potential matching equation in region 1 3.
            % They will in the 2nd row.
            M((6*j-5)*(N+1)+(m+1),(6*j-6)*(N+1)+(n+1)) =
T1(m+1,n+1,j)*(exp(-1*kayser0(1,n+1)*xjl(j)));                       %A
            M((6*j-5)*(N+1)+(m+1),(6*j-5)*(N+1)+(n+1)) =
T1(m+1,n+1,j)*(exp(+1*kayser0(1,n+1)*xjl(j)));                       %B
            M((6*j-5)*(N+1)+(m+1),(6*j-2)*(N+1)+(n+1)) =
T3(m+1,n+1,j)*(exp(-1*lambdaj(j,n+1)*xjl(j)))  *(-1);                %E
            M((6*j-5)*(N+1)+(m+1),(6*j-1)*(N+1)+(n+1)) =
T3(m+1,n+1,j)*(exp(+1*lambdaj(j,n+1)*xjl(j)))  *(-1);                %F
            M((6*j-5)*(N+1)+(m+1),(6*j-1)*(N+1)+(0+1)) =
T3(m+1,0+1,j)*(exp(+1*lambdaj(j,0+1)*xjl(j)))* xjl(j)*(-
1);             %F0  A SPECIAL PLACE

            % For left velocity matching equation in region 1 2 3.
            % They will in the 3rd row.
            M((6*j-4)*(N+1)+(m+1),(6*j-6)*(N+1)+(n+1)) =
R1(m+1,n+1,j)*(exp(-1*kayser0(1,n+1)*xjl(j)))          *(-1);        %A
            M((6*j-4)*(N+1)+(m+1),(6*j-5)*(N+1)+(n+1)) =
R1(m+1,n+1,j)*(exp(+1*kayser0(1,n+1)*xjl(j)));                       %B
            M((6*j-4)*(N+1)+(m+1),(6*j-4)*(N+1)+(n+1)) =
R2(m+1,n+1,j)*(exp(-1*kayserj(j,n+1)*xjl(j)))  *(-1)    *(-1);       %C
            M((6*j-4)*(N+1)+(m+1),(6*j-3)*(N+1)+(n+1)) =
R2(m+1,n+1,j)*(exp(+1*kayserj(j,n+1)*xjl(j)))  *(-1);                %D
            M((6*j-4)*(N+1)+(m+1),(6*j-2)*(N+1)+(n+1)) =
R3(m+1,n+1,j)*(exp(-1*lambdaj(j,n+1)*xjl(j)))  *(-1)    *(-1);       %E
            M((6*j-4)*(N+1)+(m+1),(6*j-1)*(N+1)+(n+1)) =
R3(m+1,n+1,j)*(exp(+1*lambdaj(j,n+1)*xjl(j)))  *(-1);                %F
```

```
            M((6*j-4)*(N+1)+(m+1),(6*j-1)*(N+1)+(0+1)) =
LE(m+1,0+1,j)*(exp(+1*lambdaj(j,0+1)*xjl(j)))  *(-
1);                    %F0   A SPECIAL PLACE

            % For right potential matching equation in region 1 2.
            % They will in the 4th row.
            M((6*j-3)*(N+1)+(m+1),(6*j-4)*(N+1)+(n+1)) =
S2(m+1,n+1,j)*(exp(-1*kayserj(j,n+1)*xjr(j)))  *(-1)              *(-1);%C
            M((6*j-3)*(N+1)+(m+1),(6*j-3)*(N+1)+(n+1)) =
S2(m+1,n+1,j)*(exp(+1*kayserj(j,n+1)*xjr(j)))  *(-1)              *(-1);%D
            M((6*j-3)*(N+1)+(m+1),(6*j-0)*(N+1)+(n+1)) =
S1(m+1,n+1,j)*(exp(-1*kayser0(1,n+1)*xjr(j)))                     *(-1);%A
            M((6*j-3)*(N+1)+(m+1),(6*j+1)*(N+1)+(n+1)) =
S1(m+1,n+1,j)*(exp(+1*kayser0(1,n+1)*xjr(j)))                     *(-1);%B

            % For right potential matching equation in region 1 3.
            % They will in the 5th row.
            M((6*j-2)*(N+1)+(m+1),(6*j-2)*(N+1)+(n+1)) =
T3(m+1,n+1,j)*(exp(-1*lambdaj(j,n+1)*xjr(j)))  *(-1);                  %E
            M((6*j-2)*(N+1)+(m+1),(6*j-1)*(N+1)+(n+1)) =
T3(m+1,n+1,j)*(exp(+1*lambdaj(j,n+1)*xjr(j)))  *(-1);                  %F
            M((6*j-2)*(N+1)+(m+1),(6*j-0)*(N+1)+(n+1)) =
T1(m+1,n+1,j)*(exp(-1*kayser0(1,n+1)*xjr(j)));                         %A
            M((6*j-2)*(N+1)+(m+1),(6*j+1)*(N+1)+(n+1)) =
T1(m+1,n+1,j)*(exp(+1*kayser0(1,n+1)*xjr(j)));                         %B
            M((6*j-2)*(N+1)+(m+1),(6*j-1)*(N+1)+(0+1)) =
T3(m+1,0+1,j)*(exp(+1*lambdaj(j,0+1)*xjr(j))) *xjr(j)*(-
1);          %F0   A SPECIAL PLACE

            % For right velocity matching equation in region 1 2 3.
            % They will in the 6th row.
            M((6*j-1)*(N+1)+(m+1),(6*j-4)*(N+1)+(n+1)) =
R2(m+1,n+1,j)*(exp(-1*kayserj(j,n+1)*xjr(j)))  *(-1)     *(-1);        %C
            M((6*j-1)*(N+1)+(m+1),(6*j-3)*(N+1)+(n+1)) =
R2(m+1,n+1,j)*(exp(+1*kayserj(j,n+1)*xjr(j)))  *(-1);                  %D
            M((6*j-1)*(N+1)+(m+1),(6*j-2)*(N+1)+(n+1)) =
R3(m+1,n+1,j)*(exp(-1*lambdaj(j,n+1)*xjr(j)))  *(-1)     *(-1);        %E
            M((6*j-1)*(N+1)+(m+1),(6*j-1)*(N+1)+(n+1)) =
R3(m+1,n+1,j)*(exp(+1*lambdaj(j,n+1)*xjr(j)))  *(-1);                  %F
            M((6*j-1)*(N+1)+(m+1),(6*j-0)*(N+1)+(n+1)) =
R1(m+1,n+1,j)*(exp(-1*kayser0(1,n+1)*xjr(j)))            *(-1);        %A
            M((6*j-1)*(N+1)+(m+1),(6*j+1)*(N+1)+(n+1)) =
R1(m+1,n+1,j)*(exp(+1*kayser0(1,n+1)*xjr(j)));                        %B
            M((6*j-1)*(N+1)+(m+1),(6*j-1)*(N+1)+(0+1)) =
LE(m+1,0+1,j)*(exp(+1*lambdaj(j,0+1)*xjr(j)))  *(-
1);                    %F0   A SPECIAL PLACE

            % For incident wave condition.
            % They will in the 7th row.
            M((6*J-0)*(N+1)+(m+1),(6*1-6)*(N+1)+(m+1)) = 1;
            M((6*J-0)*(N+1)+(0+1),(6*J+2)*(N+1)+(0+1)) = 1;

            % For reflect wave condition.
            % They will in the 8th row.
            M((6*J+1)*(N+1)+(m+1),(6*J+1)*(N+1)+(m+1)) = 1;
        end
    end
end
```

submerged_plate.m

```matlab
function [An,Bn,Cn,Dn,En,Fn,Cr,Ct] = submerged_plate(alpha,h,N,J,P)

% By Y. WANG @TUMSAT Oct.2016.
% INPUTs
% alpha: The radian frequency squared over g, omiga^2/g.
% h:     The water depth.
% N:     The number of evanescent wave modes.
% J:     The number of plate.
% P:     The parameters of plates.
% P = [submergence,plate length,plate thickness,midpoint coordinate]
% OUTPUTs
% Bj_n,Cj_n,Dj_n,Ej_n,Fj_n,Aj+1_n are complex values in wave potential.

% Step01
% Get water and plate parameters from matrix P.
% In matrix P values are in this table.
%%%%%%%%%%%%%%%%%%%%%%%%%%%%%%%%%%%%%%%%%%%%
%         dj        lj       tj       xj
%%%%%%%%%%%%%%%%%%%%%%%%%%%%%%%%%%%%%%%%%%%%
%  j = 1
%  j = 2
%  j = 3
%   ...
%  j = J
%%%%%%%%%%%%%%%%%%%%%%%%%%%%%%%%%%%%%%%%%%%%%%
dj = P(:,1);
lj = P(:,2);
tj = P(:,3);
xj = P(:,4);
xjl = xj - 0.5*lj;
xjr = xj + 0.5*lj;

% Step02
% Calculate the roots of the dispersion equation for the water.
% In wavenumber matrix, values are arranged below.
% For kayser0, 1st row is denoting with j =0 is wavenumber for depth h.
% For kayserj, 1st row is denoting with j =1 is wavenumber for depth dj.
% For example.
%%%%%%%%%%%%%%%%%%%%%%%%%%%%%%%%%%%%%%%%%%%%%%%%
%  n   0     1      2      3   ... N
%%%%%%%%%%%%%%%%%%%%%%%%%%%%%%%%%%%%%%%%%%%%%%%%
%  j =1
%  j =2
%  j =3
%   ...
%  j =J
%%%%%%%%%%%%%%%%%%%%%%%%%%%%%%%%%%%%%%%%%%%%%%%%
kayser0 = zeros(1,N+1);
kayserj = zeros(J,N+1);
lambdaj = zeros(J,N+1);
kayser0(1,:) = dispersion_free_surface(alpha,N,h);
for j = 1:J;
    kayserj(j,:) = dispersion_free_surface(alpha,N,dj(j));
    for n = 0:N;
        lambdaj(j,n+1) = -1*pi*n/(h - dj(j) - tj(j));
    end
end
```

```matlab
% Step03
% Resemble the eigenfunction.
% In eigenfunction matrix, values are arranged below.
% For EPSI, 1st row is denoting with j =0 is eigenfunction for depth h.
% For ZETA, 1st row is denoting with j =1 is eigenfunction for depth dj.
% For LAMB, 1st row is denoting with j =1 is eigenfunction for depth dj.
% For example.
%%%%%%%%%%%%%%%%%%%%%%%%%%%%%%%%%%%%%%%%%%%%%%
%  n    0      1      2      3   ... N
%%%%%%%%%%%%%%%%%%%%%%%%%%%%%%%%%%%%%%%%%%%%%%
%  j =1
%  j =2
%  j =3
%   ...
%  j =J
%%%%%%%%%%%%%%%%%%%%%%%%%%%%%%%%%%%%%%%%%%%%%%%
% EPSI = cos(kayser0*(z+ h))/cos(kayser0* h);
% ZETA = cos(kayserj*(z+dj))/cos(kayser0*dj);
% LAMB = cos(lambdaj*(z+ h)).

% Step04
% Taking advantage of the Orthogonality of eigenfunction.
% A(alph)={EPSI0n;EPSI0m},{ZETAjn;ZETAjm} or {LAMBjn;LAMBjm};
% B(beta)={EPSI0n;ZETAjm},{EPSI0n;LAMBjm},{ZETAjn;EPSIjm} or
{LAMBjn;EPSIjm};
zero = zeros(N+1,N+1,J);
IE = zero;  IZ = zero;  IL = zero;
EZ = zero;  EL = zero;  ZE = zero;  LE = zero;
for j = 1:J;
    for m = 0:N;
        IE(m+1,m+1,j) = alph(-1*h,                 0,kayser0(1,m+1),
h)/(cos(kayser0(1,m+1)*h))^2;
        IZ(m+1,m+1,j) = alph(-1*dj(j),
0,kayserj(j,m+1),dj(j))/(cos(kayserj(j,m+1)*h))^2;
        IL(m+1,m+1,j) = alph(-1*h, -1*(dj(j)+tj(j)),lambdaj(j,m+1),
h);
        for n = 0:N;
            EZ(m+1,n+1,j) = beta(-1*dj(j),
0,kayser0(1,n+1),kayserj(j,m+1),
h,dj(j))/(cos(kayser0(1,n+1)*h)*cos(kayserj(j,m+1)*dj(j)));
            EL(m+1,n+1,j) = beta(-1*h, -
1*(dj(j)+tj(j)),kayser0(1,n+1),lambdaj(j,m+1),    h,    h)/
cos(kayser0(1,n+1)*h);
            ZE(m+1,n+1,j) = beta(-1*dj(j),
0,kayserj(j,n+1),kayser0(1,m+1),dj(j),
h)/(cos(kayserj(j,n+1)*dj(j))*cos(kayser0(1,m+1)*h));
            LE(m+1,n+1,j) = beta(-1*h, -
1*(dj(j)+tj(j)),lambdaj(j,n+1),kayser0(1,m+1),    h,    h)/
cos(kayser0(1,m+1)*h);
        end
    end
end
% A comparing part to the eigenfunction formulation, this part can be set
as a note.
IE0 = zero;  IZ0 = zero;  IL0 = zero;
EZ0 = zero;  EL0 = zero;  ZE0 = zero;  LE0 = zero;
for j = 1:J;
    for m = 0:N;
```

```matlab
            IE0(m+1,m+1,j) = 0.5    *h*(((sin(2*kayser0(1,m+1)
*h))/(2*kayser0(1,m+1)    *h))+1)   /cos(kayser0(1,m+1)*h);    %r1
            IZ0(m+1,m+1,j) =
0.5*dj(j)*(((sin(2*kayserj(j,m+1)*(dj(j))))/(2*kayserj(j,m+1)*dj(j)))+1)
/cos(kayserj(j,m+1)*dj(j));    %s2
            IL0(m+1,m+1,j) = 0.5*(h-
(dj(j)+tj(j)));
                %t3
            IL0(  1,   1,j) = 1.0*(h-(dj(j)+tj(j)));
            for n = 0:N;
                EZ0(m+1,n+1,j) = ((kayser0(1,n+1)*sin(kayser0(1,n+1)*(h-
dj(j))))/((kayser0(1,n+1))^2-(kayserj(j,m+1))^2)*(-1))
/cos(kayser0(1,n+1)*h); %s1
                EL0(m+1,n+1,j) = ((kayser0(1,n+1)*sin(kayser0(1,n+1)*(h-
dj(j)-tj(j))))/((kayser0(1,n+1))^2-(lambdaj(j,m+1))^2)*(-1)^(m))
/cos(kayser0(1,n+1)*h);    %t1
                ZE0(m+1,n+1,j) = ((kayser0(1,m+1)*sin(kayser0(1,m+1)*(h-
dj(j))))/((kayserj(j,n+1))^2-(kayser0(1,m+1))^2))
/cos(kayserj(j,n+1)*dj(j)); %r2
                LE0(m+1,n+1,j) = ((kayser0(1,m+1)*sin(kayser0(1,m+1)*(h-
dj(j)-tj(j))))/((kayser0(1,m+1))^2-(lambdaj(j,n+1))^2)*(-
1)^(n))    ;                              %r3
            end
        end
end

% Step05
% Paraments matrix Mp and Results matrix.
M =
big_matrix(J,N,kayser0,kayserj,lambdaj,xjl,xjr,IZ0,IL0,IE0,EZ0,EL0,ZE0,LE
0);
Mp = M(1:(6*J+2)*(N+1),1:(6*J+2)*(N+1));
Re = M(:,(6*J+2)*(N+1)+1);
SOL = Mp\Re;

% Step06
An = zeros(J+1,(N+1));
Bn = zeros(J+1,(N+1));
Cn = zeros(J,(N+1));
Dn = zeros(J,(N+1));
En = zeros(J,(N+1));
Fn = zeros(J,(N+1));
for j = 1:J;
    for n = 1:N+1;
        An(j,n) = SOL((6*j-6)*(N+1)+n);
        Bn(j,n) = SOL((6*j-5)*(N+1)+n);
        Cn(j,n) = SOL((6*j-4)*(N+1)+n);
        Dn(j,n) = SOL((6*j-3)*(N+1)+n);
        En(j,n) = SOL((6*j-2)*(N+1)+n);
        Fn(j,n) = SOL((6*j-1)*(N+1)+n);
    end
end
for n = 1:N+1;
    An(J+1,n) = SOL((6*J+0)*(N+1)+n);
    Bn(J+1,n) = SOL((6*J+1)*(N+1)+n);
end
Cr = abs(Bn(1,1));
Ct = abs(An(J+1,1));
```

Appendix D   Incident and Reflection Separation for Regular Wave

A flume experiment case with 2.00 cm wave height and 1.50 sec period as target parameters is introduced in detail. Profiles in two adjacent positions can be measured by two wave gauges, see Figure A-4.

From the Eq. (3.1), the $\bar{H}^*$ and $\bar{T}^*$ are obtained by using zero crossing method, M^* is average water level of measured profile, φ^* is measured and calculated by phase lag, for the sake of convenience in coding, a trying method is used for the convenient of computational calculation, which the results show in Eq. (A.14). The Figure A-5 illustrates how the program finds the most accurate initial phases of fitting curves; the error between measured and fitting wave profile can be observed in Figure A-6; and the final fitting result of wave profile shows in Figure A-7.

$$
\eta_1^* = \frac{1}{2} \times 2.7369 \times cos(2\pi/1.5 + 2.1817) + (-0.0701)
$$
$$
\eta_2^* = \frac{1}{2} \times 0.6956 \times cos(2\pi/1.5 + 1.5359) + (-0.0423)
$$

(A.14)

By utilizing the method mentioned in chapter 3, the sine and cosine values of composed wave at the first wave gauge location can be derived, and the results are: $A_1 = -0.7849$, $B_1 = -1.1210$, $A_2 = 0.0121$ and $A_2 = -0.3476$.

The amplitude of incident and reflected wave and the corresponding phase are obtained, which the conclusive results are: $a_I = 0.9278$, $a_R = 0.6904$, $\varphi_I = -1.7055$, $\varphi_R = -3.4380$ and the $\mathcal{K}_R = 0.7411$.
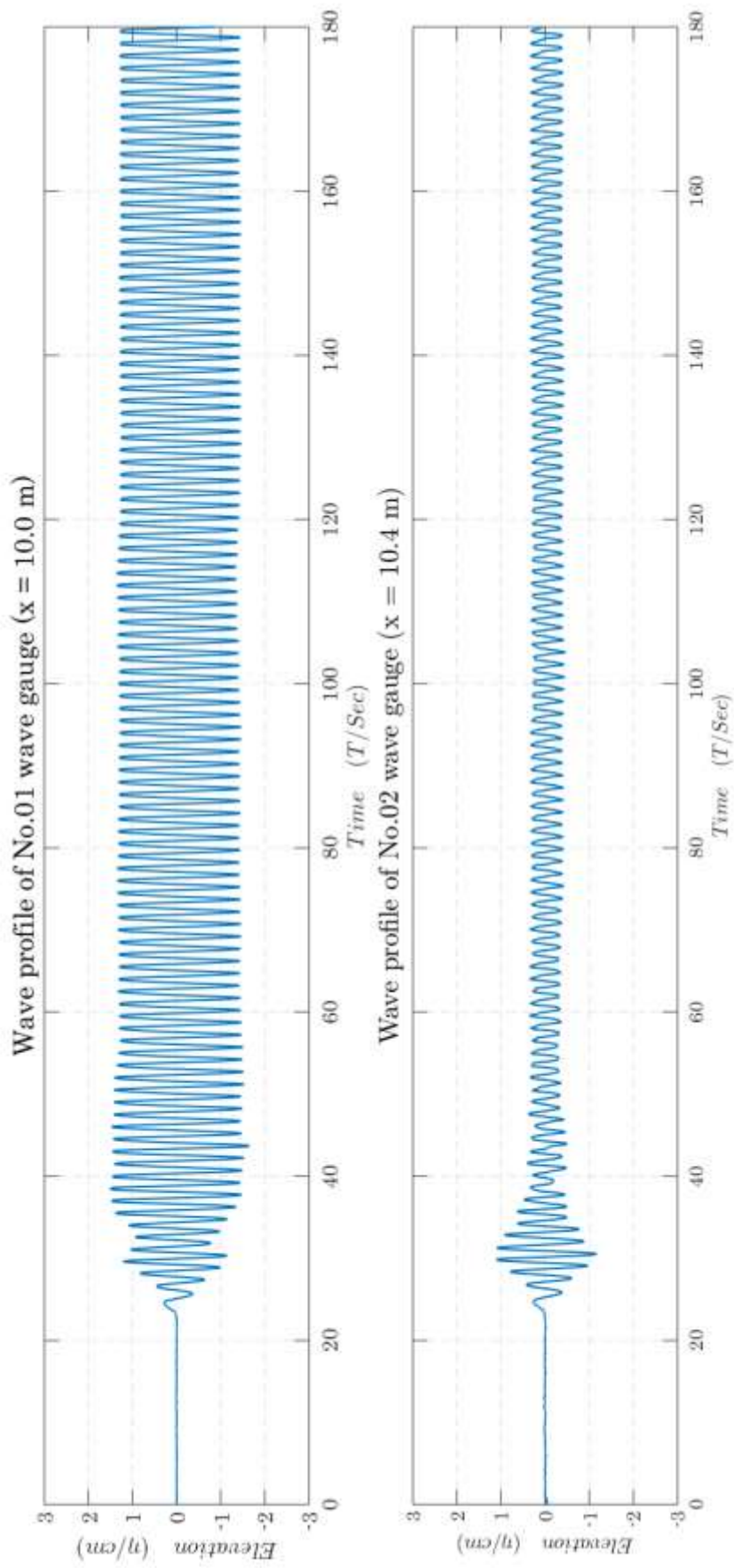
Figure A-4 Partial Profiles of Gauges in Case 1 ($\bar{H}$ = 2cm, $\bar{T}$ = 1.5s).
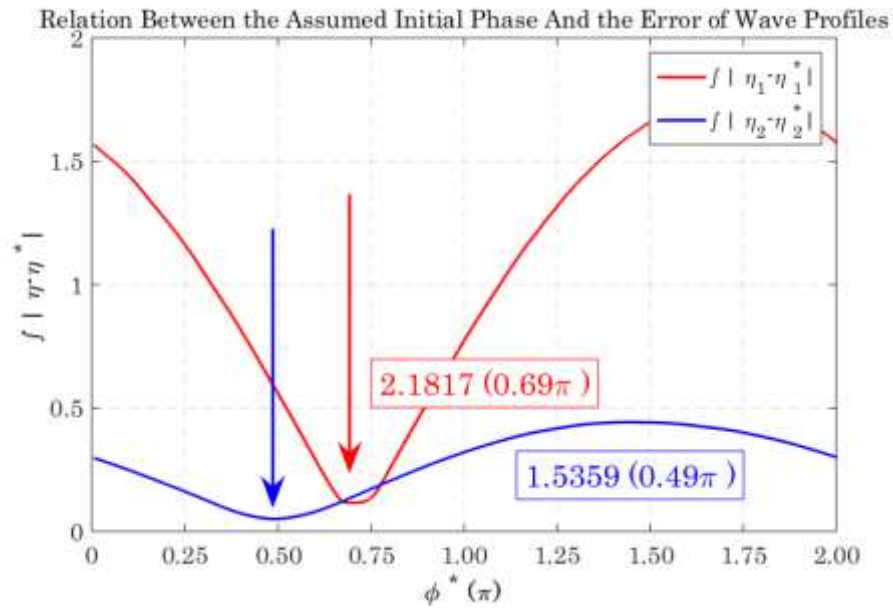
Figure A-5 Assumed Initial Phase at the Minimum Profile Error.
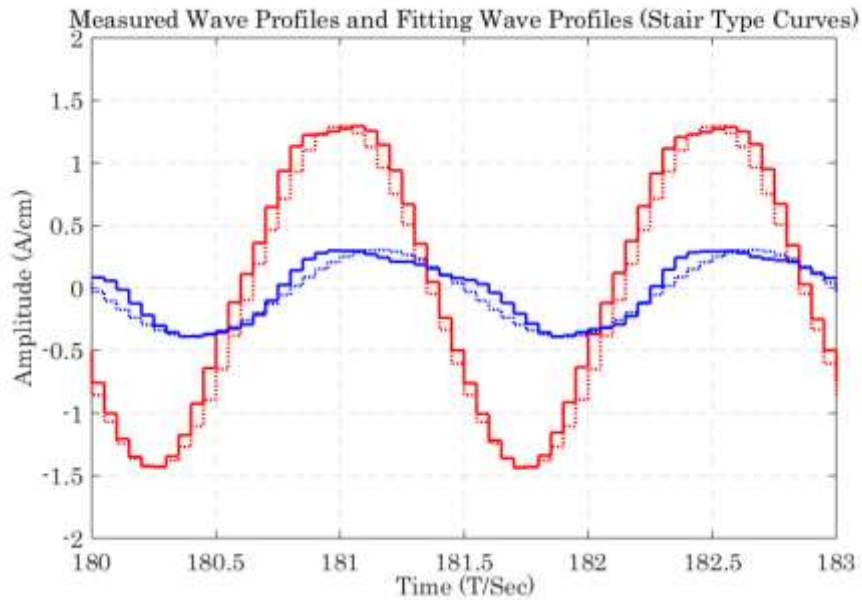
Figure A-6 Magnified Measured Profiles and Fitting Profiles.
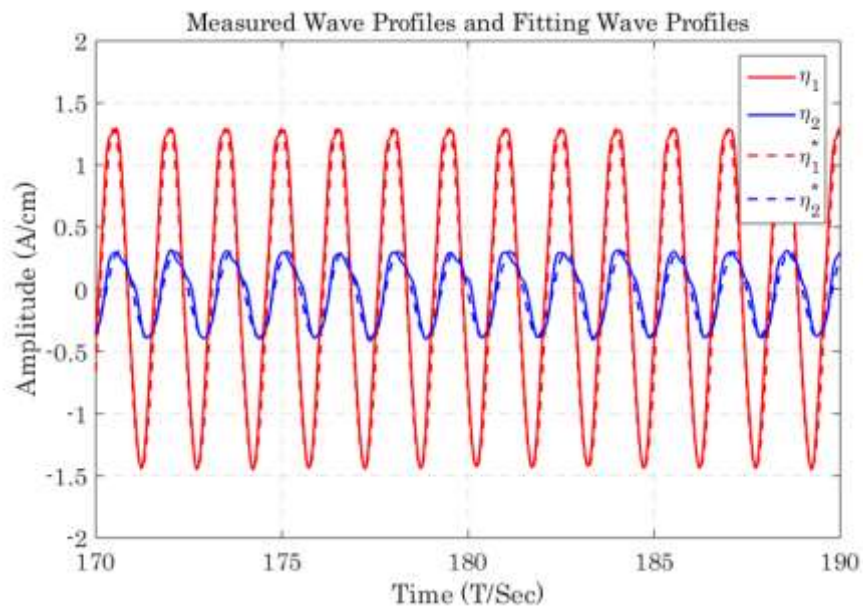
Figure A-7   Measured Profiles and Fitting Profiles.
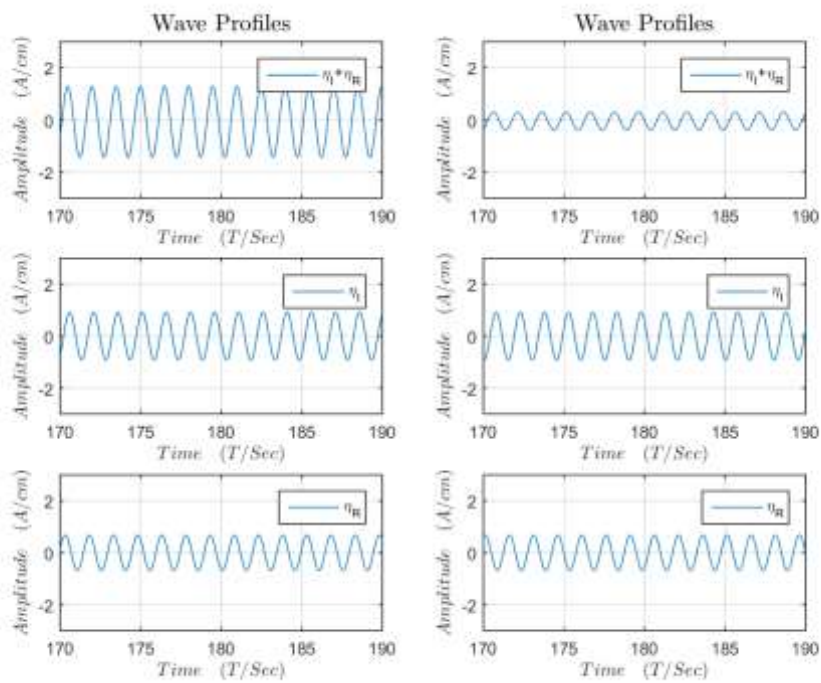
Figure A-8   Separated Wave Profiles of Gauges.